Gold-in-calcrete: A continental to profile scale study of regolith carbonates and their association with gold mineralisation

Robert Charles Dart, B.AppSc (Hons)

Geology and Geophysics
School of Earth and Environmental Sciences
The University of Adelaide

Thesis submitted as fulfilment of the requirements for the degree of Doctor of Philosophy in the Faculty of Science, University of Adelaide

March 2009

Chapter 6

Gold in the regolith profile: Pedogenic controls at White Dam, South Australia

6.1. Introduction

Previous studies have indicated that Au and Ca are correlated through the regolith profile where there are regolith carbonates (Lintern, 1989; Lintern & Butt, 1993; Lintern, 1997; Lintern & Butt, 1998b; Smee, 1998; Lintern & Sheard, 1999a; 1999b; Okujeni *et al.*, 2005; Lintern *et al.*, 2006). Less recognised but more significant however, is that this correlation is dependent on the availability of a significant amount of Au. The majority of the Ca is externally derived (demonstrated in Chapter 4), hence any relationship is due to a secondary process, and not the result of any prior association between Ca and Au within bedrock mineralogy. Two profiles at the White Dam Au-Cu prospect, South Australia, have been analysed to investigate relationships between Au and regolith carbonates.

Understanding how the profiles have developed, and the dispersion of elements within them, forms the basis of the research presented in this chapter. A detailed analysis of the profiles was undertaken and the following hypothesis investigated:

> *Au is mobilised, either chemically or physically, in association with clay minerals and the clay size fraction. Precipitation of regolith carbonates fills void space and reduces permeability. This acts as a barrier to Au movement and immobilises the clay minerals (and Au). Ongoing dissolution and re-precipitation of the carbonates leads to increased Au concentrations.*

Understanding how Au is mobilised within the regolith profile may then be applied to the interpretation of other regolith profiles where high Au values are associated with regolith carbonates, improving interpretations made from regolith carbonate sampling in Au exploration. The work presented here expands on previous PhD and honours research at the site (e.g. Cordon, 1998; Chubb, 1999; Brown & Hill, 2004; Lau, 2004; Wittwer *et al.*, 2004; Brown & Hill, 2005).

The White Dam Au-Cu deposit is approximately 25 km northeast of Olary, South Australia. The discovery and confirmation of the White Dam deposit was through geochemical sampling followed by drilling from 1989 to 1997 (McGeough & Anderson, 1998). Regional soil sampling in 1989 by Aberfoyle Resources Limited and Normandy Mining Limited, and in 1994-95 by MIM Exploration Limited, identified up to 500 ppb Au at White Dam. Drilling during 1996 and 1997 confirmed the deposit (McGeough & Anderson, 1998). Exco Resources acquired the White Dam deposit in 2006 following a joint venture with Polymetals Mining Services Proprietary Limited who took over MIM in 2001 (Exco Resources, 2006). The current Au resource is stated at 7.3 Mt at 1.09 g/t for a total of 257,400 ounces (Exco Resources, 2006).

A series of exploration costeans dug in 2003 exposed regolith profiles that were used in this study. Two profiles coinciding with areas of high Au concentrations were sampled. Bulk and undisturbed (*in-situ*) samples were collected from each soil horizon and the underlying

saprock. Additional samples were collected from thicker soil horizons or where specific features were noticed.

Analyses undertaken on the two profiles included: petrology; elemental mass balance; particle size; mineralogy; elemental chemistry; and SEM investigations on the Au morphology. Methodology of sample collection and the analytical procedures adopted are described in Chapter 3. Profile descriptions were compiled from field observations, petrological studies and analytical results. Detailed petrological observations and additional microphotographs completed during thin section analysis are included in Appendix 3. Terminology for profile descriptions is based on that used by McDonald et al. (1990). Petrological descriptions are based on terminology described in Bullock *et al.* (1985) and Stoops (2003). Colours are defined using the Munsell colour system with colour codes for moist and dry soils provided. Full results from analytical procedures are included in Appendices 4 to 7.

6.2. Geology of the White Dam Au-Cu deposit and the surrounding region

The White Dam Au-Cu deposit is located in the Olary Domain, within the southern margin of the Curnamona Province (Figure 6.1 & Figure 6.2). The Curnamona Province extends over the northeast South Australia - northwest New South Wales border. It is defined by an oval shaped, regional aeromagnetic high, approximately 250 km in diameter (Parker *et al.*, 1993; Robertson *et al.*, 1998). The Province represents a fragment of a Late Palaeoproterozoic to Mesoproterozoic basin consisting of metasedimentary rocks, metavolcanics and granitoids of the Willyama Supergroup (Table 6.1) (Robertson *et al.*, 1998; Preiss & Conor, 2001). These rocks are overlain by Neoproterozoic metasedimentary rocks of the Adelaidean, Burra and Umberatana Groups (Conor, 2004). The majority of the rocks within the Curnamona Province are buried by Cainozoic and Mesozoic sediments with only limited exposures within the Willyama, Mt. Painter and Mt Babbage Inliers (Ashley *et al.*, 1998; Robertson *et al.*, 1998).

The southern margin of the Curnamona Province is composed of the Willyama Inliers, an area that has traditionally been divided into the Olary and Broken Hill Blocks (Flint & Parker, 1993). More recently these have become known as the Olary and Broken Hill Domains (Figure 6.1) and indicate areas of different sedimentary facies and metamorphic grade (Robertson *et al.*, 1998; Preiss & Conor, 2001). The term 'Willyama Inliers' refers to a number of inliers in the cores of anticlinal domes separated by narrow corridors of Adelaidean cover (Ashley *et al.*, 1998; Preiss & Conor, 2001). The inliers mostly have curved, slightly dipping, unconformable boundaries to the east and faulted boundaries on the west (Preiss & Conor, 2001). Formal nomenclature and descriptions of the Willyama Inliers were proposed by Preiss & Conor (2001), the largest being the Kalabity Inlier, which also hosts the White Dam deposit.

Two significant periods of deformation and metamorphism have occurred in the Willyama Inliers: the Palaeoproterozoic Olarian Orogeny; and the Cambrian-Ordovician Delamerian Orogeny (Flint & Parker, 1993). The three phases of deformation defined for the Olarian Orogeny (OD_{1-3}) are the more significant, resulting in higher metamorphic grades and the formation of major structures (Clarke *et al.*, 1986; Flint & Parker, 1993). The degree of deformation and metamorphism is higher towards the south, away from the centre of the province (Robertson *et al.*, 1998). These multiple events have resulted in complex structural features and mineralogical assemblages leading to difficulties in unravelling the geological history of the area. This is illustrated by the number of previous and ongoing studies of the region (cf. Willis *et al.*, 1983; Clarke *et al.*, 1986; Stevens *et al.*, 1990; Flint & Parker, 1993;

Bierlein *et al.*, 1995; Bierlein *et al.*, 1996b; Laing, 1996; Robertson *et al.*, 1998; Conor, 2000; Conor & Fanning, 2001; Preiss & Conor, 2001; Conor, 2004; Page *et al.*, 2005; Conor, 2006a).

Figure 6.1: Extent of the Curnamona Province (Robertson *et al.*, 1998).

Mineralisation in the region includes the massive Pb-Zn-Ag deposit of Broken Hill. Smaller metalliferous deposits are widespread with Cu, U, and lesser Fe, Ba, Co, W, Au and F, significant within the Olary Domain, and Pb, Zn, Ag, with lesser W, Cu, Fe, Co, Au, Ni, Pt, Sn, Be, U and F, significant within the Broken Hill Domain (Stevens *et al.*, 1990). Various mineralisation styles exist within the Olary Domain including: stratiform; stratabound; epigenetic veins; granite- and pegmatite-related; and weathering-related (Stevens *et al.*, 1990; Conor, 2004).

Stratiform type deposits of the Olary Domain are generally disseminated to massive, sediment hosted and associated with felsic volcanism and evaporitic facies. They include: banded Fe formations and Mn silicates within the Ethiudna Subgroup and Strathearn Group; laminated sulphides associated with calc-silicates and pelite - Fe, Zn, Pb of the Bimba Formation; and, Fe formations, commonly baritic with local Cu and Au in the upper Wiperaminga Subgroup (Conor, 2004).

Epigenetic deposits are associated with all stratigraphies and granitoid intrusives (Bierlein *et al.*, 1995; Bierlein *et al.*, 1996a; Bierlein *et al.*, 1996b). Regionally however, there is an apparent Cu-Au mineralisation associated with the upper Wiperaminga Subgroup grading into the Peryhumuck Formation (Conor, 2004). Anomalous Cu-Au values are hosted in Fe formations and adjacent quartz-albite rocks in areas of biotite and magnetite alteration (e.g. Peryhumuck, Walparuta, Mary Mine and Woman-in-White, Figure 6.2) (Conor, 2004). In the

northern and eastern areas of the Olary Domain Cu-Au-(Mo) mineralisation is found within veins, stockworks and disseminated type deposits (e.g. Kalkaroo, Portia, White Dam and Waukaloo) (Conor, 2004). Many of these Cu-Au deposits show similarities with Fe-oxide Cu-Au (IOCG) deposits of other Proterozoic terranes (e.g. Olympic Dam). White Dam however, appears to be an exception with no associated Fe-oxides (Skirrow & Ashley, 2000; Skirrow, 2003).

NOTE:
This figure is included on page 124 of the print copy of the thesis held in the University of Adelaide Library.

Figure 6.2: Mineral deposits of the Olary Domain (Conor, 2004).

Table 6.1: Stratigraphy and lithological summary of the Willyama Supergroup (Olary Domain), direct relationship between some formations is uncertain (dashed lines) (adapted from Conor, 2000; Conor & Fanning, 2001; Conor, 2004; Page *et al.*, 2005; Conor, 2006a).

Age (Ma)	Igneous Suite	Willyama Supergroup			Equivalents
		Group	Sub-group	Formation: Description	
<1655		Strathearn	Mt Howden	**Dayanna:** Fine-grained sillimanite-Andalusite-staurolite schist	Paragon Group
				Mooleulooloo: Albitic psammite, locally tuffaceous	
				Alconie: Graphitic chiastolite pelite and metasiltstone	
		Saltbush		**Walparuta:** Pelite and psammopelite with minor psammite layers	Sundown Group
	Lady Louise Suite ~1685		Raven Hill	**Oonartra Creek:** Pelite and psammopelite with minor psammite layers and coticule lenses	Broken Hill Group
				Black Maria: Psammite. Psammopelite and pelite locally graphitic and locally with calc-silicate ellipsoids	
~1693			Larry Macs	**Plumbago:** Tuffaceous biotite psammite	
				Bimba: Pyritic, marble, calc-silicate, micaceous psammite	
	Basso Suite 1713-1719 Ma	Curnamona	Ethiudna	**Waukaloo:**Fine grained psammitic schist	Calc-silicate Suite of Clarke *et al.* (1986)
~1715				**Peryhumuck:** Calc-albitite metasiltstone, locally pseudomorphs after carbonate and others	
<1718				**Beewooloo:** Psammitic schist with mafic lava, volcanic conglomerate, quartz-grunerite-garnet 'exhalite' / **Toraminga:** Psammitic schist with occasional albite granofels and calc-silicate / **Cathedral Rock:** Quartzites, locally volcani-clastic	
~1718			Wiperaminga	**Tommie Wattie:** Thick upward fining package from psammites, showing sedimentary structures, top andalusite pelite. Volcanic interbeds (Abminga Substitute) / **Mooleugore:** Psammitic schist with clean epidotic cross-bedded quartzite	Quartzo-feldspathic Suite of Clarke *et al.* (1986)
~1718				**George Mine:** Pelite, psammopelite and psammite, but characterised by albite granofels. Contains numerous magnetite-rich units. Volcanic interbeds.	

Weathering-related deposits in the Olary Domain include: supergene Cu-(Co) (e.g. Dome Rock, Mt Howden, and Mary Mine); Cu-Au (e.g. Kalkaroo and Portia); Redox controlled U and Au, (e.g. Honeymoon and Beverly); and placer Au enrichments (Conor, 2004).

Mineralisation at White Dam is associated with leucosome lenses within a quartz-feldspar-biotite gneiss unit of the Wiperaminga Subgroup (Cooke, 2003; Conor, 2004; 2006b). Primary Au mineralisation is located in a stockwork of pyrite, chalcopyrite, and molybdenite veins that have been oxidised to 50 m below the surface (McGeough & Anderson, 1998; Cooke, 2003). The mineralisation consists of high Au/Cu ratios with minor molybdenite (Conor, 2004). Within the oxide zone, Au exists as small platelets up to 60 μm in diameter with occasional larger grains up to 165 μm that are associated with biotite (Cordon, 1998; Croxford, 1998; Cooke, 2003).

6.3. Regolith-landforms and vegetation of the White Dam area

White Dam is in an area of low relief with minor bedrock exposure. Alluvial sheetflow sediments, about 2 m thick, are the dominant regolith material in the area. Minor bedrock exposures in the south of the area form low rises. Towards the north-west, sediments relate to alluvial channel activity and associated alluvial plains. Vegetation is dominated by a chenopod shrubland consisting of bladder saltbush (*Atriplex vesicaria*), black bluebush (*Maireana pyramidata*) and scattered pearl bluebush (*Maireana sedifolia*). Other vegetation includes scattered belahs (*Casuarina pauper*) along the creek, and occasional mulgas (*Acacia aneura*) and rosewoods (*Alectryon oleifolius*) on the rises (Brown & Hill, 2004).

Regional regolith-landform mapping was completed by Lau (2004), and locally over the White Dam deposit, by Brown & Hill (2004). Figure 6.3 is the regolith-landform map of Brown & Hill (2004) with the exploration costeans and position of the sampled profiles shown. The area consists of depositional plains and low rises, with an alluvial channel cutting across the north-west corner. Contemporary alluvial drainage and sheetflow directions trend northwards, swinging round towards the north-east in the north of the area (Brown & Hill, 2003).

Depositional areas are characterised by red-brown to yellow-brown silts and clays, fine to coarse, sub-angular quartz with lesser feldspar sands, and minor iron oxides. A thin silt and clay surface veneer is typical within the depositional areas and surficial mud cracks are extensive towards the creek. Erosional areas consist of red-brown to yellow-brown silts and clays with abundant fine to very coarse, sub-angular to angular quartz, lesser fine to medium sized, sub-angular feldspars and minor iron oxides, micas and lithic fragments.

6.4. White Dam Profile 1: Description, petrology and analytical results

Profile 1 is within costean WDTR01 (Figure 6.3) at Geocentric Datum of Australia 1994 (GDA94) Universal Transverse Mercator (UTM) Zone 54S, 0459917 mE, 6449176 mN. This profile is directly over mineralisation with 3.2 ppm Au recorded for the underlying pegmatite and values up to 142 ppm from stockwork veins within the same costean (Cooke, 2003).

6.4.1. Profile 1 description and petrology

Profile 1 (Figure 6.4) is within a depositional plain and is approximately 4 m deep. It includes a thin, coarse textured A1 horizon, a clay-rich B1 horizon and a calcareous B2 horizon that gradually changes to a Bk horizon with carbonate nodules and rhizomorphs. Below this, the sequence is repeated with a second clay horizon (2B2) and calcareous horizon (2Bk). This is interpreted as a palaeosol where the previous A1 horizon has been eroded. Below this is the

saprolith (C horizon) consisting of a pegmatite that has intruded a biotite gneiss. Summary descriptions of each soil horizon are provided in Table 6.2.

Figure 6.3: Regolith Landform map of the White Dam deposit showing position of costeans and sample profiles, from Brown & Hill (2004).

The presence of the palaeosol represents a break in soil formation at this site and the existence of a palaeo-surface. This invalidates any mass balance calculations on the profile, since it cannot be considered to have formed *in-situ* and from uniform material (see Section 3.5.1).

Further evidence of the disconformity exists to the north of the profile, within the same costean, where at the palaeo-surface level there is a thin layer of lithic fragments that were interpreted by Lau (2004) as either a palaeo-surface or channel deposits.

The mineralogy of the coarse fragments through the profile is predominantly quartz with minor feldspars. Minor micas (biotite and muscovite) are present towards the base of the pedolith. Grains are poorly sorted and sub-rounded to sub-angular, and more angular down profile closer to the saprolith. Powdery regolith carbonates are within the B2 horizon and gradually increase in concentration into the Bk horizon. There is a change in morphology to small nodules and rhizomorphs (5 – 15 mm diameter) towards the base of the Bk horizon (Figure 6.5). Similar regolith carbonate nodules and rhizomorphs are in the 2Bk horizon.

Coarse fragment minerals have variable degrees of weathering throughout the pedolith. Feldspars show the highest degree of weathering, especially the K-feldspar, which in the majority of cases has a "dirty" grey (turbid) appearance in plane polarised light (PPL) (Figure 6.7A). Clay material is also present within fractures and along exposed feldspar grain boundaries derived from the alteration of the feldspars. Other minerals, apart from quartz, are sparse, and variations in the degree of weathering are difficult to determine. Micas are generally decayed with evidence of "splitting" along cleavage planes within grains and breakage at the ends of grains. Direct evidence of quartz weathering is limited, except that quartz is more abundant in lithic fragments towards the base of the pedolith and into the saprolith. The quartz lithic fragments have a similar sutured texture as observed in the biotite gneiss (see below).

Minor opaque minerals are present towards the top of the pedolith and become sparse towards the top of the saprolith. The majority of these are likely to be Fe-oxides as observed in the heavy mineral analysis (Section 6.4.2). In the B2 horizon birnessite [$(Na_{0.3}Ca_{0.1}K_{0.1})(Mn^{4+},Mn^{3+})O_4 1.5H_2O$] was visible in the field, which may account for some of the opaque minerals (Figure 6.6). Organic matter may also account for some of the optically opaque material.

Organic matter is sparse throughout the profile with only trace amounts within the A1 horizon. Evidence of plant activity extends into the saprolith, where plant roots have enhanced physical weathering by fracturing feldspar grains and creating fluid/clay pathways (Figure 6.7C & D).

The fine earth content is predominant in the B1 and B2 horizons and is gradually less prevalent towards the base of the pedolith. The fabric is generally random (undifferentiated) with occasional areas of alignment (mono-striated). In contrast, the regolith carbonates have a crystallitic b fabric (Figure 6.7B). A complete or partial clay cutan is on most coarse grained fragments in all horizons (Figure 6.7E). In the B1 and B2 horizons cutans tend to be more prominent on the larger grains and aggregates, with many of the smaller grains, especially those surrounded by fine material, having partial or no cutans. Apart from calcite aggregates, which have grown out from the rim of voids and in some cases completely infilling them, most voids have no cutans (Figure 6.7F).

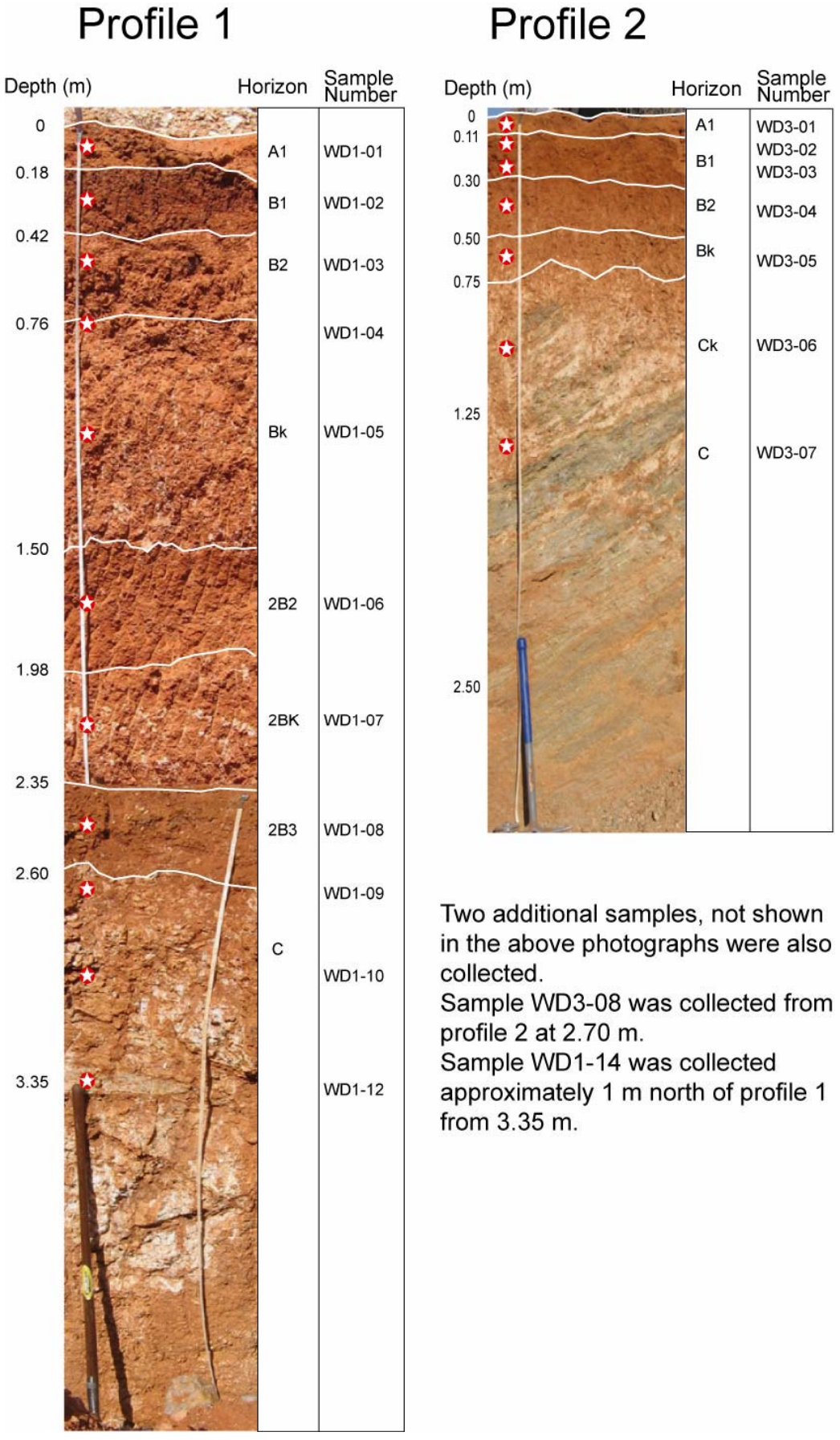

Figure 6.4: Photographs of the two White Dam profiles showing soil horizons and sample locations.

Table 6.2: Horizon properties of White Dam Profile 1.

Horizon	Depth	Colour	Contact	Macro-features	Coarse fragment mineralogy	Pedo-features
A1	0 – 0.18 m	5YR 4/6 (M) 5YR 5/6 (D)	Sharp		Poorly sorted / sub-angular / most grains 0.1 – 0.3 mm occasional larger grains & lithic aggregates up to 1 mm 80 - 85% quartz ~ 5% plagioclase ~ 2% K-feldspar < 1% other minerals (biotite, muscovite, pyroxene) ~ 5 % opaque minerals (possibly Fe-oxides or organic) ~ 10 fine fraction	**Relative-distribution:** Chito-gefuric **Ped Structure:** Apedal **Voids:** Sparse, compound packing (inter-aggregate voids) **Coatings:** thin (< 10 µm) clay cutan present on individual coarse grains **Groundmass:** None
B1	0.18 – 0.42 m	5YR 3/4 (M) 5YR 4/4 (D)	Sharp	Slightly calcareous	Poorly sorted / angular to sub-angular / average 0.5 mm diameter 25 – 30% quartz ~ 5% plagioclase ~ 1% K-feldspar < 1% other minerals (zircons, garnet) sparse opaque minerals ~ 65 – 70% fine fraction	**Rel-dist:** Double space porphyric **Ped Structure:** Angular blocky **Voids:** Inter-aggregate channels with occasion vughs **Coatings:** Sparse clay cutans on grains only **Groundmass:** Mono-striated
B2	0.42 – 0.76 m	5YR 4/6 (M) 5YR 5/6 (D)	Gradual	Highly calcareous, distinct (10 – 20%) carbonate mottles (5YR 7/4) 15 -30 mm diameter. Small cm sized black (birnessite) nodules throughout	Poorly sorted / sub-angular to sub-rounded (feldspars more lath shaped) / average 0.1 mm diameter ~ 45% quartz ~ 2% plagioclase < 1% K-feldspar calcite (small crystals and aggregates) < 1% other minerals (hornblende & zircons) Sparse opaque minerals, some with blotchy appearance ~ 45 - 50% fine fraction	**Rel-dist:** Single space porphyric **Ped Structure:** Angular blocky, (weakly defined), peds are generally free floating **Voids:** Inter-aggregate channels **Coatings:** Clay cutans on larger grains only **Groundmass:** Crystallitic b fabric
Bk	0.76 – 1.50 m	5YR 4/4 (M) 5YR 5/6 (D)	Sharp	Highly calcareous, distinct (10 – 20%) carbonate mottles (5YR 7/4) 5 – 15 mm diameter nodules and rhizomorphs	Poorly sorted/ sub-rounded (typically quartz grains) to sub-angular / average 0.1 mm diameter ~ 55% quartz ~3 plagioclase < 1% K-feldspar < 1% other minerals (hornblende, zircons, muscovite & biotite) 35 – 45% fine fraction < 1% opaque minerals	**Rel-dist:** Single space porphyric **Ped Structure:** Sub-angular blocky (weakly defined) **Voids:** Sparse inter-aggregate channels & chambers, vughs are present within some calcite aggregates **Coatings:** Partial clay cutans on most grains and aggregates **Groundmass:** Crystallitic b fabric

Table 6.2: Horizon properties of White Dam Profile 1 (continued).

Horizon	Depth	Colour	Contact	Macro-features	Coarse fragment mineralogy	Pedo-features
2B2	1.5 – 1.98 m	5YR 4/4 (M) 5YR 5/6 (D)	Gradual		Poorly sorted / sub- rounded (quartz) to sub-angular / Majority < 0.2 mm diameter ~ 65% quartz ~ 3% plagioclase < 1% K-feldspar < 1% other minerals (Actinolite, muscovite, hornblende, garnet, zircon & sparse calcite aggregates) < 1% opaque minerals 30 – 35% fine fraction	**Rel-dist:** Areas of single space porphyric and chito-gefuric **Ped Structure:** Sub-angular blocky **Voids:** Occasional inter-aggregate compound packing within chito-gefuric sections **Coatings:** Clay cutans present on most grains, voids tend to have no coatings except where a coated grain or aggregate forms void boundary **Groundmass:** Mono-striated
2Bk	1.98 – 2.35 m	5YR 4/6 (M) 5YR 5/6 (D)	Abrupt	Distinct calcareous nodules ~ 10% 15 – 30 mm diameter	Poorly sorted / sub-angular / average 0.2 mm with occasional 0.4 mm diameter ~ 65% quartz ~ 3% plagioclase < 1% K-feldspar ~ 1% biotite / muscovite < 1% Other minerals (Actinolite, orthopyroxene & hornblende) < 1% opaque minerals ~ 35% fine fraction	**Rel-dist:** Single space porphyric **Ped Structure:** Sub-angular blocky **Voids:** Inter-aggregate channels and chambers with sparse vughs. **Coatings:** Clay cutans on some larger grains and also parallel with some channels **Groundmass:** Mono-striated, with areas of calcite crystallitic b fabric
2B3	2.35 – 2.60 m	5YR 4/4 (M) 5YR 5/6 (D)	Diffuse	High proportion of lithic fragments	Poorly sorted / rounded (especially smaller grains) to sub-angular / up to 6 mm (lithic fragments) ~ 65% quartz ~ 3% plagioclase < 1% K-feldspar < 1% biotite < 1% other minerals (hornblende, microcline, muscovite) ~ 35% fine fraction	**Rel-dist:** Single space porphyric **Ped Structure:** Sub-angular blocky **Voids:** Inter-aggregate channels with occasional chambers **Coatings:** Partial clay cutans on most coarse fragments. Some large calcite aggregates have a calcite crescent capping **Groundmass:** Small scale mono-strated with crystallitic b fabric (calcite aggregates)
C (saprolith)	2.6 m to base			Pegmatite	Angular crystals that are heavily weathered and fractured 75 – 85% plagioclase, ~ 5% quartz, ~ 5% K-feldspar, < 2% microcline, < 1% biotite, ~ 15% fine fraction (decreasing with depth)	No pedo-features
				Biotite Gneiss	Fine (most < 0.5 mm occasional larger grains to 3 mm), minor alignment of biotite (larger grains tend to show weathering fractures) ~ 75% quartz, ~ 10% biotite, ~ 10% plagioclase, ~ 5% K-feldspar, ~ 5% fine fraction	No pedo-features

Figure 6.5: Rhizomorph and powdery nodule morphologies of regolith carbonates present in the Bk horizon.

Figure 6.6: Small nodules and staining by birnessite within the B2 horizon.

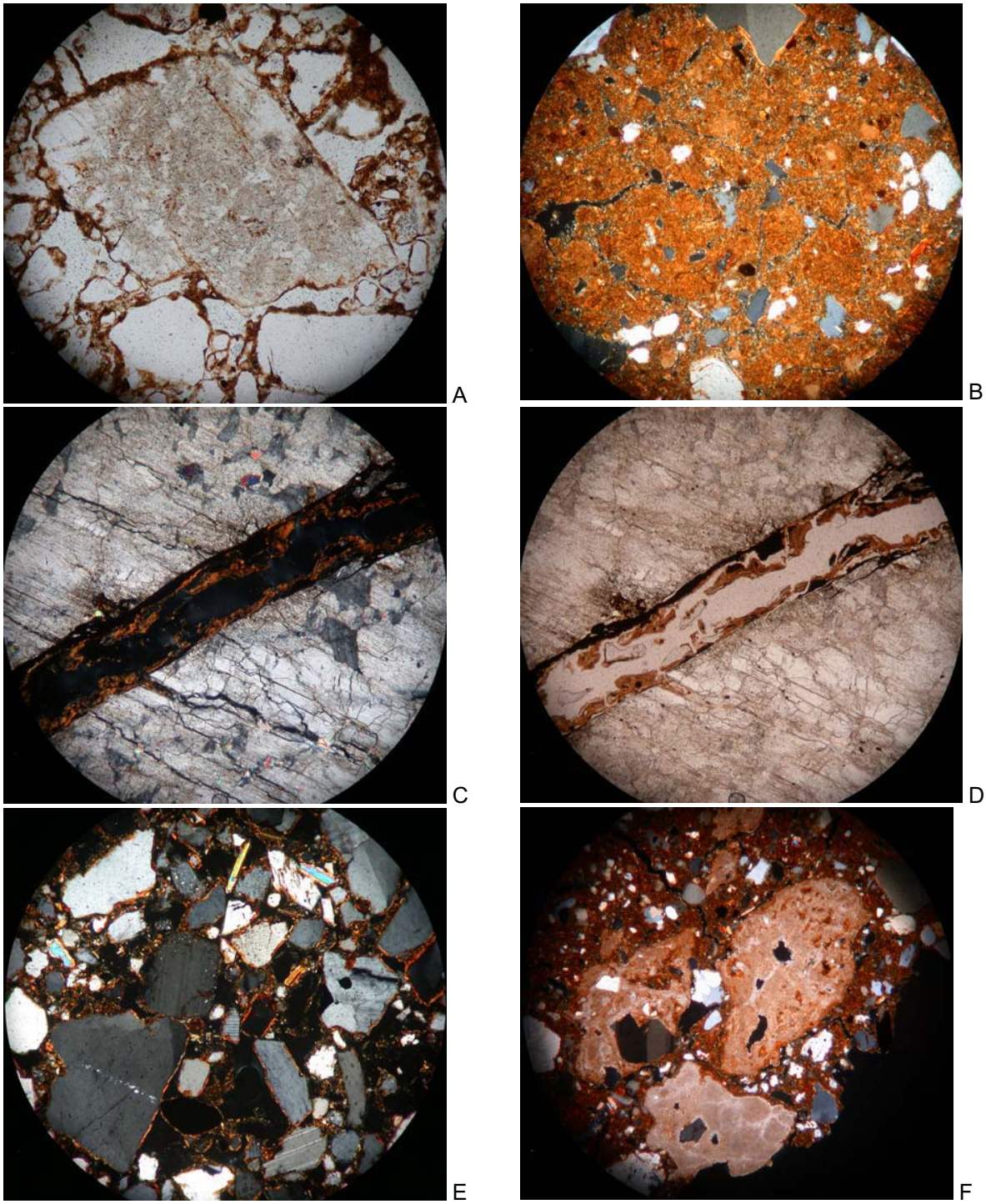

Figure 6.7: Microphotographs from Profile 1: A. Weathered feldspar (A1 horizon, FOV = 2 mm), B. Crystallitic b fabric (B2 horizon, FOV = 2 mm), C. & D. Fractured feldspar grains with plant root (C horizon, FOV = 4 mm), E. Clay cutans on coarse grains but not on voids (A1 horizon, FOV = 2 mm), and F. Calcite infilled voids (Bk horizon, FOV = 4 mm).

Despite the mineralogical differences between the gneiss and pegmatite samples, there is negligible variation in the clay fraction. The XRD analysis is included in Appendix 4 and shows that smectite and kaolin are co-dominant (>60%) with minor illite (5-20%). Upwards in the saprolith, smectite and illite gradually increase and kaolin decreases, so that at the saprolite–pedolith interface, smectite is dominant (>60%) and randomly interstratified with sub-dominant (20-60%) illite, and minor kaolin (5-20%). This is the status throughout the

pedolith apart from the A1 horizon where smectite and illite become co-dominant (Figure 6.9).

The saprolith is biotite gneiss, which has been intruded by a feldspar-rich pegmatite. The biotite gneiss consists of fine grained (0.2 – 0.5 mm) quartz, which generally has a sutured contact, feldspars (plagioclase and K-feldspar), and weakly aligned biotite. There are some larger quartz grains to ~ 5 mm. The pegmatite is predominantly coarse-grained plagioclase with minor K-feldspars, microcline and quartz.

Veins, approximately 1 – 2 cm thick, consisting of clay with minor gypsum and relict "*in-situ*" parent material are within the saprolith. Ptygmatic type folds within the gneiss continue into the veins in some parts of the profile (Figure 6.8).

According to the Australian soil classification system of *Subgroup, great group, suborder, order, family criteria (A horizon thickness, Gravel of surface and A1 horizon, A1 horizon texture, B horizon maximum texture and soil depth)* (Isbell, 1996), Profile 1 is classified as a *Calcic, haplic, Red Chromosol: medium, slightly gravelly, loamy, clay loamy and very deep*.

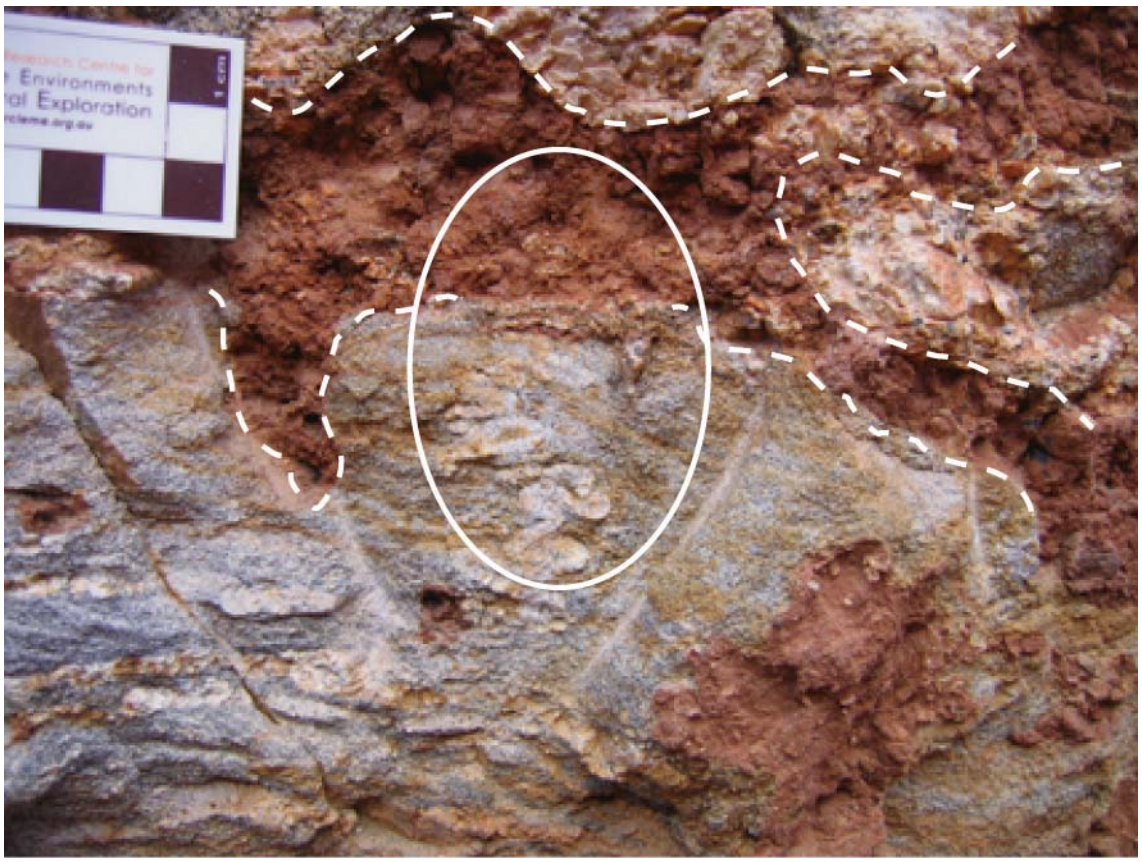

Figure 6.8: Quartz vein (circled) through gneiss showing ptygmatic type folds continuing through clay-rich vein (dashed line).

6.4.2. Profile 1 particle-size analysis

Calculated percentages of the fine earth (< 2 mm), gravel (> 2 mm), clay/silt/sand, and sand fractions for Profile 1 are shown in Table 6.3. These do not include the carbonate content (Table 6.5), which was removed during the particle separation process (see Section 3.5.2.1).

The distribution of coarse grained fragments (> 2 mm) through the profile varies from 1.2 to 28.0%. This relatively high variability can be sub-divided into distinct groups that reflect the sample position within the profile. The coarse fragments from the top of the profile, including the A1, B1, B2 and Bk horizons, are less than 2.6% of the total material. The coarse fragments of the 2B2 and 2Bk horizons are 5.6 and 4.0% respectively. There is then a significant increase in the coarse grained fragment content to 28.0% within the 2B3 horizon. The coarse grained fraction within the saprolith reflects the bedrock composition with the directly underlying pegmatite containing between 8.6 and 10.5%, and the nearby biotite gneiss 2.7%.

Table 6.3: Results from particle size analysis of samples from Profile 1.

Sample No.	Horizon	Fine earth (%)	Gravel (%)	Clay (%)	Silt (%)	Sand (%)	Sand (%)		
							Fine	Medium	Coarse
WD1-01	A1	97.4	2.6	10.4	9.2	80.4	11.1	27.0	61.8
WD1-02	B1	98.8	1.2	61.1	4.7	34.2	9.3	26.4	64.3
WD1-03	B2	97.6	2.4	46.4	7.6	46.0	10.7	25.8	63.5
WD1-04	Bk	98.0	2.0	41.8	7.2	51.1	11.0	26.0	63.0
WD1-05	Bk	98.5	1.5	32.9	6.5	60.6	10.1	29.0	60.9
WD1-06	2B2	94.4	5.6	29.8	5.7	64.5	7.1	18.4	74.5
WD1-07	2Bk	96.0	4.0	35.3	7.6	57.0	12.7	35.0	52.3
WD1-08	2B3	72.0	28.0	35.2	6.0	58.8	7.7	19.1	73.2
WD1-09	C	89.5	10.5	18.1	7.3	74.6	5.3	14.2	80.5
WD1-10	C	91.0	9.0	7.6	4.0	88.4	4.6	11.7	83.7
WD1-12	C	91.5	8.6	11.9	3.5	84.7	4.7	11.9	83.4
WD1-14*	C	97.3	2.7	6.5	3.9	89.7	6.4	20.0	73.6

* Sample WD1-14 collected approximately 1 m north of Profile 1 from 3.35 m.

The concentration of the clay-sized, silt and sand fractions for Profile 1 are plotted in Figure 6.10a. The silt fraction has the smallest variation throughout the profile, varying from 3.5 to 9.2%. There is no obvious trend with these data apart from a slight decrease within the saprolith. The content of the clay-sized fraction in the A1 horizon is relatively low at 10.4% compared with the increase to 61.1% in the underlying B1 horizon. There is then a gradual decrease in clay-sized content down the profile apart from a slight increase in the 2Bk and 2B3. In the pegmatite saprolith the clay-sized content drops from 18.0% at the top to 7.6% and then increases again to 11.9% at the base. The equivalent clay-sized content of the gneiss saprolite is 6.5%. The sand content through the profile is approximately the inverse of the clay-sized fraction.

The distribution of the three sand fractions through Profile 1 is plotted in Figure 6.10b. The fine sand (20 – 53 μm) is the most minor fraction and shows little variation through the profile. The content is lowest within the saprolith, especially the pegmatite (4.6 - 5.3%). In the pedolith the fine sand is between 7.1 and 12.7%. The variation of the fine sand fraction through the profile is similar to that observed for the silt-sized described above. The medium sand (53 – 125 μm) fraction has a moderate variation through the profile from 11.7 to 35.0%. The variations reflect their position within the profile. At the top of the profile within the A1, B1, B2, and Bk horizons, the medium sand content is relatively consistent with values between 25.8 and 29.0%. Below this the content drops to 18.4% in the 2B2 horizon, increases to 35.0% in the 2Bk horizon, and then decreases to 19.1% in the 2B3 horizon. Within the pegmatite saprolith the content is relatively stable between 11.7 and 14.2%. The value for the

gneiss was higher at 20.0%. The highest sand concentrations were in the coarse sand (125 – 2,000 μm) fraction, which varied from 52.3 to 83.7%. The distribution of the coarse sand fraction is almost the inverse of the medium sand fraction.

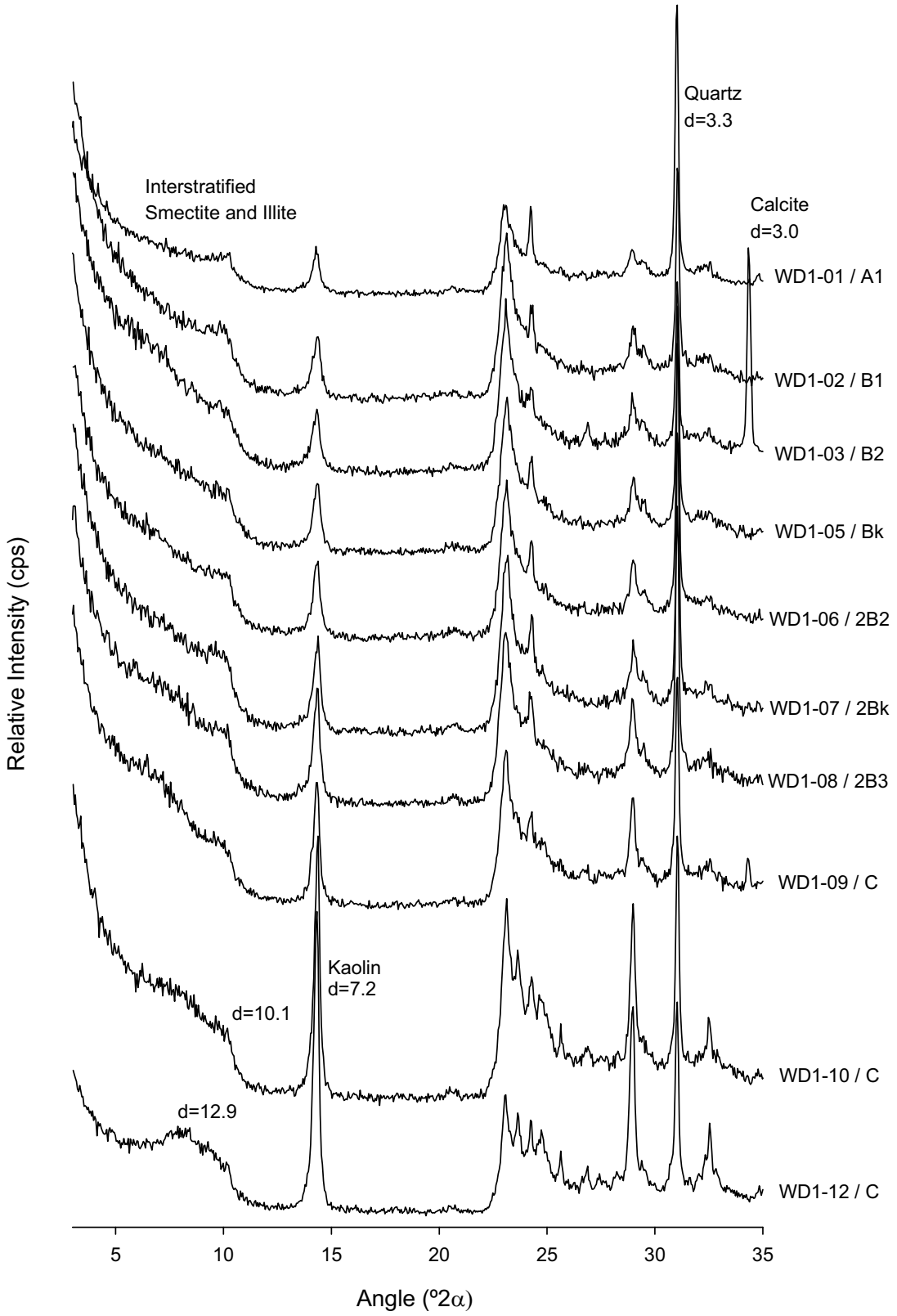

Figure 6.9: Stacked XRD plots from Profile 1 of clay-size fraction showing reduction in kaolin content and increased illite / smectite interstratification towards the surface.

Heavy mineral separation was undertaken on the fine and medium sand fractions. Variation in heavy mineral concentration within the fine sand fraction is minimal with the pedolith and saprolith zones, clearly delineated Figure 6.10c. Within the pedolith, heavy minerals account for 4.7 to 5.2% of the fine sand fraction. This drops to 2.3 to 2.8% in the saprolith. Variation in heavy mineral content within the medium sand fraction is also minimal, from 4.5 to 6.2% in the pedolith and 1.0 to 1.4% in the saprolith. The variation is greater in the medium sand fraction which has two distinctly low values of 4.6 and 4.8% within the highly calcareous Bk and 2Bk horizons respectively.

The heavy mineral fractions were inspected on the SEM and grains automatically counted as described in Section 3.5.7.1. A summary of the heavy mineral grain count analysis is provided in Table 6.4. Although details of various heavy minerals were recorded, the minerals of interest were rutile and zircon within the fine and medium sand fractions, since these are considered immobile (Fitzpatrick & Chittleborough, 2002). The immobility of these minerals means that they can provide an indication on the extent of *in-situ* weathering. This is discussed further in Section 6.6.

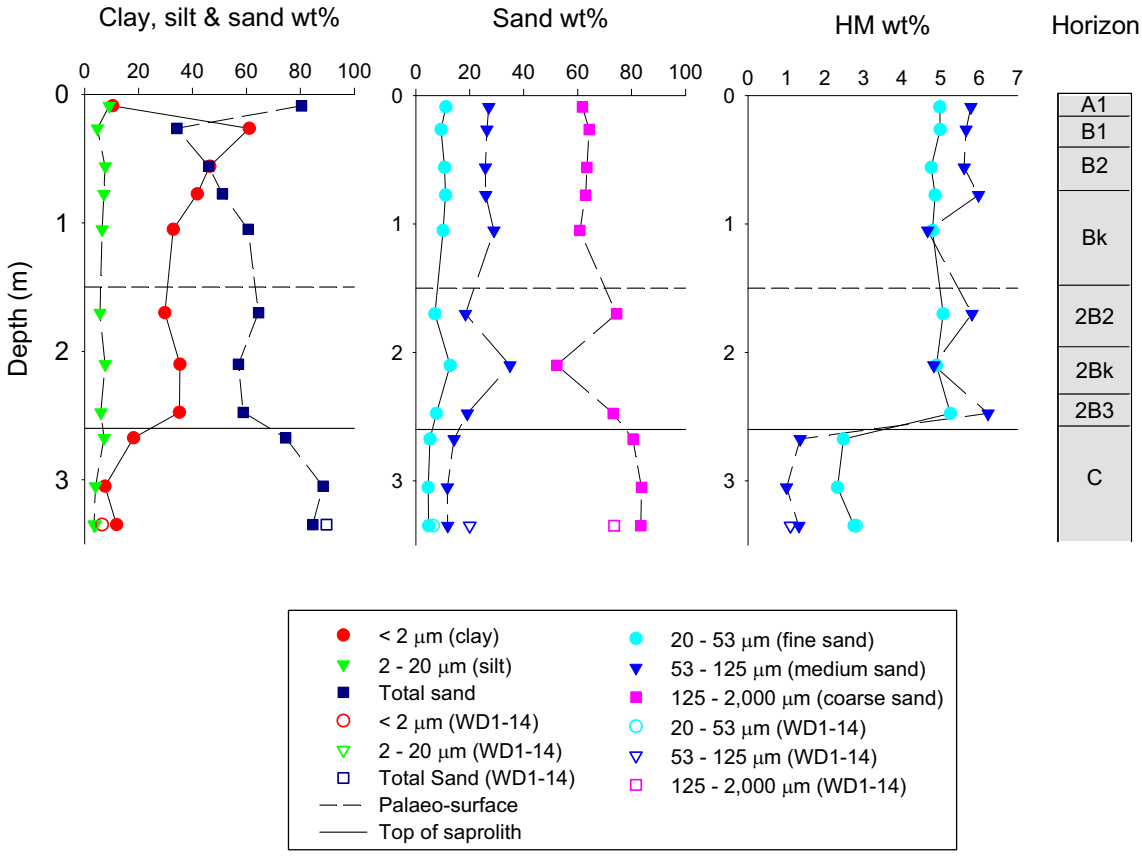

Figure 6.10: Particle size fraction and heavy mineral content of Profile 1.

In the fine sand fraction, rutile ranged from 7.4 to 20.3% in the pedolith, dropping to 2.5% in the saprolith. The rutile content of the gneiss was significantly higher at 22.7%. The zircon content ranged from 3.0 to 5.0% through the pedolith, dropping to < 0.1% in the saprolith apart from the gneiss where it was 11.4%. Iron oxides were the predominant heavy mineral with values from 43.9 to 65.2% in the pedolith, increasing to 89.6% in the saprolith. Iron oxides within the gneiss were 45.2%. Ilmenite was the other main mineral with values from

10.1 to 24.0% in the pedolith, dropping to 1.54% in the saprolith (3.1% in the gneiss). Undefinable and silicate minerals ranged from 0.8 to 6.3% and 1.4 to 10.6% respectively.

In the medium sand fraction, the percentage of rutile ranged from 3.8 to 7.1% apart from the gneiss sample which was 18.4%. Zircon content was very low with less than 1% throughout the profile. Iron-oxides were the predominant heavy minerals through Profile 1, which ranged from 37.9 to 64.7% (31.1% in the gneiss). Ilmenite also had relatively high concentrations through the pedolith, ranging from 7.9 to 11.1% dropping to 2.0% in the saprolith (5.2% in the gneiss). Biotite was typically < 5% (1.4 to 5.2%) through the profile apart from the gneiss, which was 23.7%. Unidentifiable grains and silicates represented about 17 and 20% respectively.

Table 6.4: Summary of heavy mineral grain count analysis for Profile 1.

Sample	Horizon	Al silicate (%)	Biotite (%)	Fe-oxide (%)	Ilmenite (%)	Monazite (%)	Rutile (%)	Zircon (%)	Other (%)	Total grains
Fine sand (20 - 53 μm)										
WD1-01	A1	10.63	4.72	42.52	24.02	0.79	8.27	4.72	4.33	508
WD1-02	B1	10.43	1.53	51.53	21.47	1.23	7.36	3.07	3.37	326
WD1-03	B2	6.59	1.65	43.96	16.76	1.10	20.33	3.30	6.32	364
WD1-04	Bk	6.95	1.03	44.87	21.98	0.68	15.49	5.01	3.99	878
WD1-05	Bk	4.13	0.81	50.16	21.84	0.97	13.59	4.37	4.13	1236
WD1-06	2B2	4.86	0.75	53.49	19.33	1.37	14.21	3.37	2.62	802
WD1-07	2Bk	3.59	0.95	50.63	21.04	0.63	15.22	4.97	2.96	946
WD1-08	2B3	1.43	0.44	65.24	16.94	2.20	9.02	3.19	1.54	909
WD1-09	C	2.58	0.54	59.96	10.12	8.29	15.72	1.29	1.51	929
WD1-10	C	1.86	0.34	84.43	2.20	4.48	6.35	0.00	0.34	1182
WD1-12	C	2.24	0.14	89.65	1.54	3.08	2.52	0.07	0.77	1430
WD1-14*	C	1.35	0.34	45.22	3.13	12.85	22.65	11.41	3.04	1183
Medium Sand (53 - 125 μm)										
WD1-01	A1	22.84	5.19	37.94	10.24	0.64	4.69	0.77	17.70	2198
WD1-02	B1	17.69	1.71	52.79	9.95	0.40	3.75	0.57	13.14	1758
WD1-03	B2	19.83	1.74	47.09	9.41	0.78	5.75	0.66	14.74	1669
WD1-04	Bk	18.79	1.39	44.81	10.06	0.86	7.07	0.75	16.27	1868
WD1-05	Bk	19.82	3.16	39.17	11.12	0.69	4.53	0.84	20.66	1897
WD1-06	2B2	22.73	4.42	40.59	8.16	0.74	4.99	0.57	17.80	1764
WD1-07	2Bk	19.64	3.43	41.45	10.80	1.19	5.38	0.51	17.61	2362
WD1-08	2B3	20.09	3.21	46.08	7.89	1.18	5.01	0.47	16.07	2116
WD1-09	C	15.71	2.66	51.90	9.50	3.00	6.89	0.54	9.80	2031
WD1-10	C	14.27	3.74	64.67	1.99	5.96	6.56	0.18	2.63	2165
WD1-12	C	N/A	N/A	N/A	N/A	N/A	N/A	N/A	N/A	N/A
WD1-14*	C	8.88	23.66	31.07	5.17	4.86	18.43	0.57	7.36	1915

* Sample WD1-14 collected approximately 1 m north of Profile 1 from 3.35 m.

Observations of the heavy mineral fractions on the FESEM support the above data with Fe-oxides the dominant component of most samples. Zircon grains were generally clean specimens with rounded edges above the palaeo-surface (Figure 6.11 A & B), and more angular with depth (Figure 6.11 C). Rutile and ilmenite was generally sub-angular, and then cleaner and more angular with depth (Figure 6.11 E, F, & G). Many of the ilmenite grains had dissolution features (Figure 6.11 D).

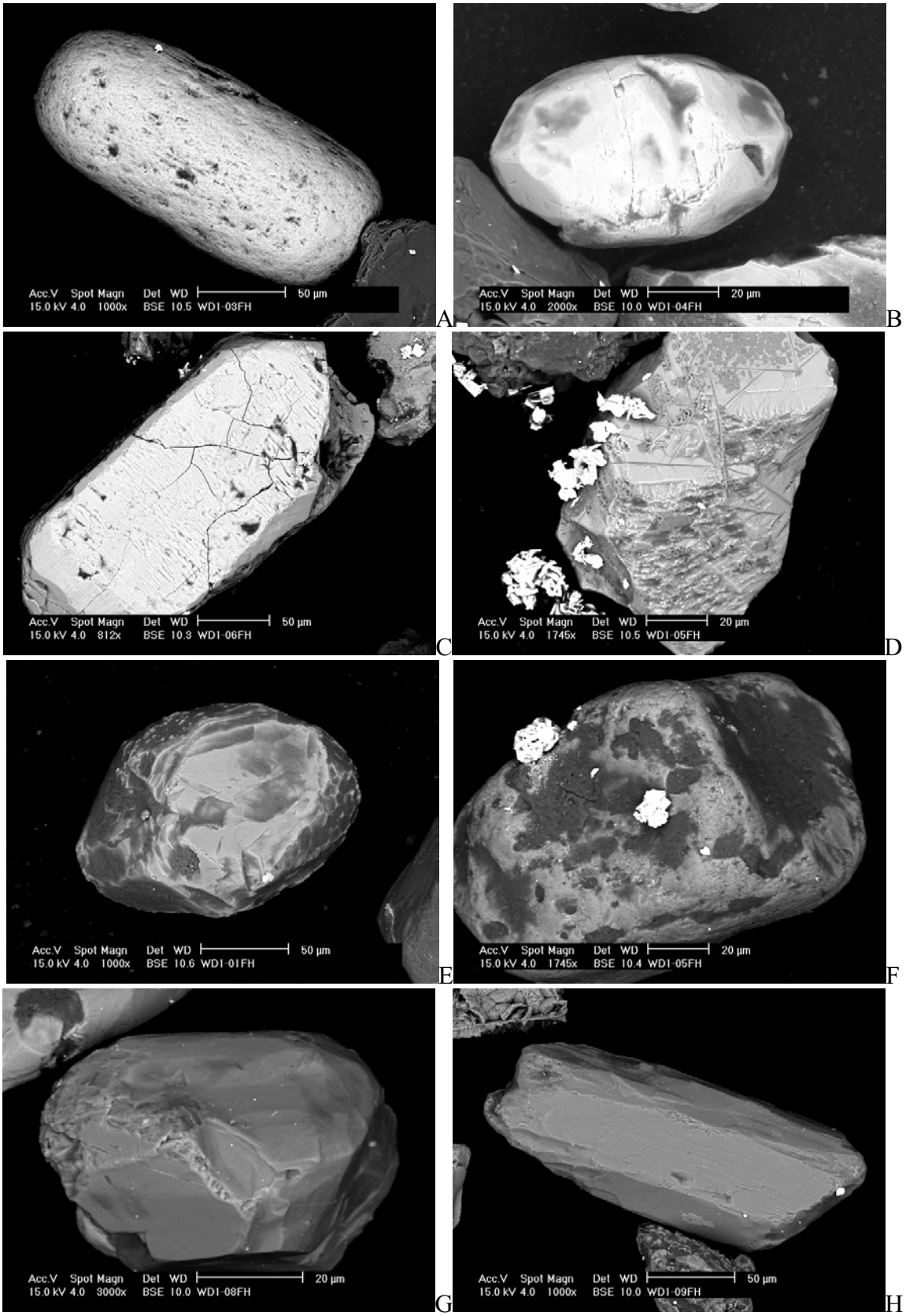

Figure 6.11: FESEM backscatter images: zircons from the B2 (A), Bk (B), and 2B2 (C) horizons; etched ilmenite grain with dissolution features (D); and rutiles from A1 (E), Bk (F), 2B3 (G) and top of the saprolith (H).

6.4.3. Profile 1: Bulk density, calcimetry, pH and EC

The pH, electrical conductivity (EC), calcium carbonate content, and bulk density results are provided in Table 6.5. Details of repeat runs for calcium carbonate content and bulk density are provided in Appendix 5.

The pH values show little variation and range between 8.4 and 8.9 for most of the profile, including the gneiss. The pegmatite at the base of the profile is the exception, which is slightly less alkaline with a pH value of 6.9.

Electrical conductivity is an indication of the soluble salt content. The highest salt content is from the B2 horizon down to the top of the saprolith.

The $CaCO_3$ content was highest at the top of the saprolith (11.4%) followed by the calcareous B2 and Bk horizons with 9.8 and 8.7% respectively. The lower calcareous horizon 2Bk recorded 5.9% $CaCO_3$.

There is a gradual increasing trend in bulk density down the profile apart from the relatively high surface value of 2.12. Below the A1 horizon, the bulk density gradually increased from 1.7 to 2.4 at the base of the profile.

Table 6.5: pH, EC, $CaCO_3$, and bulk density for Profile 1.

Sample No.	Horizon	Depth (m)	pH	EC (dS/cm)	CaCO3 (%)	Bulk density (g/cm^3)
WD1-01	A1	0.00 – 0.18	8.51	0.25	0.04	2.12
WD1-02	B1	0.18 – 0.35	8.75	0.99	0.11	1.71
WD1-03	B2	0.42 – 0.70	8.76	2.52	9.75	1.95
WD1-04	Bk	0.75 – 0.80	8.83	2.33	8.68	1.83
WD1-05	Bk	1.00 – 1.10	8.69	2.64	5.20	2.24
WD1-06	2B2	1.60 – 1.80	8.37	3.04	0.78	2.09
WD1-07	2Bk	2.00 – 2.20	8.59	2.82	5.93	2.38
WD1-08	2B3	2.35 – 2.60	8.39	1.85	4.46	2.16
WD1-09	C	2.60 – 2.75	8.46	3.44	11.35	2.40
WD1-10	C	2.95 – 3.15	8.89	1.33	1.88	2.34
WD1-12	C	3.30 – 3.40	6.87	1.18	0.00	2.37
WD1-14	C	3.30 – 3.40	8.54	0.72	0.00	2.47

6.4.4. Elemental assay results and trends for Profile 1

Results from the multi-element profile sample assays of the bulk, < 2 mm, and the five size fractions from Profile 1 are included in Appendix 6. A summary of the results, trends observed through the profile, and within the size fractions, are presented below. The elemental assay data are presented by classifying the elements into major, trace and REE. Further division is achieved by plotting the size fractions in groups of the bulk and fine earths, the three sand fractions, and the clay-sized and silt fractions. Comparison between the bulk and size fraction samples must be considered with respect to the different analytical methods and possible introduced variations resulting from the separation process. The element suites obtained for the bulk samples (ICP/MS, ICP/OES & FAA) and the size fractions, including the fine earths (INAA) are listed in sections 3.6.3 and 3.6.4 respectively.

Element assays close to or below analytical detection limit for > 20% of the samples (n = 3) from a particular size fraction are not discussed. These elements are listed in Table 6.6. Some of these elements (bracketed and in red text) were below detection in either the saprolith or pedolith and are discussed in relation to the part of the profile where they were above detection only.

The majority of below-detection elements are concentrated within the sand fractions (Table 6.6). The only element of those analysed that is below detection for the clay-sized and silt fraction is Zr, which is below detection (500 ppm) for all but the fine sand fraction. The high Zr detection limit by INNA is due to the small sample size.

Table 6.6: Elements that were at or below detection for > 20% of samples from Profile 1. Note: elements in red were only below detection for either the pedolith or saprolith.

Sample type	Elements below detection
Bulk	Ag, Cd, (Cr), In, (MnO), Sb, Sc, Se, Te, (Zr)
< 2 mm (fine earth)	(Au), (Co), Cs, (Sb), Zr
125 – 2000 μm (coarse sand)	(Au), Co, Cs, Br, Sb, As, Zn, Zr
53 – 125 μm (medium sand)	(Au), Co, Cs, Br, (Sb), As, Zn, Zr
20 – 53 μm (fine sand)	Cs, Br, (Sb), Zn
2 – 20 μm (silt)	Zr
< 2 μm (clay-size)	Zr

Major element assays for the bulk samples are plotted in Figure 6.12. A common trend for the major elements (Al_2O_3, K_2O, Fe_2O_3, MgO, and TiO_2) through the pedolith is a relatively low surface concentration with a significant increase into the B1 horizon, followed by a gradual decline through the remainder of the pedolith. Exceptions are a slight increase in K_2O concentration for the 2B2 horizon (sample WD1-06), and a significant increase in the Fe_2O_3, TiO_2, and MgO concentrations in the 2Bk horizon (sample WD1-07). Once into the saprolith there is a distinct change in concentration with Al_2O_3 and K_2O showing a significant increase, and Fe_2O_3, MgO, and TiO_2 a significant decrease.

The main component of the profile is SiO_2 with concentrations from 55 to 74%. The distribution of SiO_2 through the profile is a maximum of 74% at the surface, dropping to 58 and 55% in the B1 and B2 horizons. The SiO_2 concentration increases to 71% in the 2B2 horizon (WD1-06) followed by a fluctuating concentration from 59 to 66% through the remainder of the profile, including the saprolith.

The distribution of CaO varies from 0.7 to 6.5% through the profile. The highest concentrations are in the B2, Bk, 2Bk, 2B3 horizons and at the top of the saprolith, which corresponds with areas of high regolith carbonate content.

The concentration of MnO and P_2O_5 is < 1% for all samples, although there is still significant variation throughout the profile. There is a general decreasing trend in MnO concentration from 0.09 to < 0.01 (detection limit) through the profile, with the exception of samples WD1-03, WD1-06, and WD1-08, which are slightly elevated. The saprolith samples are all at or below analytical detection limit apart from the gneiss sample (WD1-14), which is 0.03%. The distribution of P_2O_5 is more variable. At the top of the profile the P_2O_5 concentration is 0.07%, increasing to 0.09% at the B2 – Bk boundary (WD1-04), before dropping to 0.05% in

the 2B2 horizon. This is followed by an increase in concentration to 0.10% at the base of the pedolith. Within the saprolith the P_2O_5 concentration drops again to 0.07%, before a significant increase to 0.10% at the base of the profile.

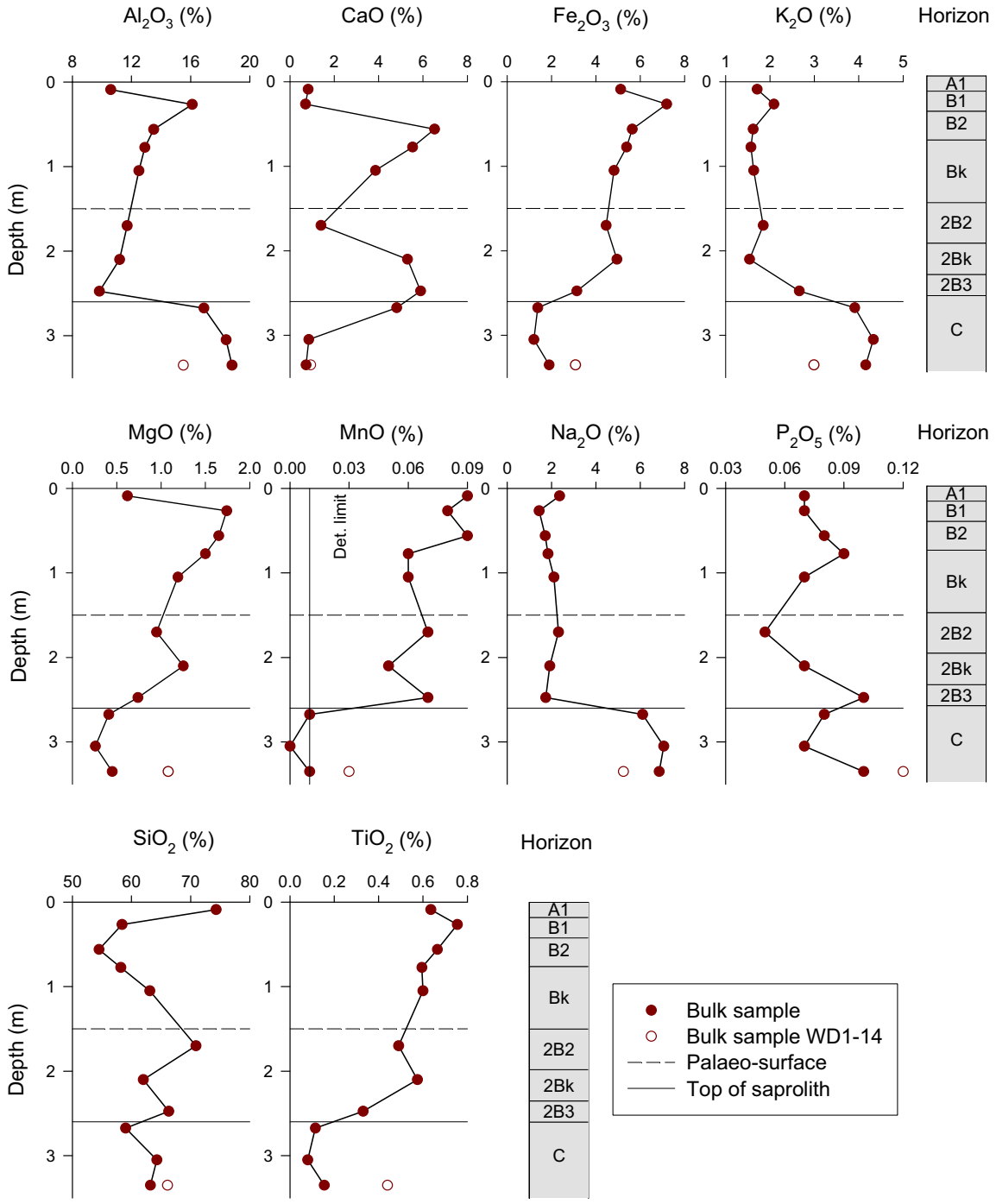

Figure 6.12: Major element depth plots of bulk soil assays for Profile 1.

Apart from a small decrease in concentration between the A1 and B1 horizons, the concentration of Na_2O is relatively uniform throughout the pedolith with a range of 1.44 to 2.36%. In the saprolith there is a significant rise in Na_2O concentration with values from 6.11 to 7.06%.

Major element concentrations in the gneiss sample (WD1-14) are distinctly different to those of the pegmatite apart from CaO and SiO_2. The concentration of Al_2O_3, K_2O, and Na_2O are significantly lower, whereas MnO, Fe_2O_3, MgO, and TiO_2 are higher. The element concentration within the gneiss tends to be nearer to the trend of the pedolith samples rather than the pegmatite samples directly underneath (WD1-09, WD1-10 & WD1-12).

The only major elements assayed for the size fractions (by INAA) were Fe and Na. Results of the total < 2 mm material are plotted in Figure 6.13. These were provided as elemental % rather than oxides, hence the comparisons presented below were made by converting the oxides to elemental weight percentages. There was minimal variation between the bulk and fine earth samples for both Fe and Na throughout the profile.

There is minor variation in Na concentration through the pedolith for all of the size fractions (Figure 6.13). The lowest concentrations (< 1%) were in the silt fraction and the highest (> 2.5%) were in the coarse sand fraction. The remaining fractions ranged from 1 to 1.6% apart from the clay-sized fraction of WD1-03 at 0.7%. In the saprolith there is an increase in Na for all the sand fractions of about 3%, whereas in the silt fraction there is an increase of about 1% and no change in the clay-sized fraction.

The highest Fe concentrations are in the clay-sized fraction, which also has the least variation with a range of 5.1 to 5.6%. This degree of variation extends through both the pedolith and saprolith. The silt fraction has a larger variation (2.8 to 4.9%); however, it is still relatively uniform through the entire profile. The Fe concentration in the sand fraction samples is relatively uniform and generally lower than the equivalent clay-sized and silt fractions, with a range of 1.8 to 3.3% through the pedolith. There is a significant decrease in Fe concentration for the sand fraction saprolith samples (WD1-09, WD1-10) of 0.4 to 1.7%. The gneiss samples of the fine and medium sand fractions have Fe concentrations that are similar to those in the pedolith of 2.3 and 2.8%.

Trace element assays for the bulk samples and size fractions are plotted in Figure 6.14 and Figure 6.16. The bulk sample plots include the assay results from the bulk and fine earth samples. The bulk and fine earth samples, including size fractions, were assayed separately by two different analytical methods (see Section 3.6). This means that some elemental assays are only available for the bulk or fine earth sample, which accounts for missing data from some plots.

There is a general pattern between the dispersion of the elements through the profile and within the size fractions that describes the majority of assayed elements. The size fraction plots are similar with only minor variations to the dispersion patterns of the elements through the profile. The main difference between the size fractions is in the concentration levels. The highest element concentration is typically in the silt and clay-sized fractions, with the lowest concentrations in the sand fractions, particularly the medium and coarse sand fractions (Figure 6.16). The bulk and fine earth assays generally lie between the two extremes (Figure 6.14).

The typical dispersion pattern, as shown in the bulk and fine earth samples through the profile is: a relatively low surface concentration in the A1 horizon (WD1–01); a moderate to high concentration in the B1 (WD1–02) clay-rich horizon, sometimes including the B2 horizon (WD1–03); a intermediate, relatively uniform or gradually decreasing concentration through the remainder of the pedolith (WD1–04 to WD1–08); and, a significant change in concentration, either lower or higher, in the saprolith (WD1–9, WD1–10, WD1–12, & WD1–

14) (Figure 6.14). The size fraction dispersion patterns are not as varied as the bulk samples. Only a few elements show a peak for the B1 horizon in the fraction plots, with most having a relatively uniform concentration through the profile. There is a change in concentration in the saprolith samples (Figure 6.16). This is not surprising given that the data have not been normalised by size fraction content, hence the higher clay content in the B1 horizon (Figure 6.10) would produce a peak in this size fraction, representative of that observed in the bulk sample.

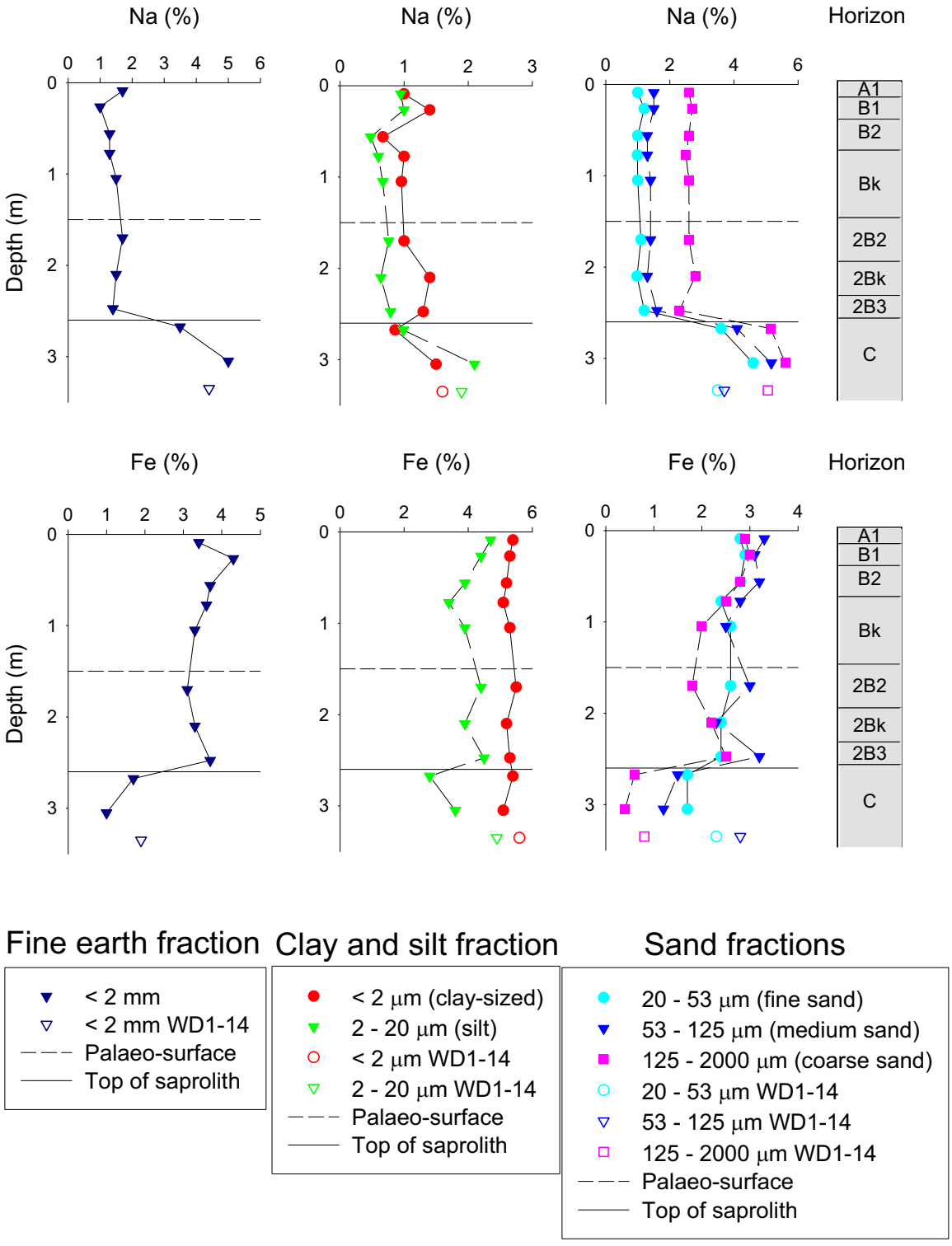

Figure 6.13: Major element depth plots of size fraction assays of Na and Fe for Profile 1.

Very few elements change significantly in concentration across the interpreted palaeo-surface boundary, in either the size or bulk sample assays. Elements that show a minor change are Cr, Mo, Rb, Sc, Sr, U, V, and Y, in the bulk samples.

Trace elements that show a large change in concentration between size fractions, or dispersion patterns through the profile, are described below. These include Au, Cu, and Mo, which are related to mineralisation at White Dam.

The presence of Au in all of the bulk samples is not evident in the fine earth samples with many concentrations being below detection, despite the lower detection limit of 5 ppb (INAA) compared with 10 ppb (fire assay/AAS) (Figure 6.15). Variation between the equivalent bulk and fine earth samples was also significant where Au was detected in both samples, including a maximum difference of 680 ppb in sample WD1-09. All of the size fractions from the saprolith had significant Au concentrations that ranged from 200 to 1,880 ppb. The highest Au concentration of 3,220 ppb however, was for the bulk sample (WD1-12). The size fractions for WD1-12 were not analysed by INAA and cannot be considered in this discussion. The Au concentrations of the gneiss sample (WD1-14) were generally lower than that of the pegmatite size fractions.

The highest Au concentrations were in the silt fraction with significant Au also in the fine sand and clay-sized fractions. In the silt fraction the concentration of Au increases from 130 ppb in the A1 horizon to 290 and 350 ppb in the B1 and B2 horizons before decreasing to 71 and 56 ppb in the Bk horizon. Below the palaeo-surface, the Au concentration in the silt fraction increases from 150 to 972 ppb. The concentration of Au in the sand fractions is mostly below 23 ppb through the pedolith. The exceptions are the B2 horizon of the fine sand fraction with a concentration of 220 ppb, and for all sand fractions at the base of the pedolith (WD1-08) with concentrations from 130 to 170 ppb. In the saprolith sand fractions, the Au content increases from 260 to 1130 ppb.

These concentrations are higher than in the equivalent clay-sized fractions of 200 to 300 ppb Au, but lower than the silt fractions of 1600 to 1880 ppb Au. The concentration of Au in the clay-sized fraction through the pedolith is uniform, particularly above the palaeo-surface, with a range of 52 to 65 ppb. Below the palaeo-surface the Au concentration decreases to 43 ppb before increasing to a maximum pedolith concentration of 140 ppb at the base of the pedolith (WD1-08). The concentration of Au within the size fractions of the gneiss (WD1-14) is slightly lower, but comparable with the equivalent pegmatite assays.

Assays of Cu and Mo, the other mineralisation-related elements, were only carried out on the bulk samples. The Cu concentration is relatively uniform through the pedolith, gradually decreasing from a high surface value of 76 ppm (WD1-01) to 34.5 ppm in the 2Bk horizon (WD1-07). Below this the concentration increases to 74 ppm at the base of the pedolith (WD1-08), continuing through the saprolith to a high 320 ppm at the base (WD1-12). The equivalent gneiss sample (WD1-14) is significantly higher (550 ppm). The Mo concentration ranges from 0.9 to 2.9 ppm through the profile, where it has a step-like concentration pattern related to the various horizons. There are four apparent groups through the profile, in which Mo concentration varies by < 0.2 ppm in the pedolith and < 0.5 ppm in the saprolith. In the A1, B1 and B2 horizons the concentration of Mo ranges from 0.9 to 1.0 ppm, then increases to 2.2 and 2.3 ppm in the Bk horizon. Below the palaeo-surface the Mo concentration increases to a range of 2.7 to 2.9 ppm, and falls to a range of 1.4 to 1.9 ppm (2.3 ppm for the gneiss sample WD1-14) in the saprolith.

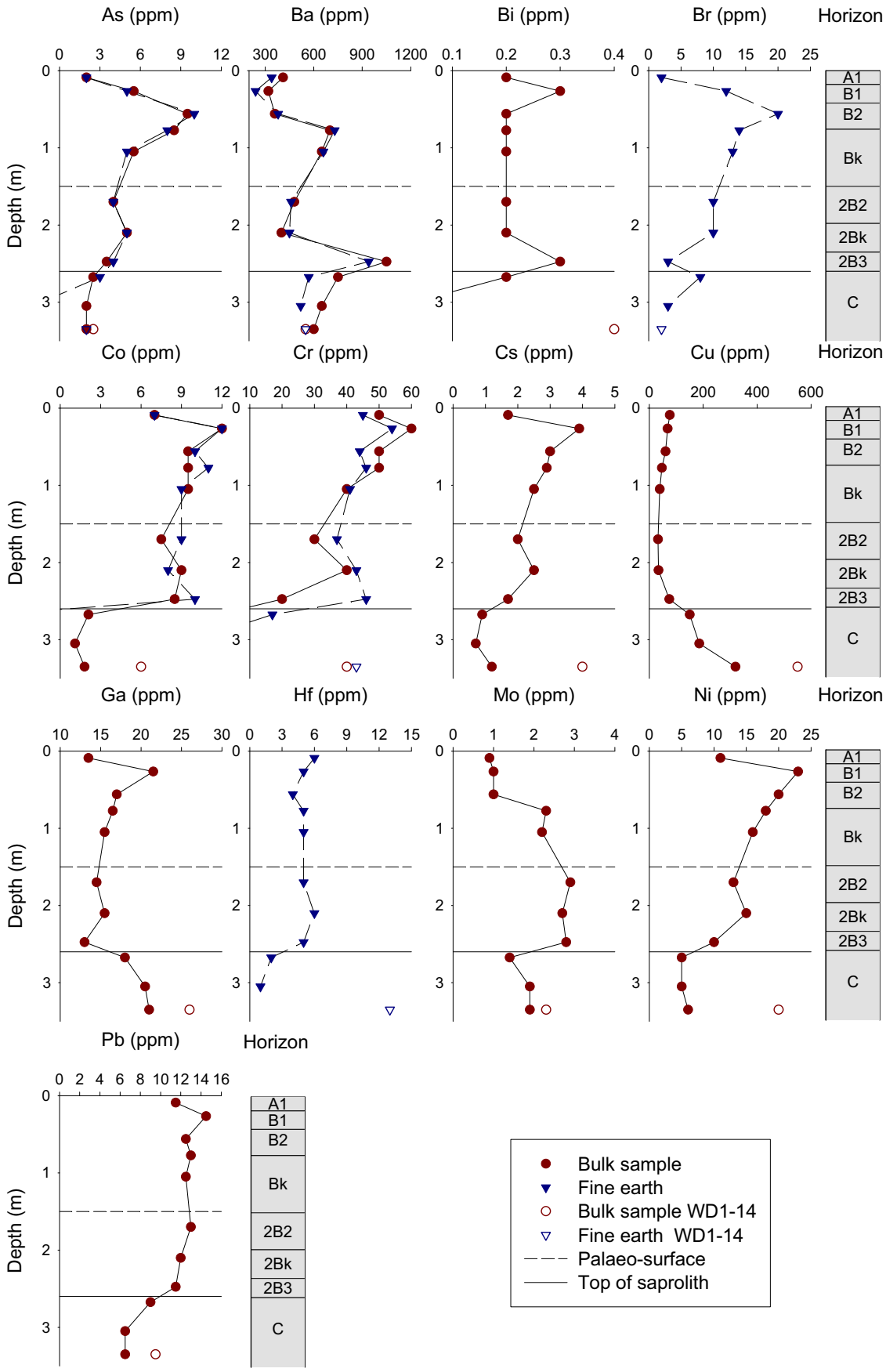

Figure 6.14: Trace element depth plots of the bulk and fine earth soil assays for Profile 1. Some samples were below detection limits for As (2 ppm), Bi (0.1 ppm), Cr (10 ppm), Sb (0.2 ppm), and V (20 ppm).

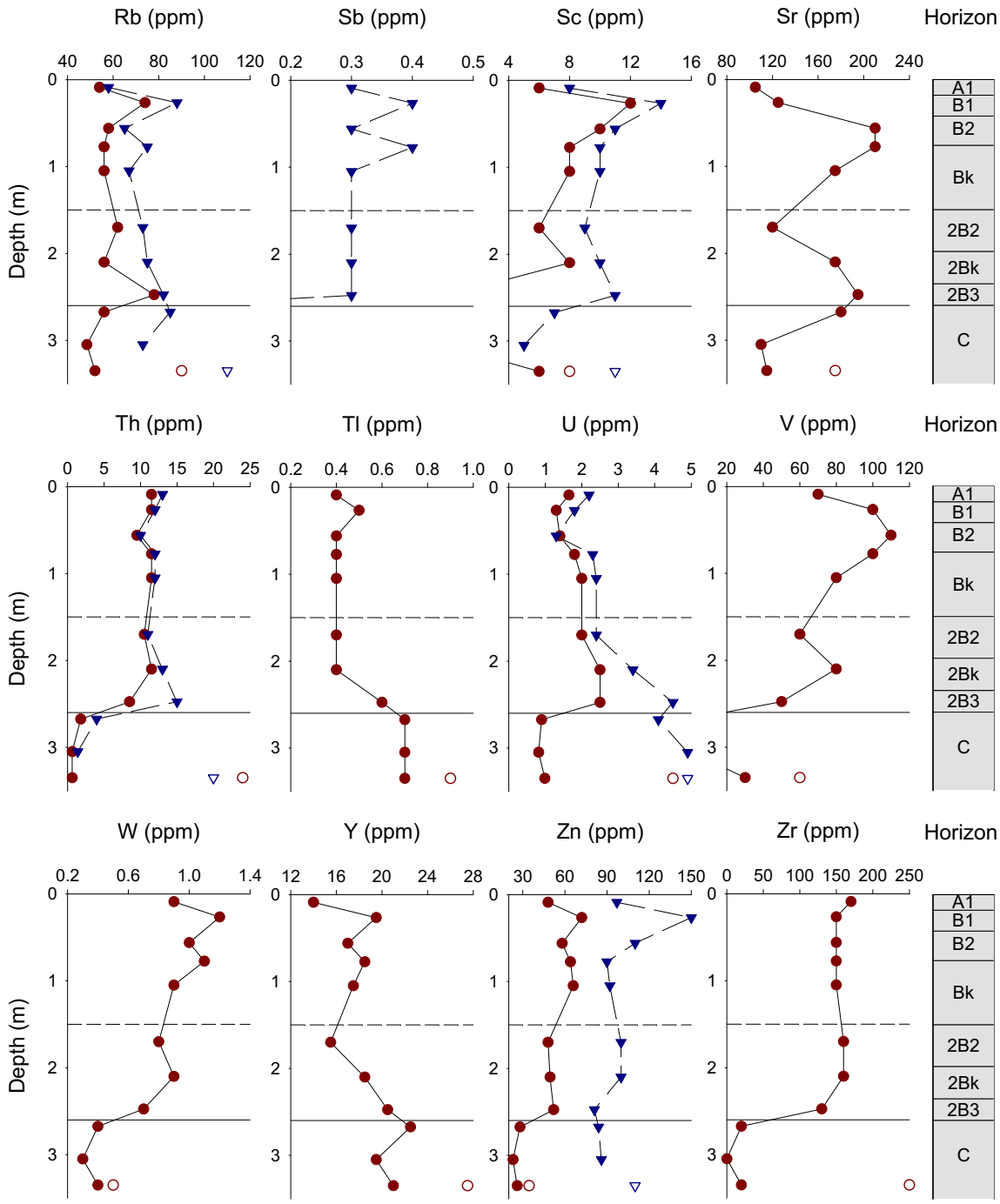

Figure 6.14: Trace element depth plots of the bulk and fine earth soil assays for Profile 1. Some samples were below detection limits for As (2 ppm), Bi (0.1 ppm), Cr (10 ppm), Sb (0.2 ppm), and V (20 ppm) (continued).

Whereas the majority of elements in the bulk and fine earth samples have their highest concentration in the B1 horizon (WD1-02), As, Br, Sr, and V, have highest concentrations in the underlying B2 horizon (WD1-03). Below the B2 horizon As, Br, and V, gradually decrease in concentration through the remainder of the pedolith and into the saprolith, although As and V have a minor increase below the palaeo-surface in the 2Bk horizon (WD1-07). The concentration of Sr closely follows that of CaO with another concentration peak in the 2Bk and 2B3 horizons (WD1-07 & WD1-08).

The analysis of Zr concentrations were only carried out on the bulk samples. Apart from the high surface Zr concentration of 170 ppm, there is only minor variation with values between 150 and 160 ppm through the remainder of the pedolith. At the base of the pedolith the Zr concentration decreases to 130 ppm in the 2B3 horizon, decreasing abruptly through the saprolith to the detection limit of 20 ppm. The exception is the gneiss sample (WD1-14) with a concentration of 250 ppm.

The moderately high surface concentration followed by relatively uniform values through the pedolith reported for Zr, is similar to the dispersion patterns of Hf and Th. Assays for Th were available for both the bulk and fine earth samples, but Hf was not available for the bulk samples. The total < 2 mm Hf concentrations ranged from 4 to 6 ppm throughout the pedolith, dropping to 1 ppm at the base of the saprolith. These concentration levels and the dispersion pattern is similar for all size fractions apart from the fine sand fraction, which had significantly high concentrations through the pedolith ranging from 24 to 31 ppm. The gneiss sample (WD1-14) had relatively high Hf concentrations for the clay-sized, silt, and fine sand fractions, and total fine earth material of 22, 37, 36, and 13 ppm respectively. The medium and coarse sand fractions had significantly lower concentrations of 8 and 6 ppm respectively.

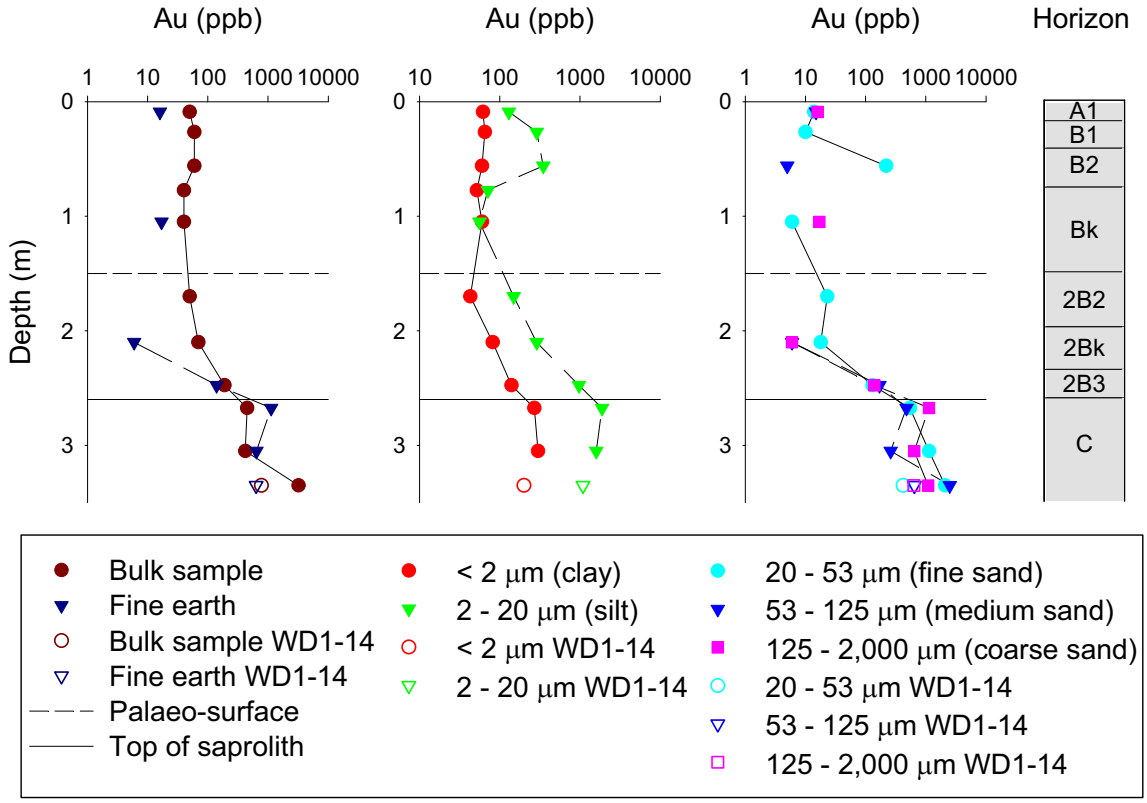

Figure 6.15: Bulk and size fraction depth plots of Au vs depth for Profile 1.

The Th concentrations ranged from 9.5 to 11.5 ppm (bulk sample) and 10 to 15 ppm (fine earth sample) through the pedolith, before dropping to 0.65 and 1.4 ppm in the bulk (WD1-10 & WD1-12) and fine earth (WD1-10) samples at the base of the saprolith. Within the individual size fractions, variations are also minor through the pedolith. The concentration varies from a low 6.4 to 10 ppm in the coarse sand fraction, to a maximum 24 to 31 ppm in the fine sand fraction. The clay-sized and silt fractions have Th concentrations of 10 to 15 ppm and 13 to 23 ppm respectively. In the saprolith the Th concentrations are significantly

lower with an overall range from 1.3 to 13 ppm. The gneiss sample (WD1-14) has significantly higher Th concentrations from 20 to 77 ppm.

The Zn assays of the fine earth samples are significantly higher than for their corresponding bulk samples, with differences between equivalent samples in the fractions ranging from 26 to 78 ppm through the profile with most samples ~50 ppm higher in the fine earth fraction. The exceptions are in the B1, B2 to Bk, 2B3 and gneiss samples. The largest difference is in the B1 horizon and coincides with the highest Zn concentration for both the bulk (72 ppm) and fine earth (150 ppm) assays. The least differences occur in the samples directly above the palaeo-surface (WD1-04 & WD1-05) and saprolith (WD1-08). The trend of Zn concentration for both the bulk and fine earth samples is a moderate surface concentration, a significant increase in the B1 horizon, then a general decreasing trend through the remainder of the profile (Figure 6.14).

In the silt and clay-sized fractions the Zn concentrations do not follow the same trends as the bulk and fine earth samples. In the clay-sized fraction the Zn concentrations range from 110 to 150 ppm. There is a gradual decreasing trend down through the pedolith to a low of 110 ppm at the base with a minor deviation from the trend to a low 120 ppm in the B2 (WD1-03) and B2/Bk boundary (WD1-04) samples. The Zn concentration in the silt fraction is generally lower than the fine earth fraction, but higher than the bulk assays with values from 73 to 130 ppm. Concentration variation through the profile is similar to the clay-sized fraction apart from a small peak directly above the saprolith (WD1-08) of 93 ppm.

The concentration of Ba varies significantly through the profile and has no distinctive trend. Assays were available for both the bulk and fine earth samples and results were similar. The Ba concentrations at the surface were a relatively low 410 ppm (bulk) and 340 ppm (fine earth) which drops to 320 ppm (bulk) and 240 ppm (fine earth) in the B1 horizon, followed by an increase to 700 ppm (bulk) and 730 ppm (fine earth) at the B2-Bk boundary (WD1-04). Below this the Ba concentrations gradually decrease to 400 ppm (bulk) and 450 ppm (fine earth) in the 2Bk horizon (WD1-07), before climbing again to 1050 ppm (bulk) and 940 ppm (fine earth) at the base of the pedolith (WD1-08). In the saprolith the concentrations decrease to a low of 600 ppm (bulk) and 520 ppm (fine earth) at the base of the profile, which is similar to the gneiss sample concentration of 550 ppm for both the bulk and fine earth gneiss samples. This dispersion pattern is similar to that of the size fractions. The largest variation occurs in the silt fraction with a range of 470 (WD1-01) to 3100 ppm (WD1-08). The dispersion pattern is reasonably uniform between the sand fractions despite the large variation between the fractions, up to ~400 ppm.

The difference in Rb concentration between the bulk and fine earth assays ranges from 4 to 29 ppb. The < 2 mm samples have higher Rb concentrations through the profile with a large peak of 88 ppm in the B1 horizon (WD1-02) and a smaller peak of 75 ppm at the B2/Bk boundary (WD1-04). Rubidium concentrations in the < 2 mm samples below the B2/2Bk boundary, after a slight decrease to 67 ppb, gradually increase to a maximum 85 ppm at the top of the saprolith (WD1-09). In the bulk samples the Rb concentration is more uniform with the majority of assays between 54 and 58 ppm. Two small peaks of 74 and 78 ppm are in the B1 and 2B3 horizons respectively with only the B1 peak corresponding directly to the equivalent bulk assay. The gneiss samples (WD1-14) have high Rb concentrations of 90 and 110 ppm for the bulk and fine earth assays respectively. Dispersion and concentration of Rb through the profile is more uniform between and within the individual fractions. Clay-sized and silt fractions have the highest Rb content ranging from 92 to 140 ppm (200 ppm in the gneiss silt fraction) through the profile compared with a range of 37 to 86 ppm in the pedolith

and 84 to 130 ppm in the saprolith sand fractions. Gneiss sample assays for Rb are higher for all fractions apart from the coarse sand, with a range of 49 to 200 ppm.

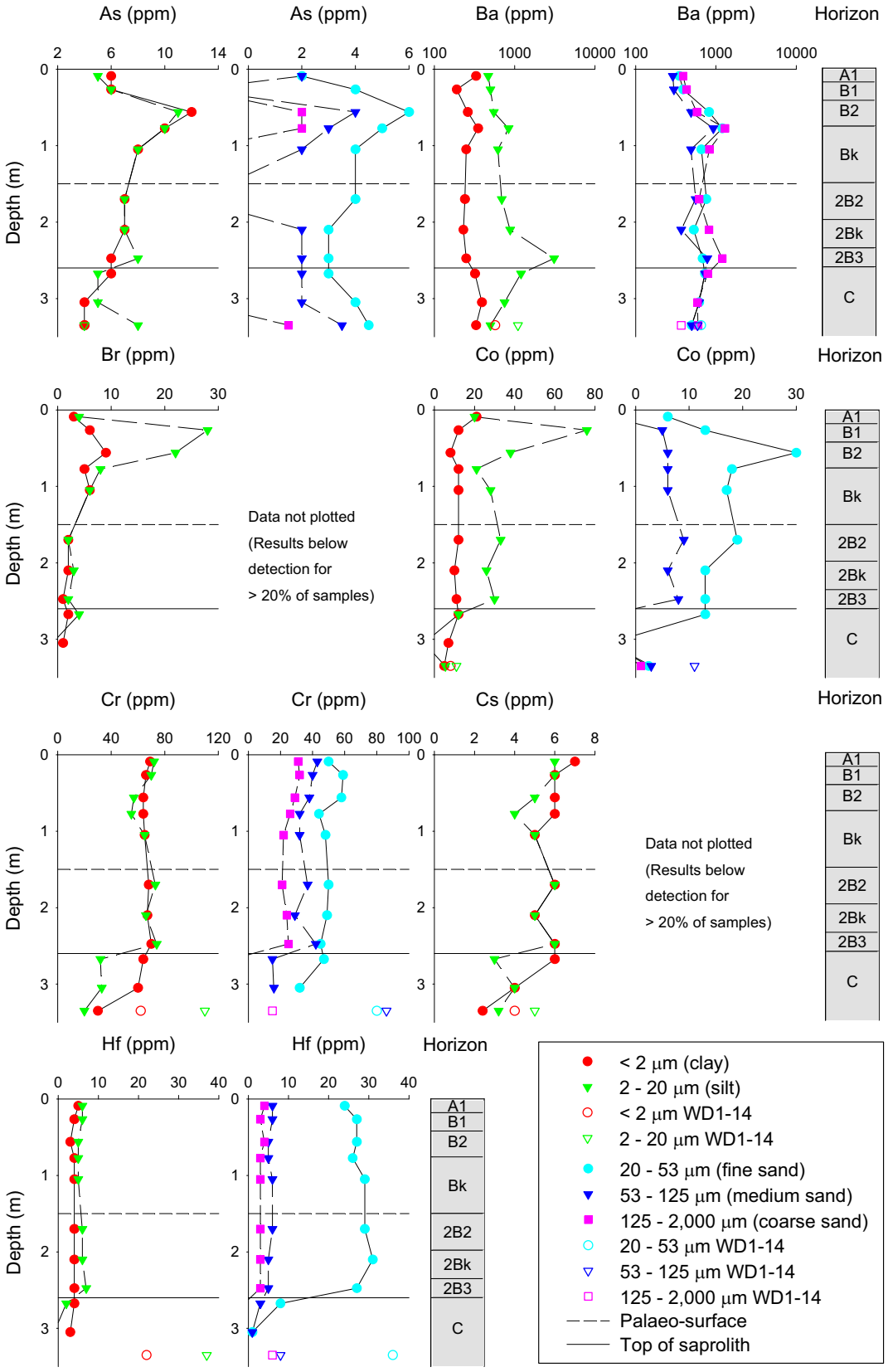

Figure 6.16: Trace element depth plots of size fraction assays for Profile 1. Some samples were below detection limits for As (2 ppm), Br (1 ppm), Co (5 ppm), Cr (10 ppm), Hf (1 ppm), and Sb (0.2 ppm).

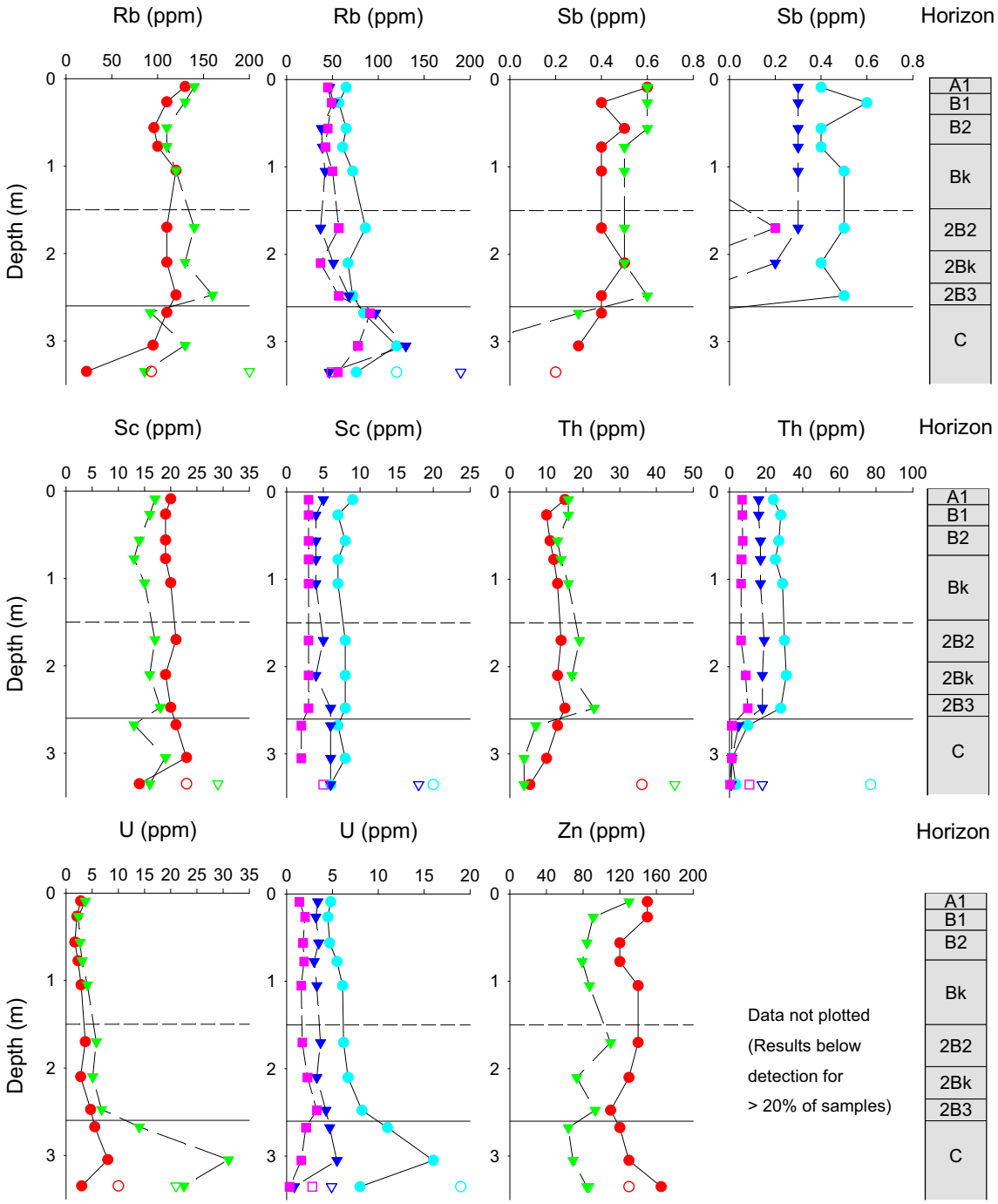

Figure 6.16: Trace element depth plots of size fraction assays for Profile 1 Some samples were below detection limits for As (2 ppm), Br (1 ppm), Co (5 ppm), Cr (10 ppm), Hf (1 ppm), and Sb (0.2 ppm) (continued).

Concentration of U in the bulk and fine earth samples is similar through most of the pedolith. At the base of the pedolith and into the saprolith however, there is a gradual increase in U in the fine earth samples compared with a decrease in the bulk samples. Above the palaeo-surface the U concentration ranges from 1.3 to 2.4 ppm with the lowest concentrations in the B1 (WD1-01) and B2 (WD1-02) horizons. Below the palaeo-surface the U concentration in the bulk sample is relatively uniform, but in the fine earth samples it increases to 4.5 ppm directly above the saprolith. This increasing trend continues into the saprolith, reaching 4.9 ppm for both the pegmatite (WD1-10) and gneiss (WD1-14) samples. The U

concentration decreases in the pegmatite (WD1-10) to 0.8 ppm for the bulk sample; however, the gneiss is at 4.5 ppm. Within the size fractions the U concentrations are relatively uniform with only minor variations through the pedolith. The highest U concentrations are in the fine sand fraction with values ranging from 4.5 (WD1-02) to 8.2 (WD1-08) in the pedolith, increasing to 19 ppm in the gneiss sample (WD1-14).

The bulk, fine earth, and size fraction assay results for the REEs are plotted in Figure 6.17 and Figure 6.18. Only La, Ce, Nd, (LREEs) Sm, Eu, Tb, (MREEs) Yb, and Lu (HREEs) were included in the size fractions assays.

In the bulk and fine earth samples the LREEs are relatively uniform through the pedolith apart from a slight increase at the base prior to a moderate decrease through the saprolith. The concentration in the gneiss sample (WD1-14) is higher than the equivalent pegmatite sample by approximately three times. This dispersion pattern is repeated in the size fractions, but there is significant variation in concentrations between the fractions. The highest concentrations are in the fine sand fraction. The silt and medium sand fractions have similar concentrations to each other, which is lower than the fine sand fraction but only slightly higher than the clay-sized fraction.

The trend of the MREEs is relatively uniform above the palaeo-surface with a slight peak in the B1 horizon (WD1-02). Below the palaeo-surface the concentration increases slightly. In the saprolith the bulk sample assays tend to decrease, or remain constant in concentration, whereas the fine earth samples significantly increase. In the size fractions, variations in concentration are similar to those observed for the LREEs, but the variations are not as large. Hence the highest concentrations are in the fine sand fraction but not as significantly as in the LREEs.

In the bulk samples the HREEs generally have a lower surface concentration followed by a relatively uniform concentration down to the palaeo-surface, however, Er and Tm also have a moderately high B1 concentration. Below the palaeo-surface there is a slight increasing trend followed by a slightly decreasing or constant concentration through the saprolith. In the fine earth there is less variation above the palaeo-surface and a more noticeable increase below it, followed by a significant increase in the saprolith. The size fractions are very uniform through the profile with a very minor increase below the palaeo-surface and a significant increasing trend through the saprolith. Although there is a slight difference in concentrations between the size fractions, it is significantly less than in the MREEs or LREEs. The concentration of the HREEs in the gneiss samples is significantly higher than in the pedolith samples, but not has high as the in the pegmatite samples.

Plots of the REEs normalised to chondrite and post Archaean Australian shales (PAAS) are shown in Figure 6.19 (Taylor & McLennan, 1985; McLennan, 1989). These plots highlight the difference between the saprolite and pedolith samples. The gneiss sample (WD1-14) is enriched in the LREEs and MREEs, whereas the pegmatite samples are generally depleted (WD1-09 to WD1-12) in the LREEs, compared with the pedolith samples. There is minimal variation between the saprolite and pedolith samples in the HREEs.

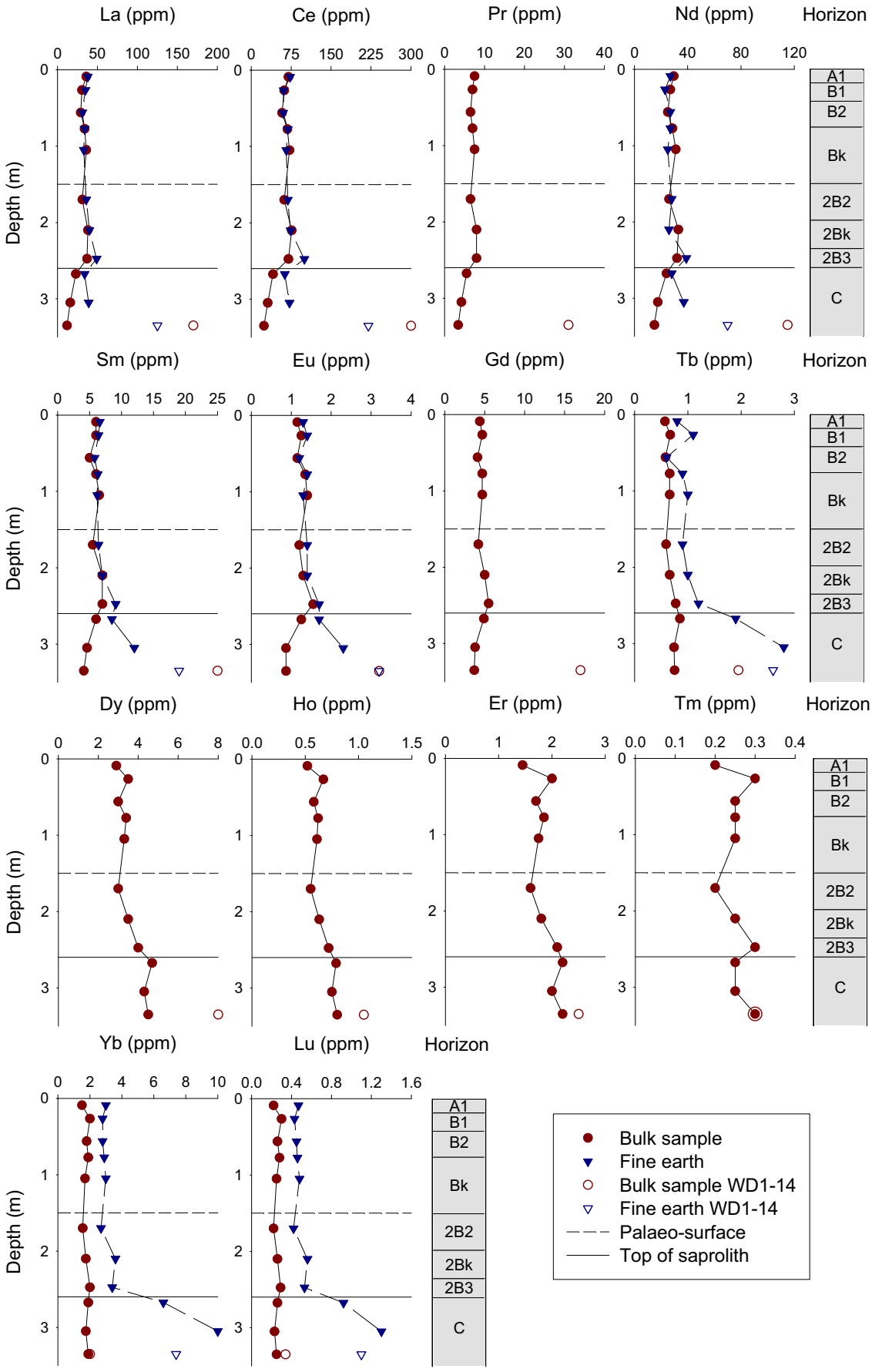

Figure 6.17: REE depth plots of the bulk and fine earth soil assays for Profile 1.

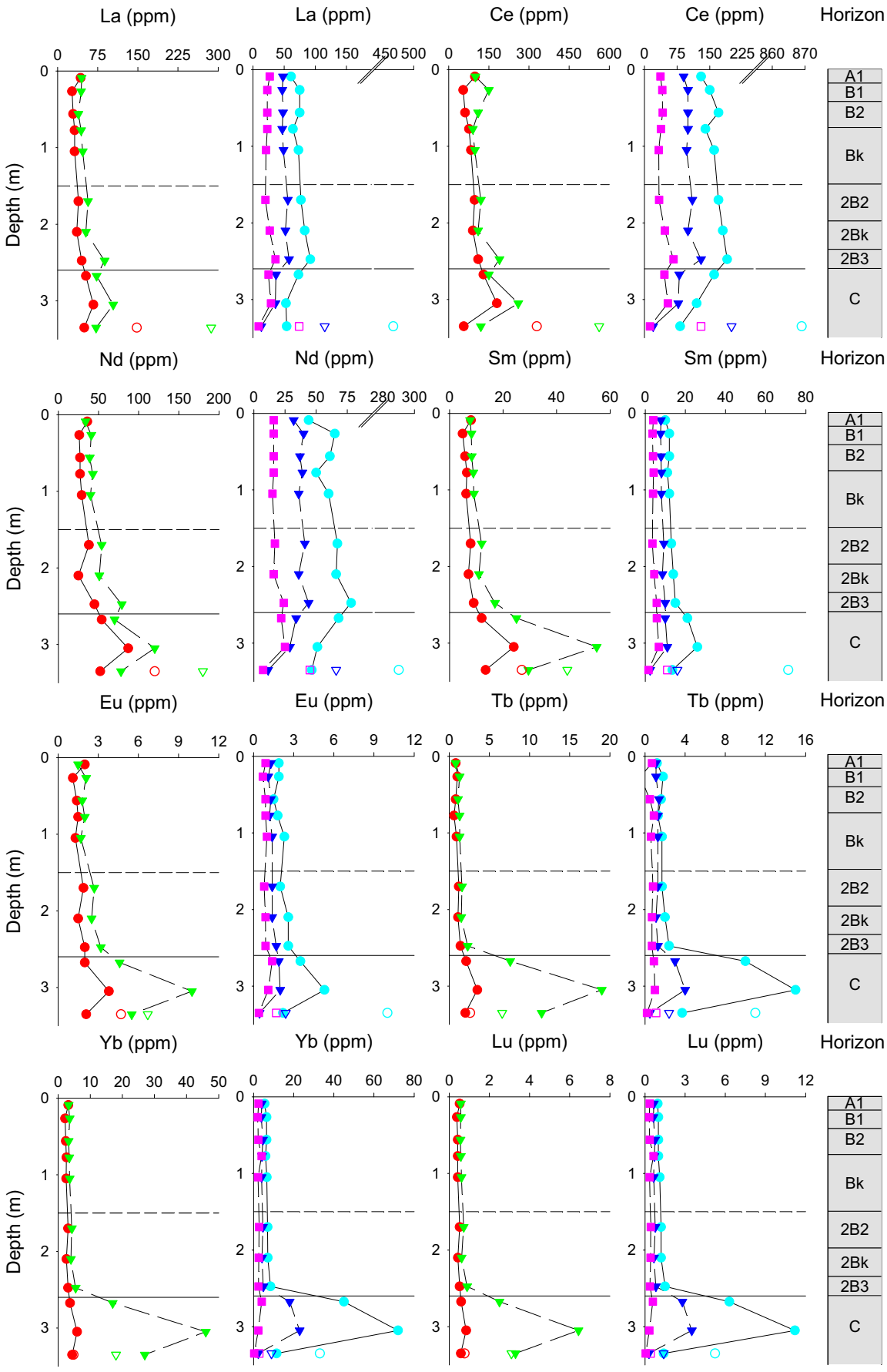

Figure 6.18: REE depth plots of size fraction assays for Profile 1.

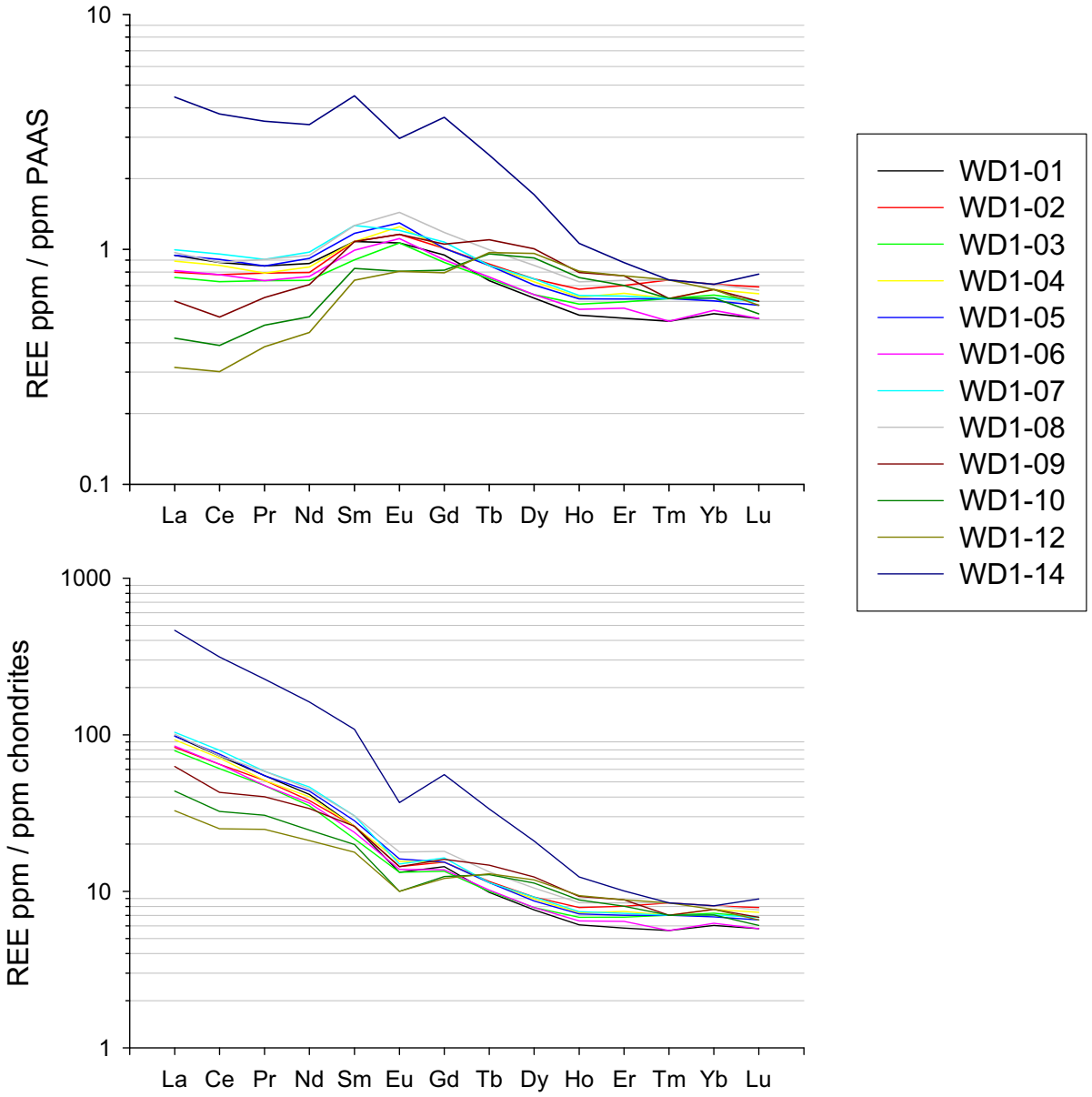

Figure 6.19: Chondrite and PAAS normalised REEs for Profile 1 (Taylor & McLennan, 1985; McLennan, 1989).

6.5. White Dam Profile 2, description, petrology and analytical results

Profile 2 is from costean WDTR03 (Figure 6.3) at GDA94, UTM Zone 54 south, 0460060 East, 6449009 North. This profile is just off the main zone of mineralisation.

6.5.1. Profile 2 description and petrology

The profile, shown in Figure 6.4, is on an erosional rise (Figure 6.3) and is approximately 3 m deep. It consists of a thin coarse-textured A1 horizon underlain by a sandy clay B1 horizon. Increasing carbonate content with depth marks a gradual change to a B2 horizon followed by a highly calcareous Bk horizon. Increasing coarse grains and lithic fragments with depth characterise the Bk horizon, which gradually merges into the saprolith over a depth interval of

approximately 0.5 m. The saprolith consists of highly weathered biotite gneiss. A summary description of each soil horizon is provided in Table 6.7.

The mineralogy of the coarse fragments through the profile is predominantly quartz with minor feldspars and micas (biotite and muscovite). The majority of grains through the profile are generally poorly sorted and sub-angular to sub-rounded. There is a gradual increase in regolith carbonates down the profile. These are in powdery form and are in the B2 horizon and extend through the Bk horizon and into the top of the saprolith.

Table 6.7: Horizon properties of White Dam Profile 2.

Horizon	Depth	Colour	Contact	Macro-features	Coarse fragment mineralogy	Pedo-features
A1	0 – 0.11 m	5YR ¾ (M) 5YR 5/6 (D)	Sharp		Poorly sorted / sub-angular to sub-rounded some coarse fragments to ~ 7 mm diameter ~ 80% Quartz ~ 5% Plagioclase ~ 2% K-feldspar 5 – 8 % Opaque minerals < 1% Other minerals (garnet, clinopyroxene, hornblende, sparse muscovite and biotite) ~ 10% Fine fraction	**Relative-distribution:** Chito-gefuric **Ped Structure:** Apedal **Voids:** Inter-aggregate, complex packing **Coatings:** Clay cutans present on most coarse grain and also on some larger opaque grains **Groundmass:** None
B1	0.11 – 0.30 m	5YR 4/4 (M) 5YR 5/6 (D)	Gradual	Slightly calcareous, increasing with depth	Moderately sorted / sub-angular to sub-rounded / average ~ 0.5 mm ~ 70% Quartz ~ 5% Plagioclase < 2% K-feldspar ~ 2% Opaque minerals < 1% Other minerals (hornblende, muscovite & biotite) ~ 20% Fine fraction	**Relative-distribution:** Mainly chitonic **Ped Structure:** Angular blocky **Voids:** Inter-aggregate channels with areas of complex packing **Coatings:** Clay cutans on majority of coarse grains **Groundmass:** Occasional areas of crystallitic b fabric (calcite aggregates)
B2	0.30 – 0.50 m	5YR 4/6 (M) 5YR 5/6 (D)	Diffuse	Highly calcareous, powdery regolith carbonates	Poorly sorted / sub-angular to angular / 0.05 to 2 mm ~ 60% Quartz < 2% Plagioclase < 2% K-feldspars ~ 2% Opaque minerals < 1% other minerals (Orthopyroxene, muscovite, biotite, microcline & hornblende) ~ 30% Fine fraction	**Relative-distribution:** Single spaced porphyric **Ped Structure:** Angular blocky (poorly defined) **Voids:** Mainly inter-aggregate voids, sub-angular shape and small (~ 0.2 mm) with occasional inter-aggregate channels and chambers **Coatings:** Clay cutans present on larger grains only **Groundmass:** Generally undifferentiated with areas of crystallitic b fabric

Table 6.7: Horizon properties of White Dam Profile 2 (continued).

Horizon	Depth	Colour	Contact	Macro-features	Coarse fragment mineralogy	Pedo-features
Bk	0.5 – 0.70 m	5YR 4/4 (M) 5YR 6/4 (D)	Gradual	Highly calcareous, distinct (10 – 20%) carbonate mottles (5YR 8/3) 15 - 30 mm diameter	Moderately sorted / sub-rounded to sub-angular / majority ~ 0.3 mm diameter ~ 60% Quartz ~ 2% Plagioclase ~ 2% K-feldspars ~ 1% micas (mainly biotite) ~ 2% Opaque minerals < 1% other minerals (Clinopyroxene & hornblende) ~ 30% Fine fraction	**Relative-distribution:** Single spaced porphyric **Ped Structure:** Angular blocky (poorly defined) **Voids:** Inter-aggregate channels with occasional chambers and vughs **Coatings:** Partial clay coatings on select grains only. Calcite coatings present on several grains, especially coarser grains **Groundmass:** Crystallitic b fabric
C (saprolith)	0.70 m to base			Highly calcareous (Ck horizon) at the top (~ 0.4 m thick) Grading into a more consolidated, but still highly weathered Biotite Gneiss with depth	Fine (most < 0.5 mm occasional larger grains to 3 mm), slight alignment of biotite ~ 75% quartz ~ 15% biotite ~ 7% plagioclase ~ 5% K-feldspar ~ 15% fine fraction at top to < 1% at base	No pedo-features

Most feldspar grains show signs of weathering similar to those described for Profile 1. Although there is a higher proportion of coarse grains (see particle-size analysis results below) suggesting that weathering is less extensive within this profile.

Small (~ 0.1 – 0.2 mm) opaque minerals are in all pedolith horizons. Larger (up to ~ 3 mm) optically opaque minerals were observed in the B2 and A1 horizon. Most of these are likely to be Fe-oxides as observed in the heavy mineral fractions (Section 6.5.2). One large opaque mineral with a calcite coating has an organic cellular, internal structure and is possibly a cross section of a plant root (Figure 6.20 A & B).

The fine fraction increases from approximately 10% in the A1 horizon to approximately 30% in the B2 and Bk horizon. There is then a gradual decrease to less than 1% within the saprolith. The fine fraction fabric is generally undifferentiated apart from calcite areas, which have a crystallitic b fabric. Clay cutans coat most coarse fragments within the A1 and B1 horizons. Within the B2 and Bk horizons only the larger grains tend to have cutans and many of these are only partially coated. No coatings were observed around voids. Also, no coatings were observed on aggregate lithic fragments in the B2 and Bk horizons (Figure 6.20 D). A coating of calcite is present on many of the coarse grains in the Bk horizon. A laminated calcite capping was observed on one particularly large feldspar grain in the Bk horizon (Figure 6.20 C).

Stacked XRD plots of the clay-sized fraction samples are presented in Figure 6.21. A copy of the analytical report is included in Appendix 4. At the base of the profile (WD3-08)

phlogopite is co-dominant (>60%) with kaolin and smectite. This reflects the primary composition of the parent material since this sample is composed of less weathered minerals, as indicated by the very low clay-sized content (see next section). Overlying this, but still within the saprolith, sample (WD3-06) consists of > 60% smectite with minor kaolin (5-20%) and trace illite (<5%). This sample has seen a higher degree of weathering, which is reflected in the loss of phlogopite and very pure non-interstratified smectite. In the Ck horizon and through the overlying pedolith, smectite and illite are co-dominant and become increasingly interstratified towards the surface (Figure 6.21). Calcite was present as a co-dominant mineral in the Ck horizon and minor mineral in the B2 and Bk horizons, despite the removal of $CaCO_3$ from the fine earth fraction prior to particle separation.

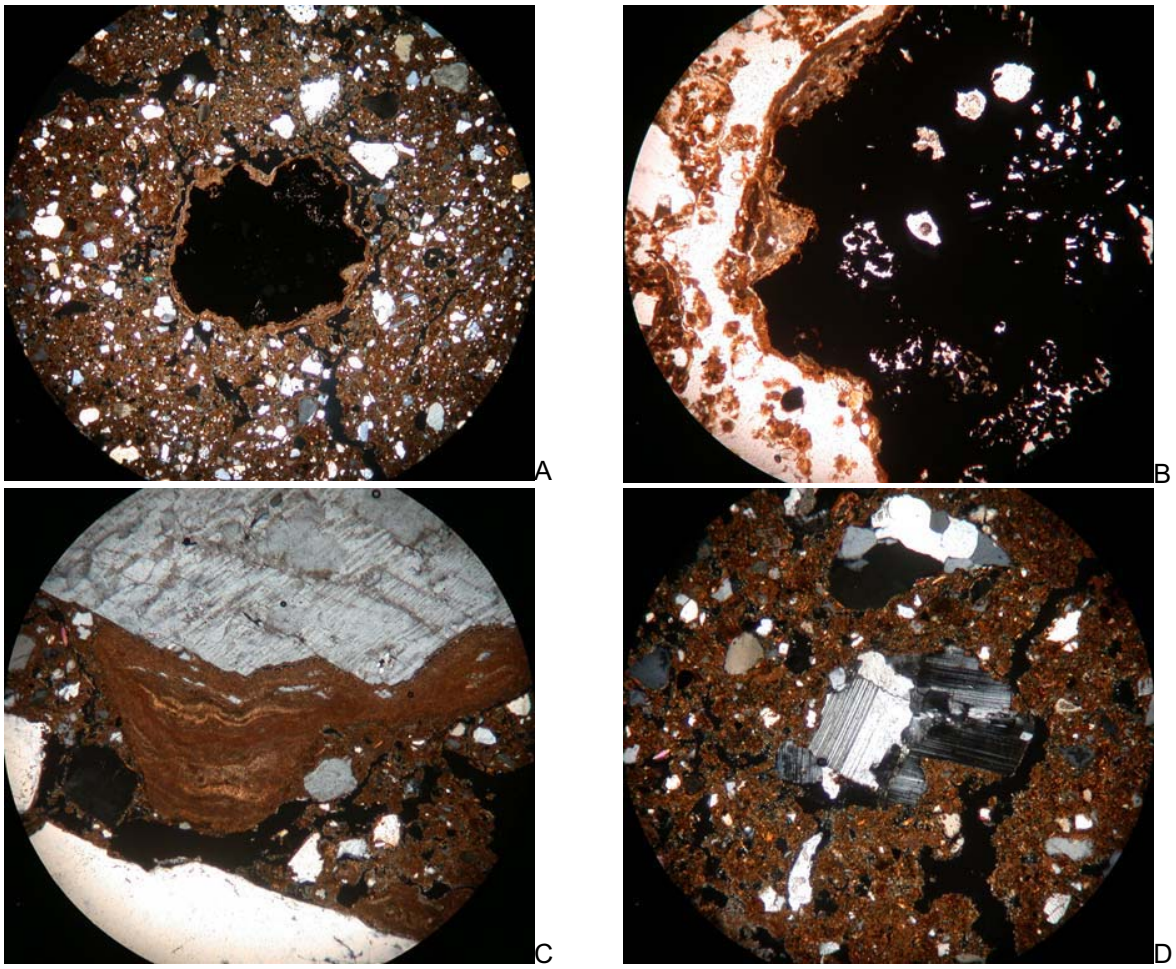

Figure 6.20: Microphotographs from Profile 2: A. and B. Organic particle with calcite coating (B2 horizon, FOV A = 12 mm, B = 4 mm), C. Calcite laminations forming capping on large feldspar grain (Bk horizon, FOV = 4 mm), D. Feldspar and quartz aggregates, note lack of coatings (B2 horizon, FOV = 4 mm).

The boundary between the saprolith and pedolith is gradual (between 5 to 10 cm thick) with highly friable and weathered areas at least 0.5 m into saprolith (Figure 6.22). This area, defined as a Ck horizon, is highly calcareous and merges into the overlying Bk horizon. The Ck horizon gradually changes to a more consolidated, but still highly weathered C horizon consisting of biotite gneiss, which is similar to that described for Profile 1.

According to the Australian soil classification system of *Subgroup, great group, suborder, order, family criteria (A horizon thickness, Gravel of surface and A1 horizon, A1 horizon*

texture, B horizon maximum texture and soil depth) (Isbell, 1996), the profile is classified as: *calcic, haplic, Red Chromosol: medium, slightly gravelly, loamy, clay loamy, moderate.*

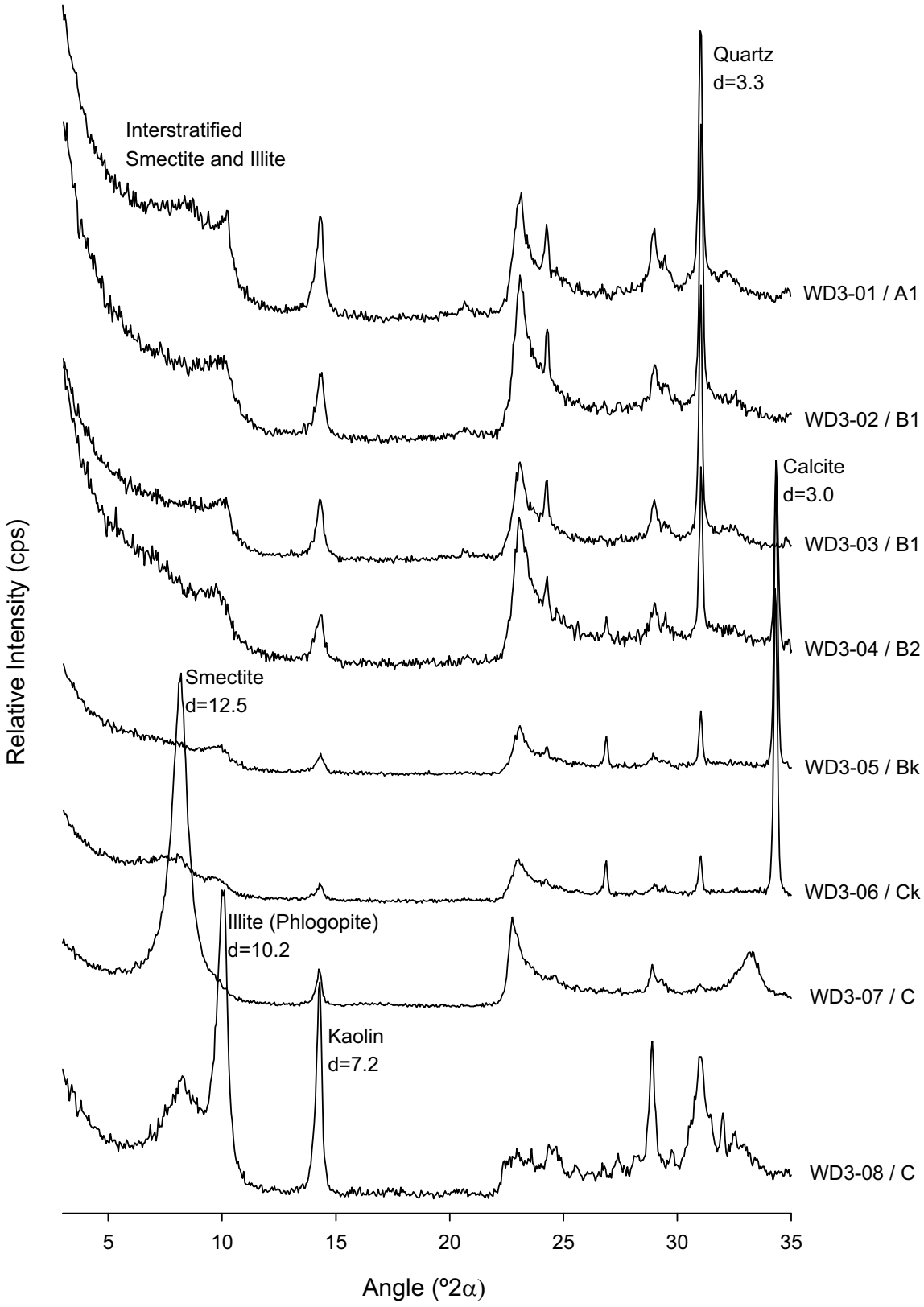

Figure 6.21: Stacked XRD plots of the clay-size fraction illustrating the breakdown of illite and its interstratification with smectite towards the surface.

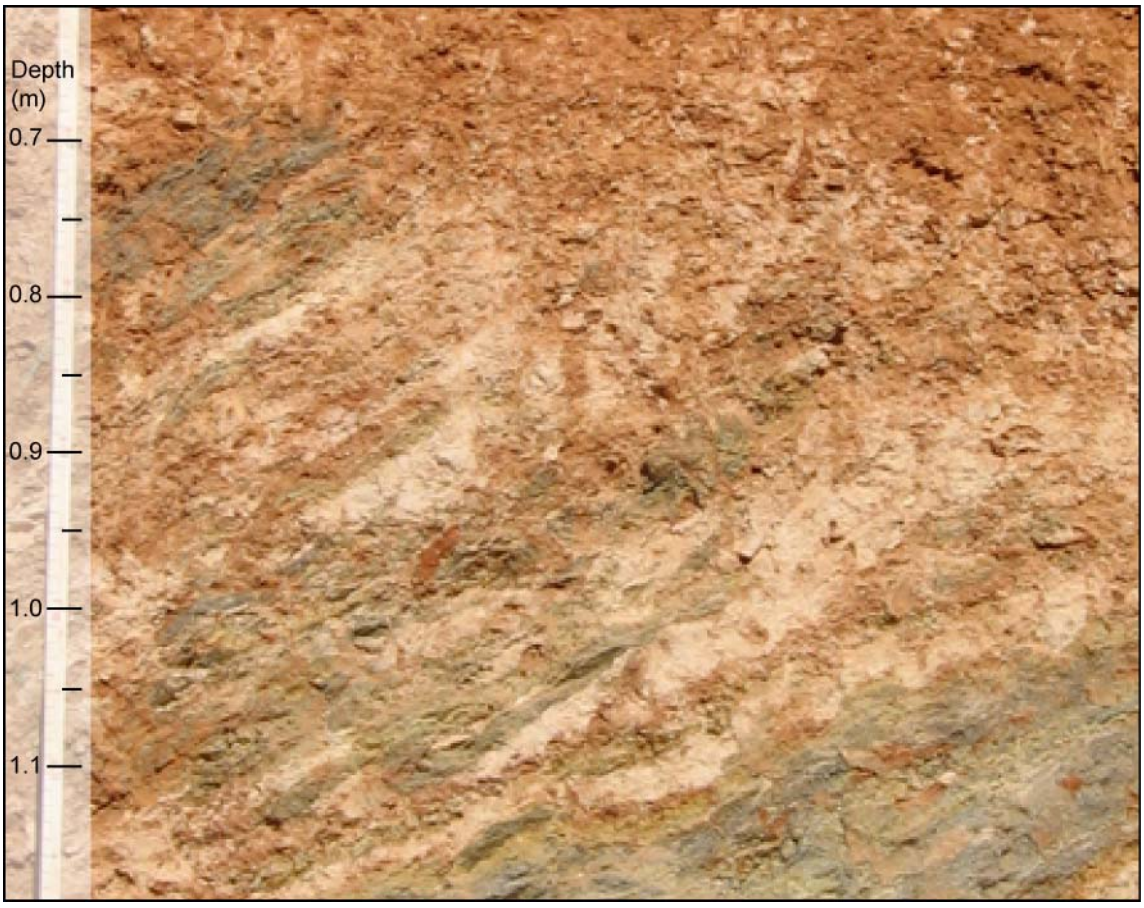

Figure 6.22: Top of saprolith (Ck horizon) showing the gradual contact with the overlying Bk horizon and the gradation into a more consolidated C horizon.

6.5.2. Profile 2 particle-size analysis

Calculated percentages of the fine earth, gravel; clay-sized/silt/sand; and fine/medium/coarse sand fractions for Profile 2 are shown in Table 6.8. These are carbonate-free values, since carbonate material was removed during the separation process (see Section 3.5.2.1).

The distribution of fine earths and coarse fragments through Profile 2 is relatively consistent. The largest variation is within the saprolithic gneiss, from 3.4 and 3.0% at the base to 9.9% at the top. Within the pedolith the variation is from 3.9 and 6.9%. The distribution records a slight increase between the A1 and B1 horizons, but then gradually decreases down to the saprolith.

The distribution of the clay-sized, silt, and sand fractions is plotted in Figure 6.23. The silt fraction has the least variation (1.6 to 9.8%). The silt content of the A1 and B2 horizons is similar at 7.1 to 7.3%. The content then increases slightly in the B2 (9.8%) and Bk (9.7%) horizons, before dropping rapidly to 1.6% at the base of the profile. The clay-sized fraction gradually increases from 10.2 to 35.6% through the A1, B1, and B2 horizons. It then drops to 32.7% for the Bk horizon. There is then a significant drop to 17.4% at the top of the saprolith, to less than 1% at the base of the saprolith. The abundance of the sand fraction is almost the inverse of the clay-sized fraction and is the major component of the profile with values from 54.6 to 98.0%.

The distributions of the individual sand fractions for Profile 2 are plotted in Figure 6.23. Apart from the lowest saprolith sample, the variation between all fractions through the profile is relatively minor. The fine sand fraction decreases from 9.5 to 8.0% between the A1 and B1 horizons before gradually increasing to a maximum 12.8% within the Bk horizon. The fine sand content then drops through the saprolith from 10.0% at the top to 3.1% at the base. The medium sand fraction has a similar distribution pattern, except at a higher concentration. Through the pedolith the medium sand ranges from 20.3 to 25.5% and drops to a low 10.6% at the base of the profile. The coarse sand fraction makes up most of the sand fraction and ranges from 61.7 to 86.3%. In the A1 horizon the coarse sand content is 67.1% which increases to 71.7% in the B1 horizon. There is then a gradual decrease to 61.7% in the Bk horizon before a gradual increase within the saprolith, to a maximum 86.3% at the base of the profile.

The heavy mineral concentration of the fine sand fraction has minimal variation of 4.8 to 5.5% through the pedolith, including the top of the saprolith (Figure 6.23). There is then a significant increase to 11.8 and 12.5% in the deeper, less weathered saprolith. The heavy mineral concentration in the medium sand fraction is similar, but slightly higher than in the fine sand fraction. Variation through the pedolith is minimal, from 5.7 to 7.0%. This is followed by an increase to 9.7%, and substantial rises to 24.7 and 30.0% with depth through the saprolith.

Table 6.8: Results from particle size analysis of samples from Profile 2.

Sample No.	Horizon	Fine earth (%)	Gravel (%)	Clay (%)	Silt (%)	Sand (%)	Sand (%)		
							Fine	Medium	Coarse
WD3-01	A1	95.4	4.6	10.2	7.3	82.5	9.5	23.4	67.1
WD3-02	B1	93.1	6.9	15.6	7.1	77.3	8.0	20.3	71.7
WD3-03	B1	94.1	5.9	22.5	7.6	69.9	9.5	22.8	67.8
WD3-04	B2	95.5	4.5	35.6	9.8	54.6	11.2	24.8	64.0
WD3-05	Bk	96.1	3.9	32.7	9.7	57.7	12.8	25.5	61.7
WD3-06	Ck	90.2	9.9	17.4	8.2	74.4	10.0	22.0	68.1
WD3-07	C	97.1	2.9	2.0	2.8	95.3	6.4	21.0	72.7
WD3-08	C	96.7	3.4	0.5	1.6	98.0	3.1	10.6	86.3

Results from the heavy mineral grain count analysis are summarised in Table 6.9. In the fine sand fraction, rutile ranged from 7.3 to 12.3% with minor variation between the pedolith and saprolith. Zircon content ranged from 3.4 to 6.8%, decreasing to 1.5% in the saprolith. Iron oxides were the predominant mineral through the pedolith, ranging from 34.9 to 56.5%, dropping to 12.2 and 32.7% in the saprolith. Biotite was very low through the pedolith, ranging from 0.8 to 6.3%, jumping significantly within the saprolith to 68.1 and 45.1%. Ilmenite was also predominant in the pedolith with values from 11.8 to 17.2%, although in the saprolith this was only 1.6 and 1.8%. Unidentified and silicate minerals ranged from 2.2 to 16.3% and 0.8 to 18.0% respectively, with the lower values occurring in the saprolith.

In the medium sand fraction rutile ranged from 2.4 to 6.5% in the pedolith dropping to 0.5% in the saprolith. Zircons are $< 1\%$ throughout the profile with values of $< 0.1\%$ in the saprolith. Iron oxides were the predominant mineral in the pedolith (41.0 to 56.1%), while biotite was predominant in the saprolith (73.9 to 93.6%) (Figure 6.24 F). Ilmenite was

significantly lower in this fraction with values from 7.5 to 8.6% in the pedolith and < 1.6% in the saprolith. Unidentified and silicate minerals ranged from 15.3 to 18.4% and 13.8 to 18.3% respectively in the pedolith, dropping to 1.85 to 4.5% and 1.8 to 3.9% respectively in the saprolith.

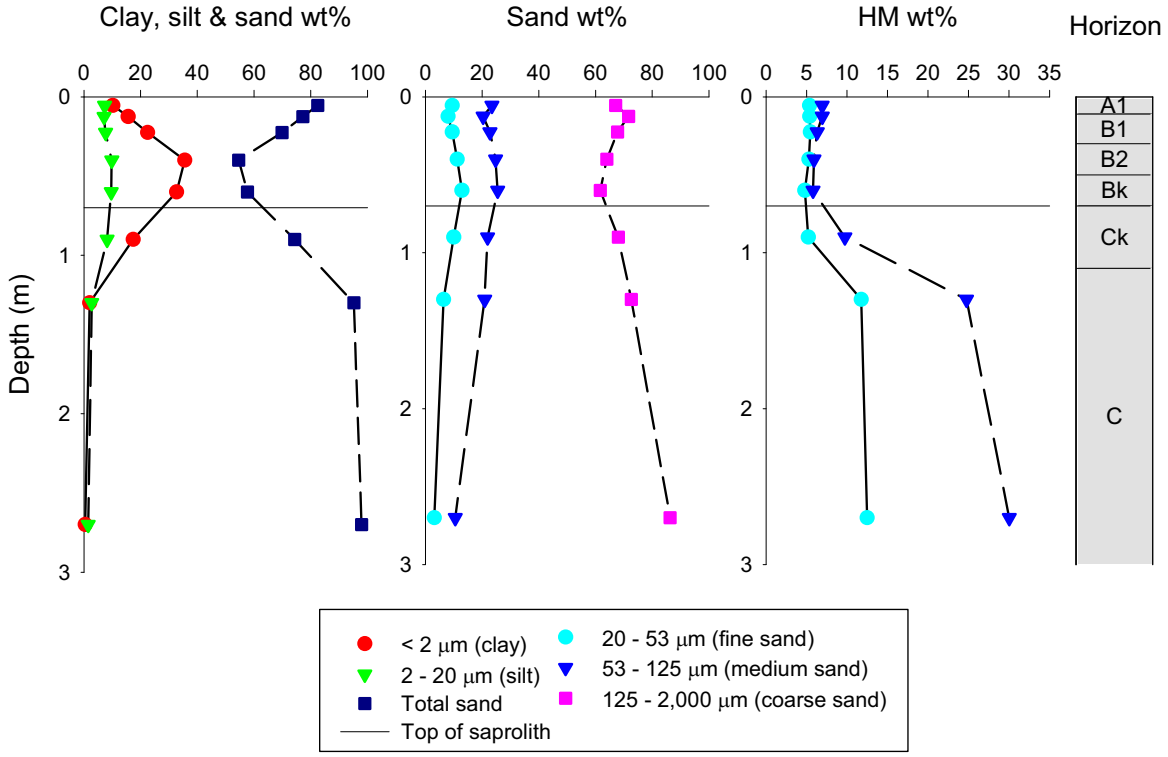

Figure 6.23: Depth plots of particle size fractions and heavy mineral content of Profile 2.

Observations of the heavy mineral fractions by electron microscopy supported the above data. Iron-oxides were dominant in the pedolith samples and biotite was dominant in the saprolith (Figure 6.24 F). Zircons viewed by electron microscopy generally had a clean appearance with smooth sides and rounded edges (Figure 6.24 A & B). The rutile and ilmenite grains were generally less rounded and had angular features on the surfaces (Figure 6.24 C & D). Many of the rutile and ilmenite grains showed evidence of dissolution features (Figure 6.24 E).

6.5.3. Profile 2: Bulk density, calcimetry, pH and EC

A summary of the pH, EC, calcium carbonate content and bulk density results is provided in Table 6.10. Full details of the repeat runs for the calcium carbonate and bulk density measurements are provided in Appendix 5.

There is a general alkaline trend through the profile with a pH range of 8.8 to 10.3. The EC values are very low with an increasing trend through the pedolith from 0.05 to 0.34 dS/cm followed by a rapid decrease in the saprolith from 0.21 to 0.06 dS/cm. Calcium carbonate content is highest within the calcareous B2 and Bk horizons, and at the top of the saprolite (Ck horizon) with 9.1, 18.6 and 17.5% respectively. Bulk density gradually increases with depth from 1.8 to 2.6 g/cm^3, apart from the surface, A1 horizon where the density was 2.2 g/cm^3.

Table 6.9: Summary of heavy mineral grain count analysis for Profile 2.

Sample	Horizon	Al silicate (%)	Biotite (%)	Fe-oxide (%)	Ilmenite (%)	Monazite (%)	Rutile (%)	Zircon (%)	Other (%)	Total grains
Fine sand (20 - 53 μm)										
WD3-01	A1	17.95	3.09	36.62	17.24	0.48	9.04	5.23	10.34	841
WD3-02	B1	7.59	0.76	56.46	16.20	2.28	7.34	6.84	2.53	395
WD3-03	B1	9.02	2.42	41.95	13.50	1.21	12.29	3.93	15.68	1652
WD3-04	B2	10.57	6.26	39.92	11.82	1.81	9.87	3.48	16.27	719
WD3-05	Bk	14.41	4.16	34.92	13.97	0.74	11.00	6.09	14.71	673
WD3-06	Ck	12.78	5.28	38.34	14.19	0.82	8.21	5.28	15.12	853
WD3-07	C	0.84	68.13	12.21	1.77	2.14	11.18	1.49	2.24	1073
WD3-08	C	2.87	45.10	32.72	1.57	1.29	9.70	1.66	5.08	1082
Medium Sand (53 - 125 μm)										
WD3-01	A1	14.99	2.43	53.94	7.29	0.17	2.43	0.34	18.43	1194
WD3-02	B1	16.07	2.61	51.12	7.51	0.74	3.41	0.19	18.36	1612
WD3-03	B1	16.59	5.73	45.69	8.56	0.79	3.82	0.53	18.30	1519
WD3-04	B2	13.80	1.36	56.14	8.10	0.82	4.08	0.33	15.38	1840
WD3-05	Bk	18.26	2.83	41.04	7.97	0.28	6.50	0.34	22.78	1769
WD3-06	Ck	3.93	73.92	11.96	1.61	0.27	3.58	0.21	4.52	3738
WD3-07	C	1.96	92.87	1.71	0.25	0.09	1.18	0.09	1.84	3214
WD3-08	C	1.76	93.62	2.07	0.12	0.00	0.49	0.09	1.85	3243

6.5.4. Elemental assay results and trends for Profile 2

Results of multi-element assays for the bulk, fine earth, and size fractions from Profile 2 are included in Appendix 6. A summary of these results and observed trends is presented below. Further discussion of the element assays for Profile 2 is presented in Section 6.6 with pedogenic implications of the mass balance analysis.

Table 6.11 lists the elements that were assayed, but found to be at or below detection for > 20% (n=2) of the samples. Those elements bracketed and in red text were below analytical detection for either the pedolith or saprolith samples only. The majority of these are below analytical detection in the saprolith. The exceptions are Co and Zn. Cobalt was below analytical detection at the top of the pedolith (WD3-01 and WD3-02) for the medium sand fraction, and Zn was below or close to analytical detection through most of the pedolith in the medium and coarse sand fractions. Of those elements below analytical detection, most were in the sand-size fractions, especially the medium and coarse sand fractions. In the pedolith Zr was the only element of those assayed to be below analytical detection (500 ppm) in the clay-sized and silt fractions.

Major element assays for the bulk samples are plotted in Figure 6.25. Apart from K_2O, they all have wide variation through the pedolith. The concentration of K_2O through the pedolith varies from 1.68 to 1.95%, with the highest values in the B1 horizon (WD3-02 & WD3-03). There is a significant increase towards the base of the profile within the saprolite where the K_2O concentration increases to 9.68%.

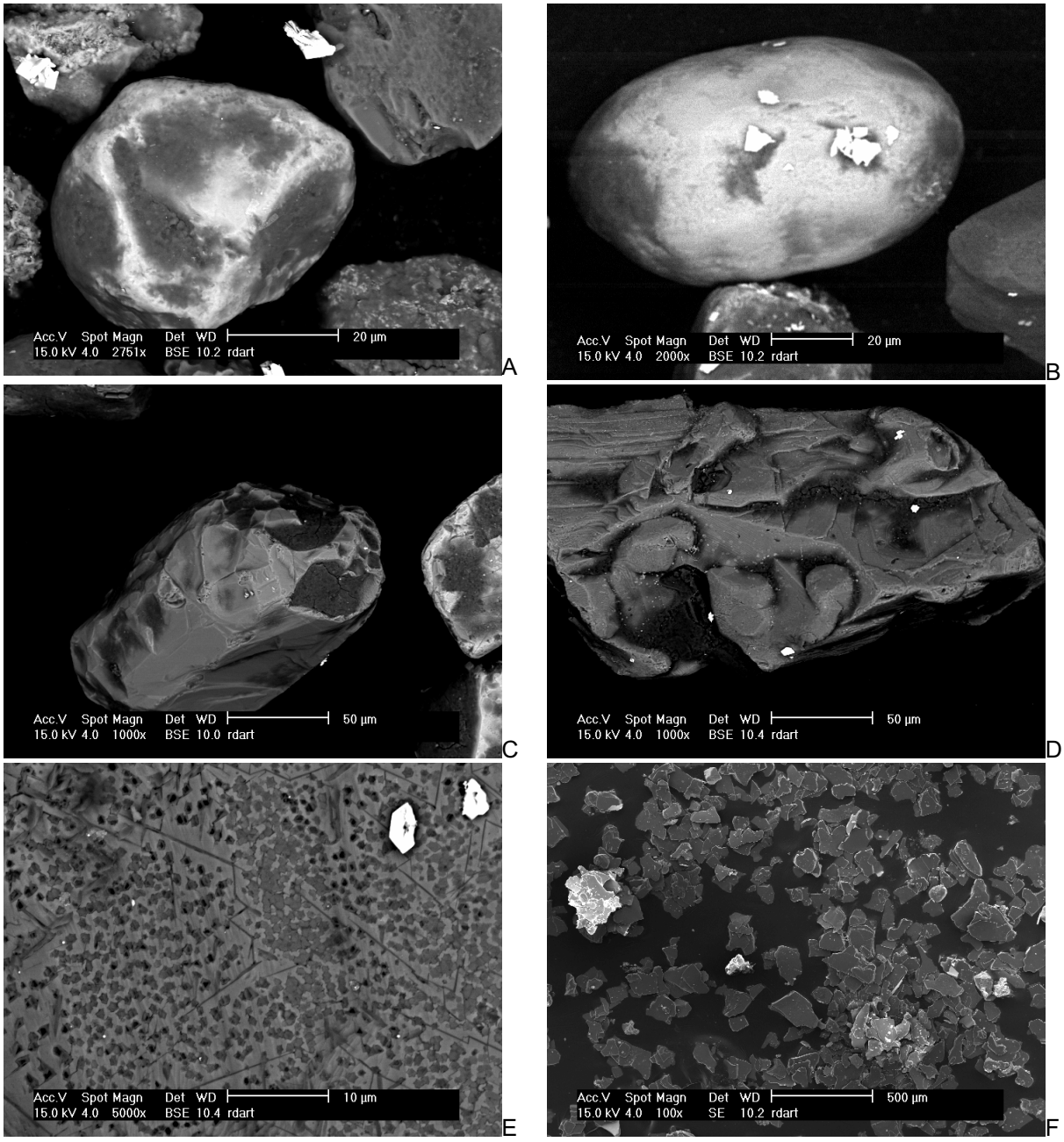

Figure 6.24: Backscatter images: A & B) zircon grains from the A1 and B2 horizons respectively; C & D) rutile grains from the B1 and Bk horizons respectively; E) dissolution feature on surface of ilmenite grain, darker areas contain more TiO_2; and, F) general view of prepared sample stub for sample WD3-07 showing high biotite percentage.

The dominant major element through the profile is Si with SiO_2 concentrations ranging from 50.1 to 70.4%. There is a gradual decrease in concentration from the maximum at the surface to the minimum in the Ck horizon (WD3-06) before increasing to ~62% for the remaining two saprolith samples. The concentration of Na_2O decreases from 3.09% at the surface to 2.95 (WD3-04) and 2.05% (WD3-05) at the base of the pedolith. In the saprolith the Na_2O concentration increases to 4.27% (WD3-07) before dropping to 2.87% (WD3-08) at the base of the profile. The dispersion of Fe_2O_3 increases from 5.16% at the surface to 5.59% in the B2 horizon (WD3-04), before dropping to 4.21% in the Ck horizon (WD3-06). Below this the concentration increases to 4.84% (WD3-07) and then decreases again at the base of the profile to 3.76% (WD3-08). Despite a gradual decrease in TiO_2 concentration through the pedolith

from 0.58 to 0.48% there is a minor increase to 0.55 and 0.56% at the base of the B1 (WD3-03) and within the B2 (WD3-04) horizons. In the saprolith there is a gradual increase from a profile low value of 0.43% (WD3-06) to a maximum 0.66% (WD3-08) at the base.

Table 6.10: pH, EC, $CaCO_3$, and bulk density for Profile 2.

Sample No.	Horizon	Depth (m)	pH	EC (dS/cm)	CaCO3 (%)	Bulk density (g/cm^3)
WD3-01	A1	0.00 – 0.11	8.77	0.05	0.00	2.24
WD3-02	B1	0.11 – 0.15	9.12	0.10	0.23	1.80
WD3-03	B1	0.15 – 0.30	9.19	0.13	2.24	2.17
WD3-04	B2	0.30 – 0.50	9.04	0.17	9.13	2.11
WD3-05	Bk	0.50 – 0.70	8.76	0.29	18.60	2.16
WD3-06	Ck	0.70 – 1.10	9.20	0.34	17.46	2.26
WD3-07	C	1.20 – 1.40	10.27	0.21	0.32	2.54
WD3-08	C	2.65 – 2.75	9.22	0.06	0.00	2.55

Table 6.11: Elements that were at or below detection for > 20% of samples from Profile 2. Note: elements in red were only below detection for either the pedolith or saprolith.

Sample type	Elements below detection
Bulk	Cd, In, Sb, Se, Te
Tot < 2 mm (fine earth)	Cs, (Sb), Zr
125 – 2000 μm (coarse sand)	As, Br, Co, Cs, Sb, (Zn), Zr
53 – 125 μm (medium sand)	Br, (Co), Cs, (Sb), (Zn), Zr
20 – 53 μm (fine sand)	Br, Cs, (Sb)
2 – 20 μm (silt)	(Br), (Sb), Zr
< 2 μm (clay-size)	(Br), (Cs), (Sb), Zr

Both CaO and P_2O_5 have an increasing trend towards the base of the pedolith before significantly decreasing in the saprolith. The only deviation from this trend is with P_2O_5 from the A1 and B1 horizons where there is an initial decrease from 0.08 to 0.06% in concentration before reaching a maximum 0.11% in the Bk horizon (WD3-05). The concentration of CaO increases from 0.7% at the surface to 12.4% in the Bk horizon before reaching a maximum 13.4% in the Ck horizon. The dispersion of MgO is similar insofar as it increases from the surface concentration of 0.69%, but only as far as the B2 horizon where the concentration of 1.42% (WD3-04) is followed by a decrease to the Ck horizon of 1.24% (WD3-06) before increasing once more to a profile maximum of 1.70% (WD3-08).

The dispersion pattern of MnO is relatively uniform throughout most of the profile between 0.09 and 0.15%. The exception is at the top of the pedolith and also at the top of the saprolith where there are significant increases in concentration to 0.64 and 0.55% for the A1 (WD3-01) and Ck (WD3-06) horizons respectively.

The remaining major element, Al_2O_3, increases from a surface concentration of 11.4 to 12.3% at the base of the B1 horizon (WD3-03), before decreasing to a low 10.1% at the base of the pedolith (WD3-05) and at the top of the saprolith (WD3-06). This is followed by an increase to a maximum of 16.2% at the base of the profile (WD3-08).

The major elements included in the size fraction assays were Fe and Na (Figure 6.26). The dispersion patterns for the fine earth samples are similar to that of the bulk samples for both Fe and Na, apart for a minor decrease in Fe concentration from the A1 to B1 horizons in the fine earth sample, instead of the minor increases in the bulk sample.

Within the size fractions, the highest Fe concentrations were in the clay-sized and silt fractions. In the pedolith the concentrations ranged from 4.2 to 5.9% and 3.1 to 5.3% for the clay-sized and silt fractions respectively compared with a range of 2.5 to 3.9% for all of the sand fractions. The trend for all fractions is a gradual decrease from the surface to the base of the pedolith. There is a major increase in Fe from the top of the saprolith to sample WD3-07 for all size fractions, followed by only minor variation to the base of the profile (WD3-08).

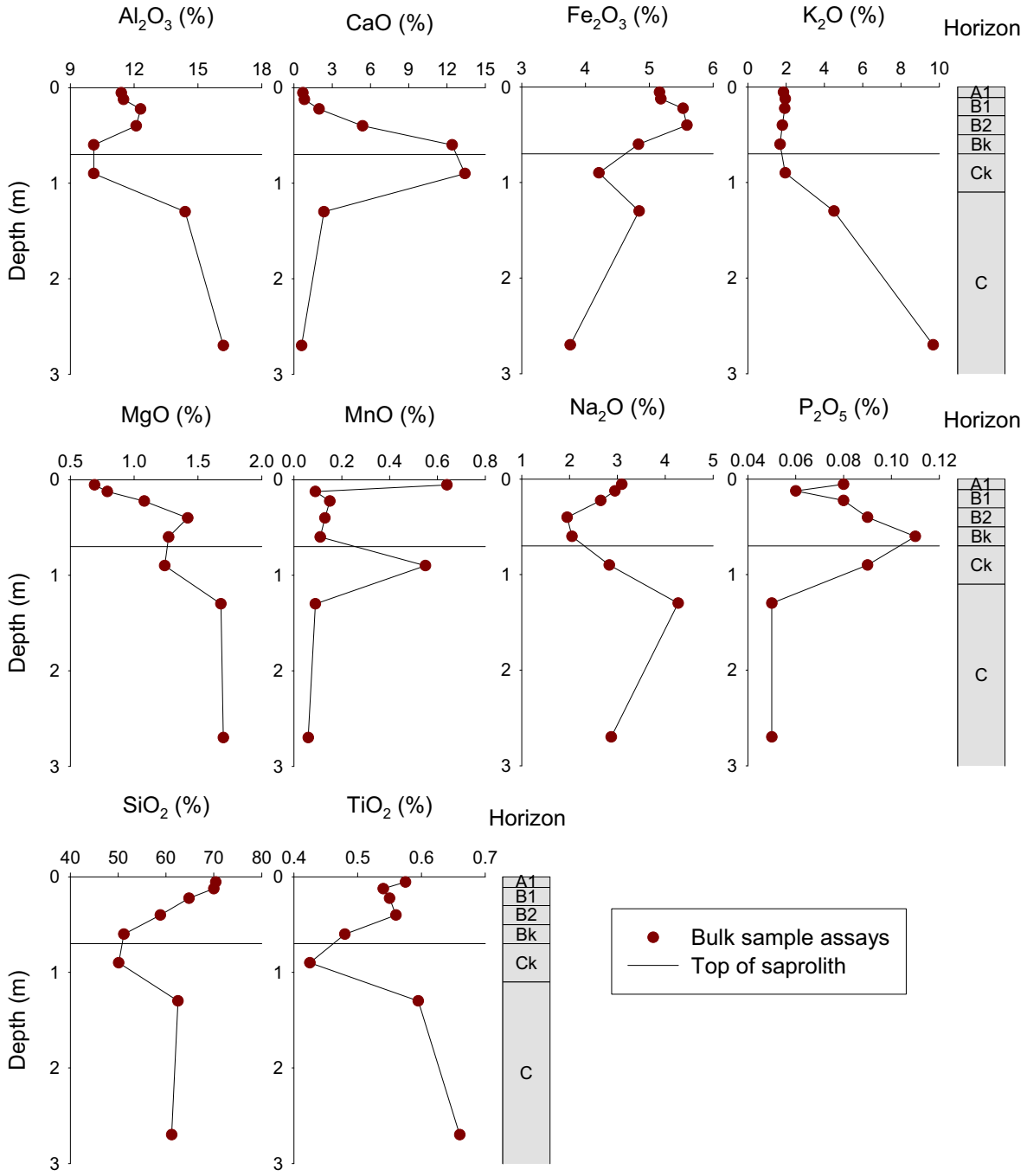

Figure 6.25: Major element depth plots of bulk soil assays for Profile 2.

The coarse sand fraction has the highest concentrations of Na, ranging from 3.2 to 3.5%, apart from a minimum of 2.5% at the base of the profile. This is more than twice the concentration of the other size fractions from the pedolith. Higher concentrations are in the saprolith, but apart from the base (WD3-08) of the clay-size fraction at 3.6%, all are lower than those in the coarse sand fraction. Variation of Na concentration in the sand fractions through the pedolith is minor with a slight increase at the top of the saprolith before decreasing at the base of the profile. In the clay-sized and silt fractions there is a larger variation with the samples from the B2, Bk, and Ck horizons (WD3-04, WD3-05, & WD3-06) having marginally lower Na concentrations than the remainder of the profile.

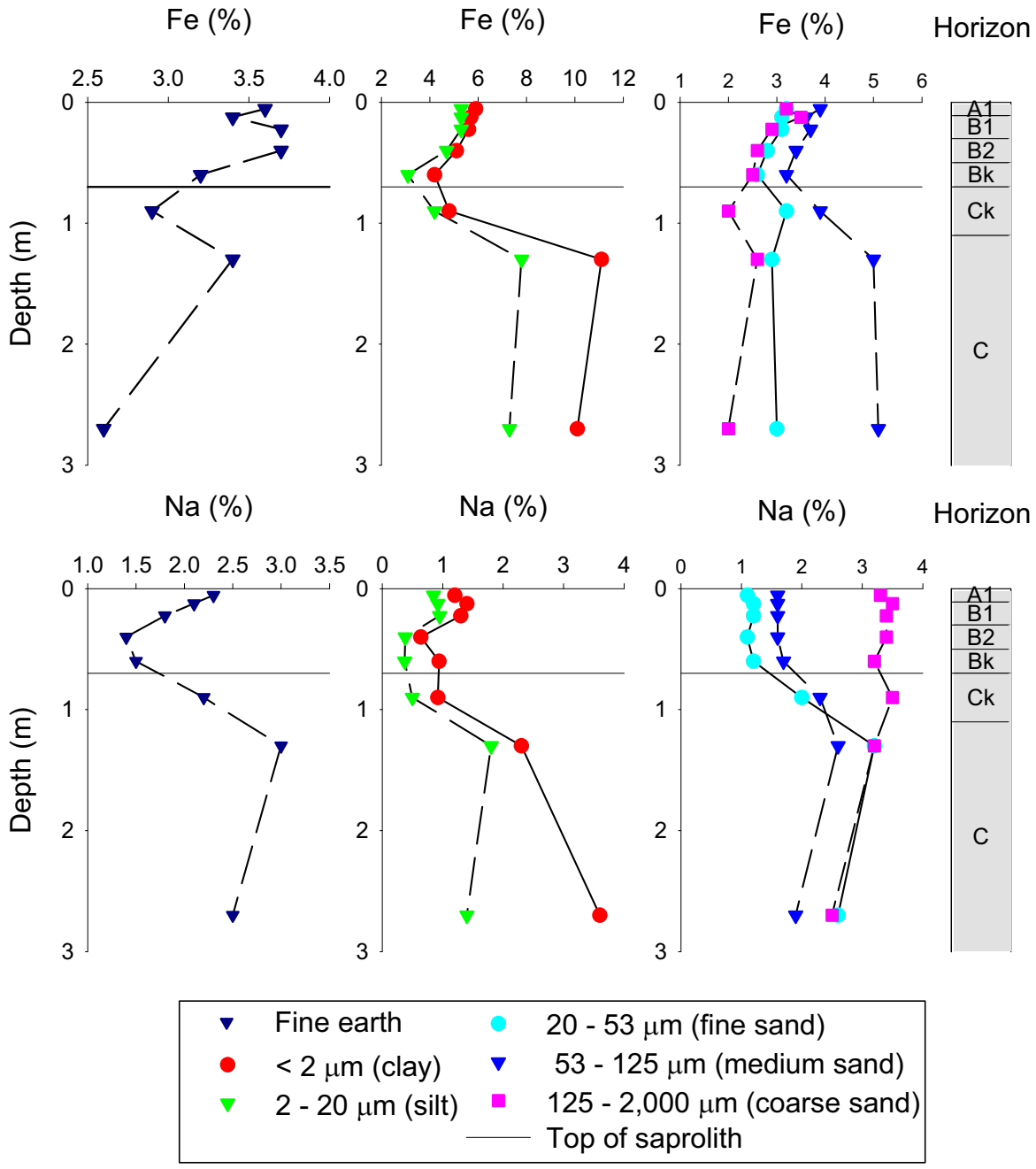

Figure 6.26: Major element depth plots of size fraction assays of Fe and Na for Profile 2.

Trace element assay results of the bulk and fine earth fraction are plotted in Figure 6.27 and of the size fractions in Figure 6.28. Due to the different analytical methods there is a difference in the acquired elements between the bulk and size fractions (see Section 3.6), which is why some plots are missing the bulk or size fraction data. In general, where both the bulk and fine earth element assays are available, the dispersion patterns have minor differences. The exception is Co, which is discussed in more detail below.

The elemental dispersion patterns through the pedolith can be grouped into:

1. those that increase (As, Au, Ba, Br, Mo, Ni, & Sr);
2. those that decrease (Pb);
3. those that are relatively uniform (Ag, Bi, Cu, Ga, Hf, Rb, Sb, Th, Tl, U, Y, & Zn); and,
4. those that have distinct variations (Co, Cr, Cs, Sc, V, W, & Zr).

Dispersion patterns of elements through the pedolith in the size fractions are generally similar to their bulk and fine earth equivalents.

There is a significant variation in the assay results between the pedolith and saprolith for both the bulk and size fraction assays. Many elements also have a distinct variation within the saprolith between the Ck and basal C horizons. The variations through the saprolith for the individual size fractions were generally similar to those in the bulk and fine earth samples.

The following elements, As, Au, Ba, Br, Co, Cu, & Hf had distinct variations between the size fractions and/or change in trend, between the pedolith and saprolith. These are are discussed in more detail below.

The dispersion pattern of As was relatively uniform between the bulk and fine earth samples and between the silt and clay-sized fractions, however, there was distinct variation in the concentration levels between these and the individual sand fractions. All the fractions increase to the Ck horizon (WD3-06) and then decrease to, or below, the detection limit of 2 ppm apart from the silt fraction. The lowest As concentrations were in the coarse sand fraction with most samples below detection. The highest concentrations of As were in the clay-sized and silt fractions with ranges of 5 to 9 ppm and 6 to 15 ppm respectively.

There is considerable variation in Au concentration between individual samples or size fractions. Concentrations range from below analytical detection limit (5 ppb) to 330 ppb in the pedolith, and from 34 to 350 ppb in the saprolith. The concentration of Au decreases in the basal sample (WD3-08) with the highest concentrations in sample WD3-07. The lowest concentrations overall were in the fine sand fraction, which ranged from below analytical detection at the surface to 55 ppb in the saprolith. The medium and coarse sand fractions both had Au concentrations below analytical detection at the surface followed by concentrations of < 30 ppb through the remainder of the pedolith. Gold increased in the saprolith to 120 ppb (53 – 125 μm) and 320 ppb (125 – 2000 μm). The highest Au concentrations were in the clay-sized and silt fractions with the clay-sized fraction having the highest saprolith concentrations (340 & 350 ppb in WD3-05 & WD3-06) and the silt fraction having the highest pedolith concentration (330 & 220 ppb in WD3-03 & WD3-04).

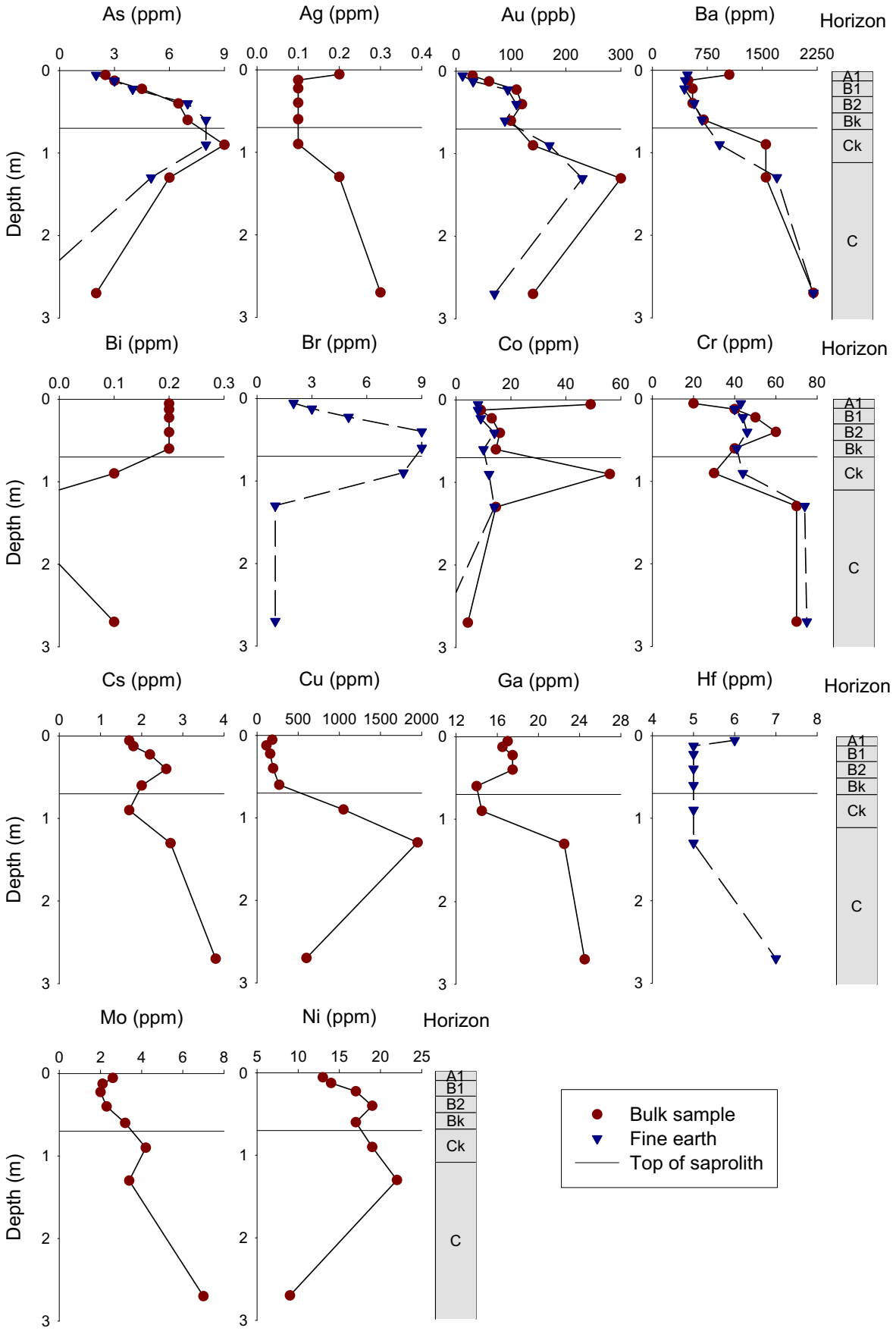

Figure 6.27: Trace element depth plots of the bulk and fine earth soil assays for Profile 2. Some samples were below detection limits for As (2 ppm), Bi (0.1 ppm), Co (5 ppm), and Sb (0.2 ppm).

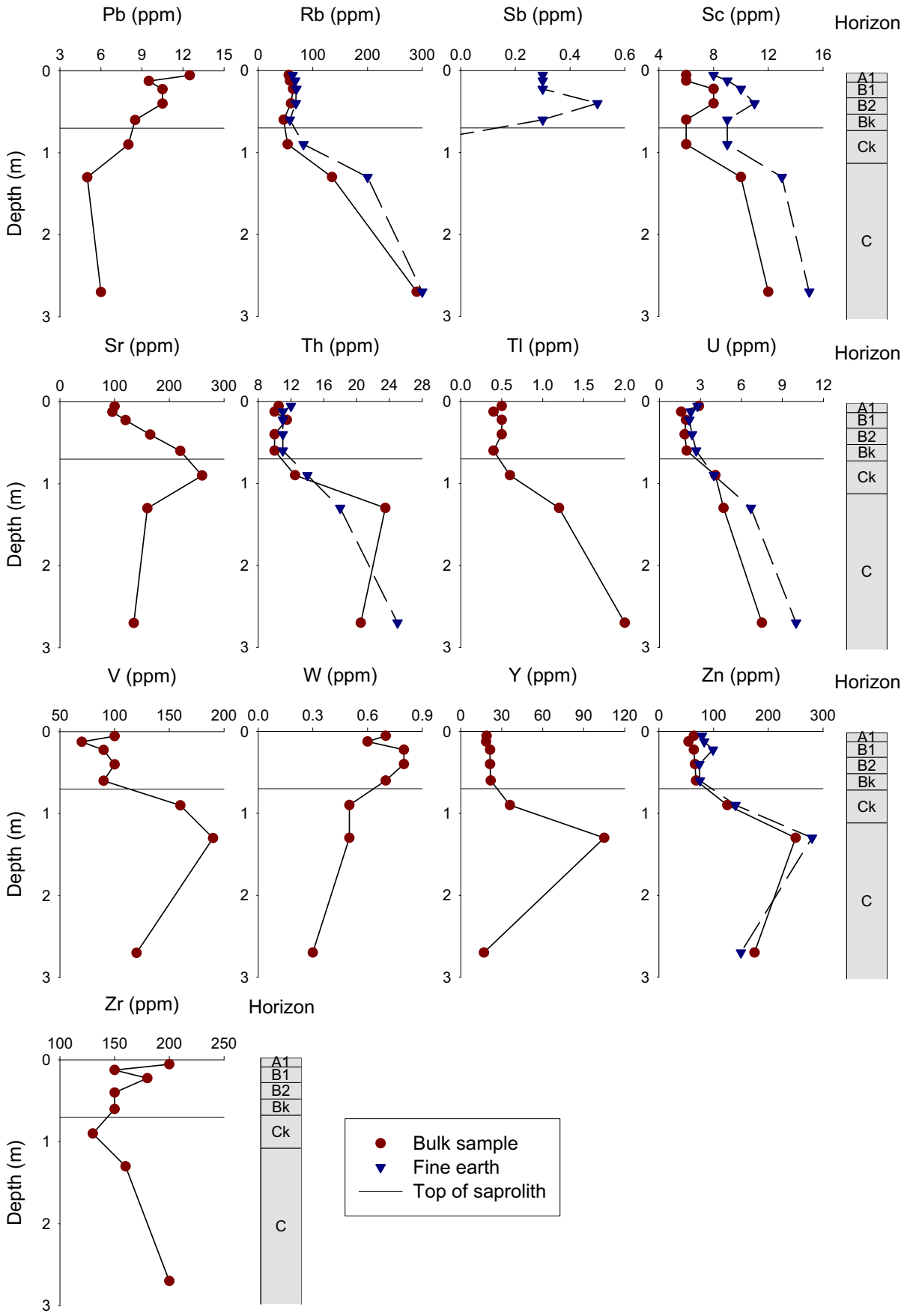

Figure 6.27: Trace element depth plots of the bulk and fine earth soil assays for Profile 2. Some samples were below detection limits for As (2 ppm), Bi (0.1 ppm), Co (5 ppm), and Sb (0.2 ppm) (continued).

In general, Ba concentration was relatively uniform through the pedolith, increasing significantly into the saprolith and towards the base of the profile apart from the clay-sized fraction. The Ba concentrations in the clay-sized fraction ranged from 220 ppm in the pedolith to 940 ppm at the base of the saprolith compared with a typical range of 350 to 2,200 ppm for the other size fractions. The coarse sand fraction had the overall highest concentrations with a range from 550 to 2,200 ppm.

In the bulk samples for Co, two concentration peaks are at the top of the pedolith (49 ppm WD3-01) and saprolith (56 ppm WD3-06). This is significantly higher than the equivalent fine earth assays and the remainder of the bulk samples, which range from 8 to 16 ppm, not including the basal sample from the fine earth that was below detection (5 ppm). In the sand fractions many samples were close to or below analytical detection, especially in the medium and coarse sand fractions through the pedolith. In the saprolith however, a Co concentration of 21 ppm (WD3-07) was measured for the medium sand fraction. The basal sample (WD3-08) has low concentrations for all size fractions and below analytical detection for the fine and coarse sand fractions, and total fine earth material. The highest Co concentrations were in the silt fraction, which increased through the pedolith from 21 to 36 ppm at the B2 horizon (WD3-04) before decreasing to 23 ppm in the Bk horizon (WD3-05).

This is almost the inverse of the clay-sized fraction, in which Co decreases through the pedolith from 21 ppm at the surface to 13 ppm in the Bk horizon. In the saprolith the clay-sized and silt fractions increase to 36 and 26 ppm respectively for sample WD3-07 before decreasing to 18 and 12 ppm.

The Cu assays were only available for the bulk samples. The dispersion pattern through the pedolith was relatively uniform from 115 to 195 ppm, increasing to 270 ppm in the Bk horizon (WD3-05). In the saprolith, there is a significant increase to 1,050 (WD3-06) and 1,950 ppm (WD3-07), before Cu decreases to 600 ppm in the basal sample (WD3-08).

Profile 2 REE assays for the bulk, fine earth, and size fractions are plotted in Figure 6.29 and Figure 6.30. The majority of the REE dispersion patterns show similar trends between all the fractions, including the bulk and fine earth samples. Although the patterns are similar the concentration levels are significantly different between the size fractions for several of the REEs.

The dispersion trend of the LREEs (La, Ce, Pr, & Nd) through the profile is relatively uniform in the pedolith, before a significant increase at the Ck horizon (WD3-06). Below this there is an initial decrease followed by a similar or slightly elevated concentration at the base. There are significant concentration variations of around $10-20$ ppm between the size fractions. In the pedolith, the highest overall concentrations are in the fine sand fraction with decreasing concentrations towards the coarser and finer fractions. In the saprolith however, the clay-sized and silt fractions are generally higher, particularly for the basal sample (WD3-08), where the increase is up to six times larger than the pedolith assays. After an increase in concentration at the top of the saprolith, the fine and medium sand fractions decrease to concentration levels similar to those in the pedolith, whereas the other size fractions do not decrease to the same extent. In the clay-sized and silt fractions the concentration increases at the top of the saprolith are minor or within the range of the overlying samples, although sample WD3-07 has a significant increase. Unlike the majority of other size fractions, the clay-sized fraction LREE concentration does not decrease towards the base of the profile, but increases, reaching the highest individual concentration of any fraction. In the clay-sized

fraction at the top of the pedolith (WD3-01) the concentration is much higher than through the remainder of the pedolith, which is relatively uniform.

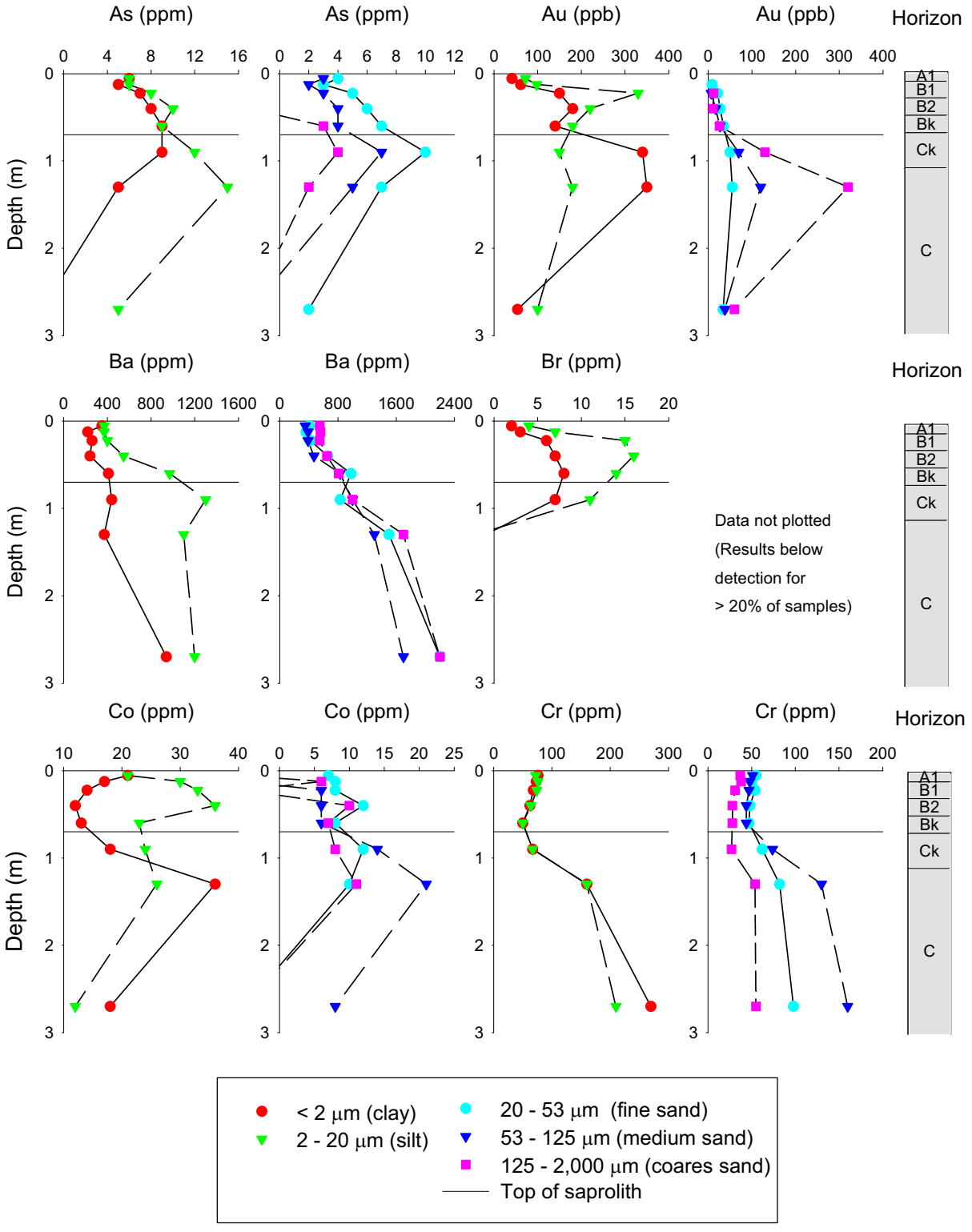

Figure 6.28: Trace element depth plots of size fractions from Profile 2. Some samples were below detection limits for As (2 ppm), Br (1 ppm), Cs (3 ppm), Rb (30 ppm), Sb (0.2 ppm), and Zn (50 ppm).

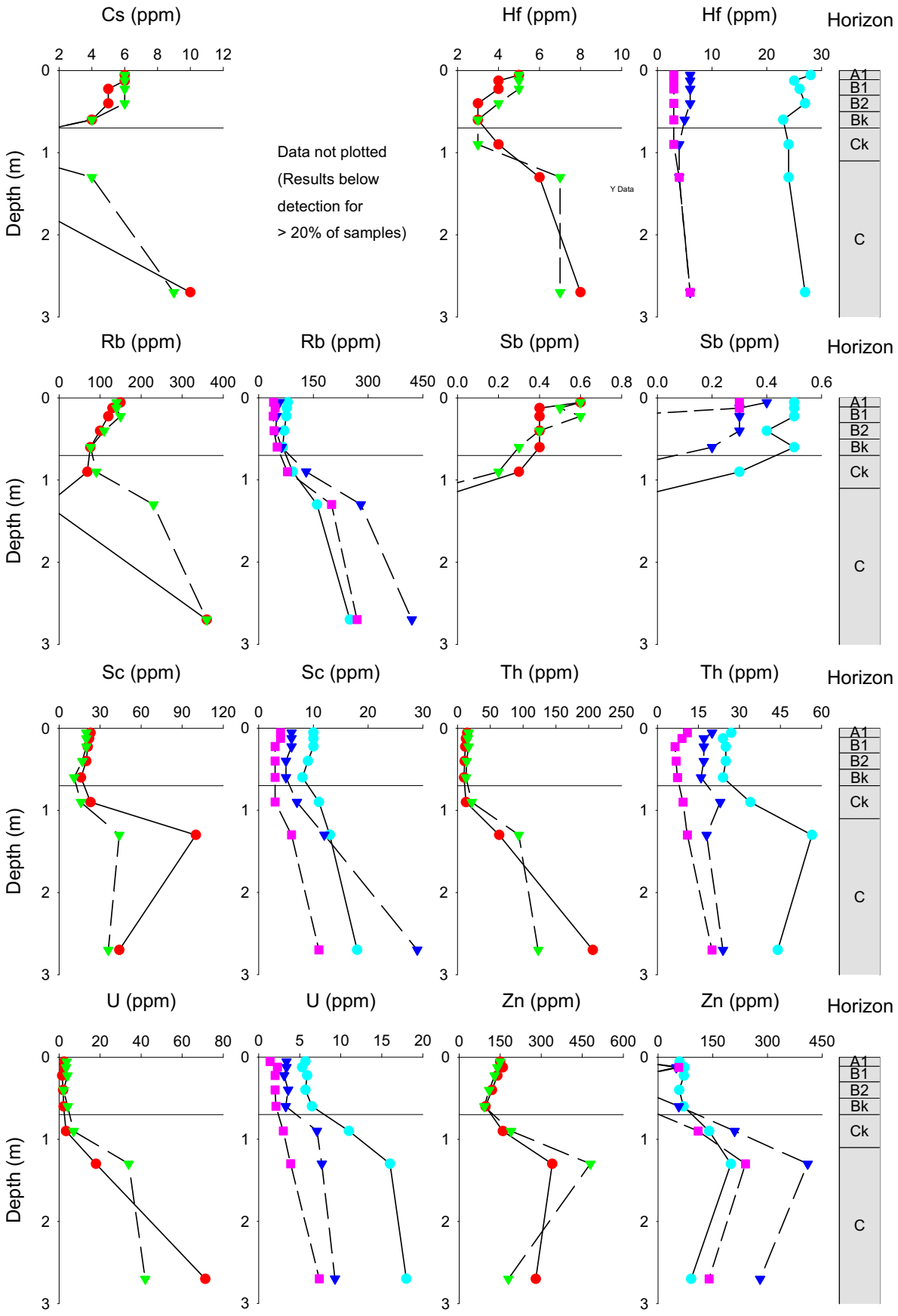

Figure 6.28: Trace element depth plots of size fractions from Profile 2 Some samples were below detection limits for As (2 ppm), Br (1 ppm), Cs (3 ppm), Rb (30 ppm), Sb (0.2 ppm), and Zn (50 ppm) (continued).

Similar trends and variations are in the MREEs (Sm, Eu, Gd, Tb, Dy, & Ho). Only Sm, Eu, and Tb were included in the size fraction assays. The concentrations are close to uniform through the pedolith, and then increase through the saprolith, and decrease or remain similar for the basal sample. Variation is minor between the bulk and fine earth samples through the pedolith, although the fine earth samples mostly have higher concentrations. In the pedolith the highest overall concentrations are in the fine sand fraction with decreasing concentrations towards the coarser and finer fractions. In the saprolith the sand fractions have concentrations similar to or slightly higher than those in the pedolith. Clay-size and silt concentrations however, are significantly higher in sample WD3-07, which decrease to similar or moderately higher concentrations for the basal sample (WD3-08). There is an increase in concentrations at the surface (WD3-01) for Sm in the clay-sized and medium sand fractions, and Tb in the fine sand fraction, compared with the remainder of the pedolith samples.

There are minor variations in the bulk, fine earth, and size fractions through the pedolith for the HREEs (Er, Tm, Yb, & Lu). In the Ck horizon (WD3-06), the bulk fractions are all slightly higher than those in the pedolith; however, in the majority of the fine earth samples and size fractions the concentration is similar to those in the pedolith. Below this the concentrations increase in the bulk, fine earth, and size fractions, apart from the medium and coarse sand fractions, which are relatively uniform throughout the profile. In the basal sample (WD3-08) the concentrations decrease to levels similar to or slightly elevated to those in the pedolith. Only Yb and Lu concentrations were available in the size fractions. The variations between the size fractions are similar to those in the LREEs and MREEs. The overall highest concentrations are within the fine sand fraction, but significantly higher concentrations are in the saprolith clay-sized and silt fractions of sample WD3-06.

Plots of the REEs normalised to chondrite and PAAS are shown in Figure 6.31 (Taylor & McLennan, 1985; McLennan, 1989). Compared with the basal saprolith sample (WD3-08) most of the pedolith samples are depleted in LREEs and MREEs with minor enrichment in the HREEs. The C and Ck horizons (WD3-07 & WD3-06) have similar values to WD3-08 for LREEs, but are enriched in MREEs and HREEs with the C horizon being approximately twice as enriched as the Ck horizon.

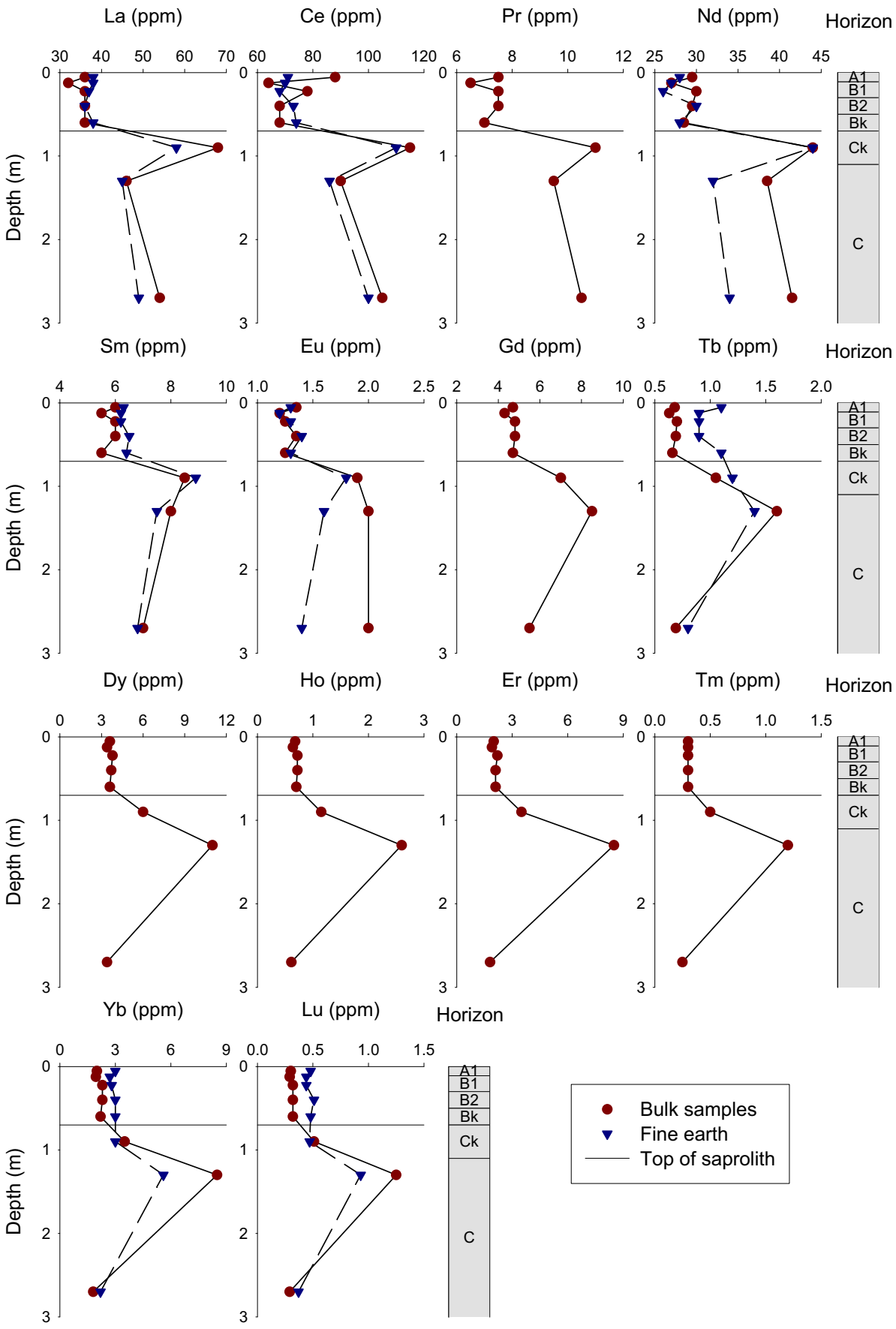

Figure 6.29: REE depth plots of the bulk and fine earth soil assays for Profile 2.

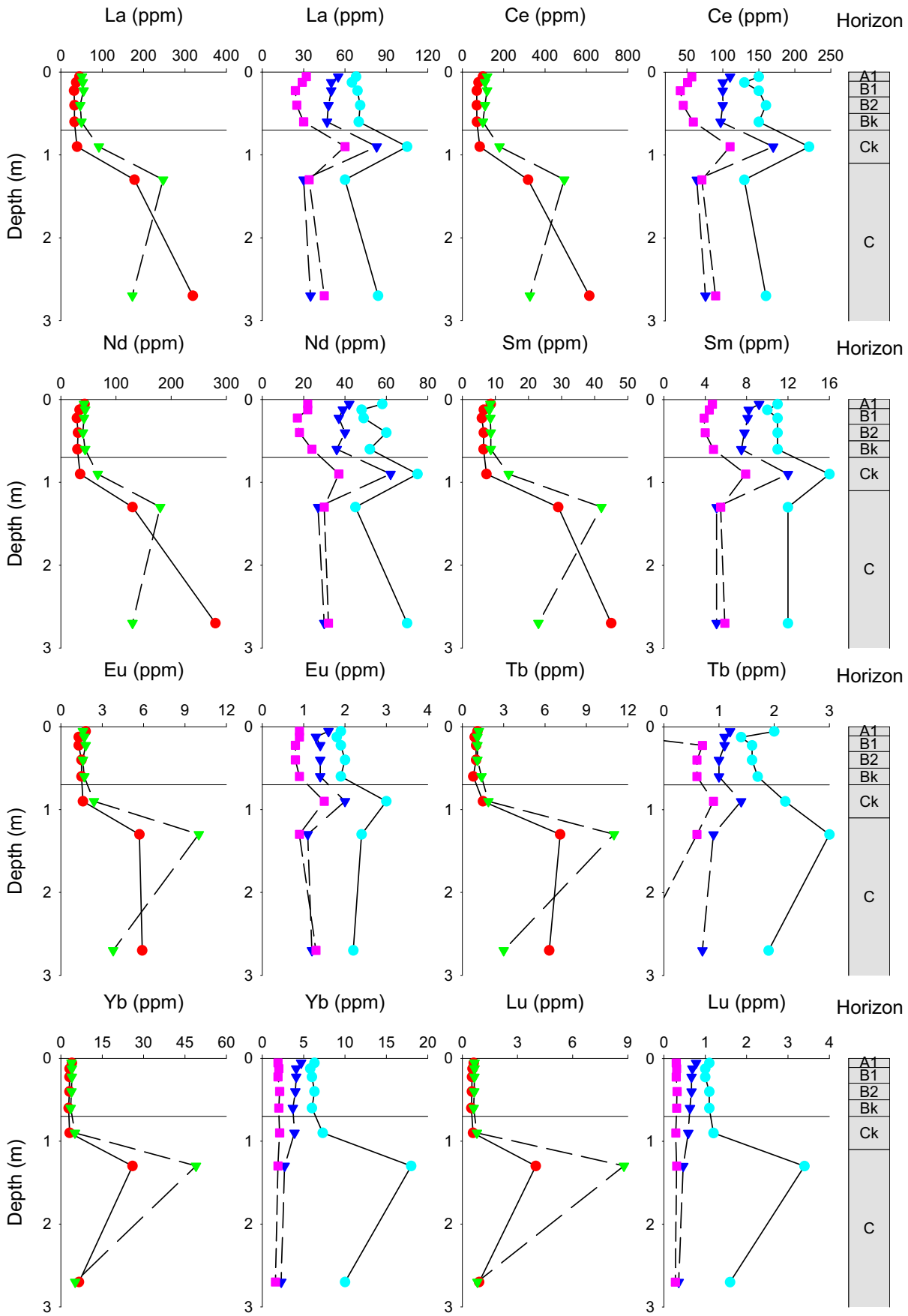

Figure 6.30: REE depth plots of size fraction assays for Profile 2.

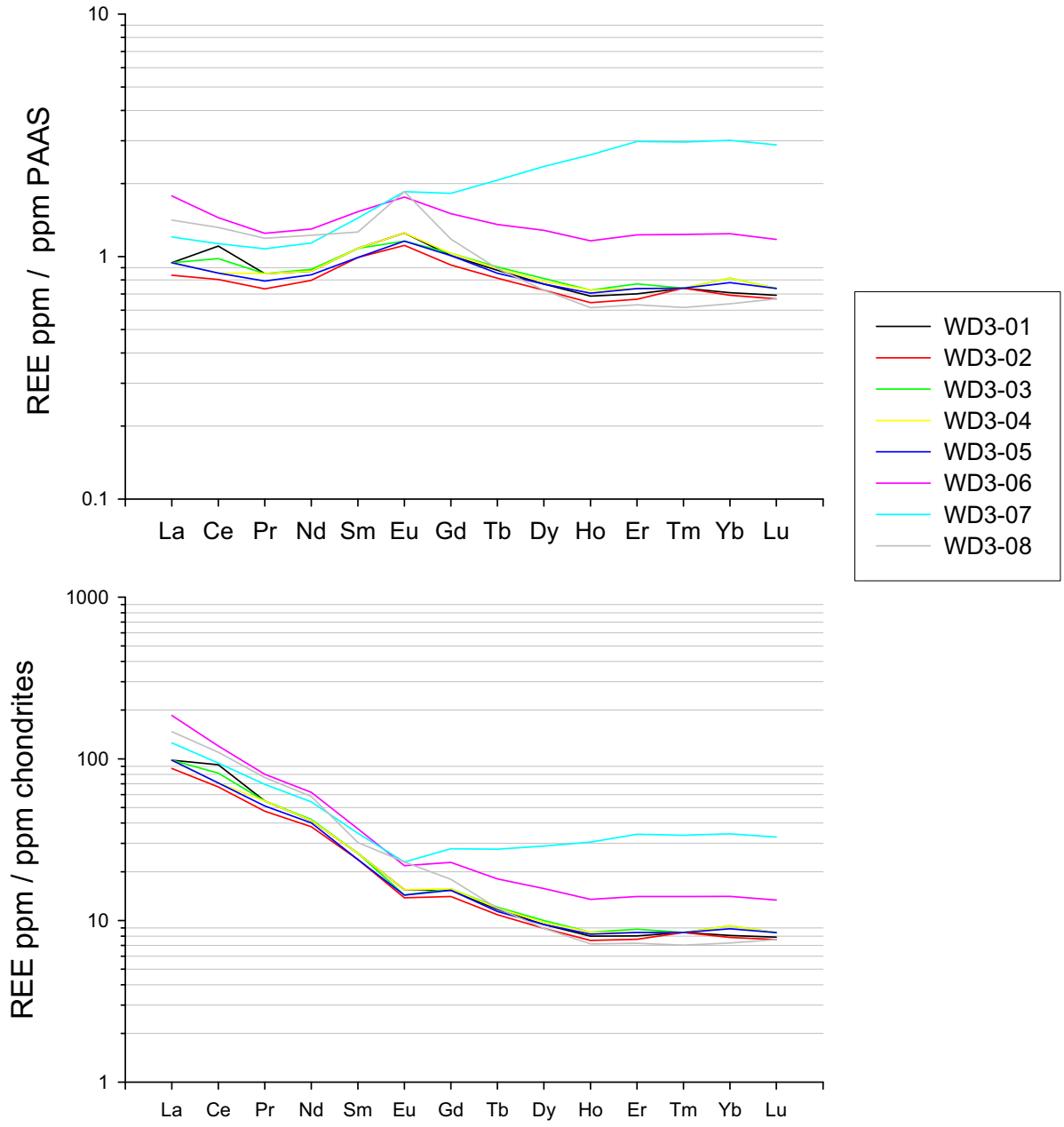

Figure 6.31: Chondrite and PAAS normalised REEs for Profile 2 (Taylor & McLennan, 1985; McLennan, 1989).

6.6. Mass balance analysis

Mass balance techniques described in Section 3.5.1, are applied to the data obtained for Profile 2 to determine gains and losses of major and trace elements. Results from this analysis are presented in this section. The critical factor of mass balance analysis is the determination of the uniformity of the profile and accurate determination of the parent material (Barshad, 1964; Brewer, 1964; Evans, 1978; Chadwick *et al.*, 1990; Brimhall *et al.*, 1991). Descriptions of Profile 1 presented above, show the existence of a palaeo-surface within the profile. It therefore does not meet this criterion and is unsuitable for the mass balance techniques described here. There is no obvious break in Profile 2, but the tests presented in the next section were undertaken to confirm this and to determine the parent material.

Physical appearance and macro-scale descriptions reveal a potential palaeo-surface in Profile 1, but it is not clearly expressed in the geochemical data. The majority of elements analysed have minor variations in concentration levels between the samples above and below the palaeo-surface, as discussed in Section 6.4.4. The best indication of the discontinuity is a change in the medium and coarse sand sand content between samples WD1-05 and WD1-06 of > 10% (Table 6.3). The 10% change is considered an indication of a discontinuity (Schaetzl, 1998). A similar change occurs at the saprolith-pedolith boundary (WD1-08 & WD1-09) where there is a sharp increase in gravel from 4 to 28%, suggesting that the entire pedolith is within transported material. A decrease in bulk density (Table 6.5) in sample WD1-06 differs from the otherwise gradual increasing trend down the profile; however, but this may be a function of soil formation rather than an indicator of a break in soil formation. Zircon grains in the heavy mineral fractions were rounded and etched above the palaeo-surface, suggesting that they have been transported (Figure 6.11 A & B).

Profile 1 is continuing to develop, and transported material was deposited in at least two stages. The reason for a limited geochemical expression of the palaeo-surface in Profile 1 is possibly due to the material being derived from the same source. Hence, following deposition of sediment, a soil developed and was exposed to erosion resulting in the formation of the palaeo-surface. Following this, further deposition occurred from the same source as the initial material. The current soil profile is now developing within this additional sediment. The similarities between the two soils are therefore due to the same source material. The directly underlying pegmatite and biotite gneiss that it intrudes are therefore not the parent material for this profile; however, the gneiss extends over a large area of the landscape and is therefore the most likely initial source material.

6.6.1. Tests for uniformity in Profile 2 and selection of parent material

No discontinuities were recognised within the macro-features of Profile 2. Instead, the diffuse and gradual boundaries (Figure 6.22) between the saprolith and overlying soil horizons (Table 6.7) support uniformity. The profile is in an erosional setting (Figure 6.3), hence deposition of the overlying material is restricted to minor amounts of aeolian, colluvial, or sheetwash material. The profile is therefore more likely to have been formed *in-situ*, however, this should not be assumed.

The distribution of weathering resistant minerals such as, zircon, rutile, tourmaline, garnet, and quartz are useful in determining uniformity (Marshall & Haseman, 1942; Barshad, 1964; Brewer, 1964; Evans, 1978; Santos *et al.*, 1986; Beshay & Sallam, 1995). Sand fractions are generally used for this analysis because: 1) they tend to have the highest concentration of primary minerals; and, 2) minerals in these fractions are less likely to have been translocated than the clay and silt fractions (Barshad, 1964; Brewer, 1964; Fitzpatrick & Chittleborough, 2002). Ratios of two resistant minerals within a size fraction, or the same mineral in two size fractions are generally used. The basis of the analysis is that collapse or expansion of a soil horizon reflects flux changes, which affect the concentration of a mineral; however, the ratio between two immobile constituents remains constant. A profile formed from uniform material will plot as a near vertical line (Santos *et al.*, 1986).

Uniform ratios through a profile indicate that two constituents have behaved the same way; hence they may have both been removed from the profile by equal amounts. Therefore this does not guarantee that two constituents are immobile, and presents a potential problem in the use of ratios (Brimhall *et al.*, 1991). Another problem arises when the values are very low. If the low values are in the denominator then the differences in the ratios may be amplified and difficult to interpret (Beshay & Sallam, 1995; Schaetzl, 1998).

Grain count results for the fine and medium sand fractions are discussed in Section 6.5.2 and presented in Table 6.9. Results and associated ratio plots of the rutile, zircon, and ilmenite grain counts are plotted in Figure 6.32. Ilmenite is included because of its Ti content ($FeTiO_3$). The ratios for the medium sand fraction are generally lower and less variable than for the fine sand. All ratios are < 1 and are reasonably uniform through the pedolith apart for the zircon/rutile ratio where the fine sand fraction varies from 0.3 to 0.9 in the pedolith. In the saprolith, the zircon/ilmenite ratios for both size fractions increases significantly towards the base. This may be because of the very low ilmenite percentage. Similar increases, but not as large, in the other ratio values may reflect low rutile percentages and are therefore a sampling and counting error. Variations within the ratios are shown in Table 6.12 and are discussed along with element ratios below.

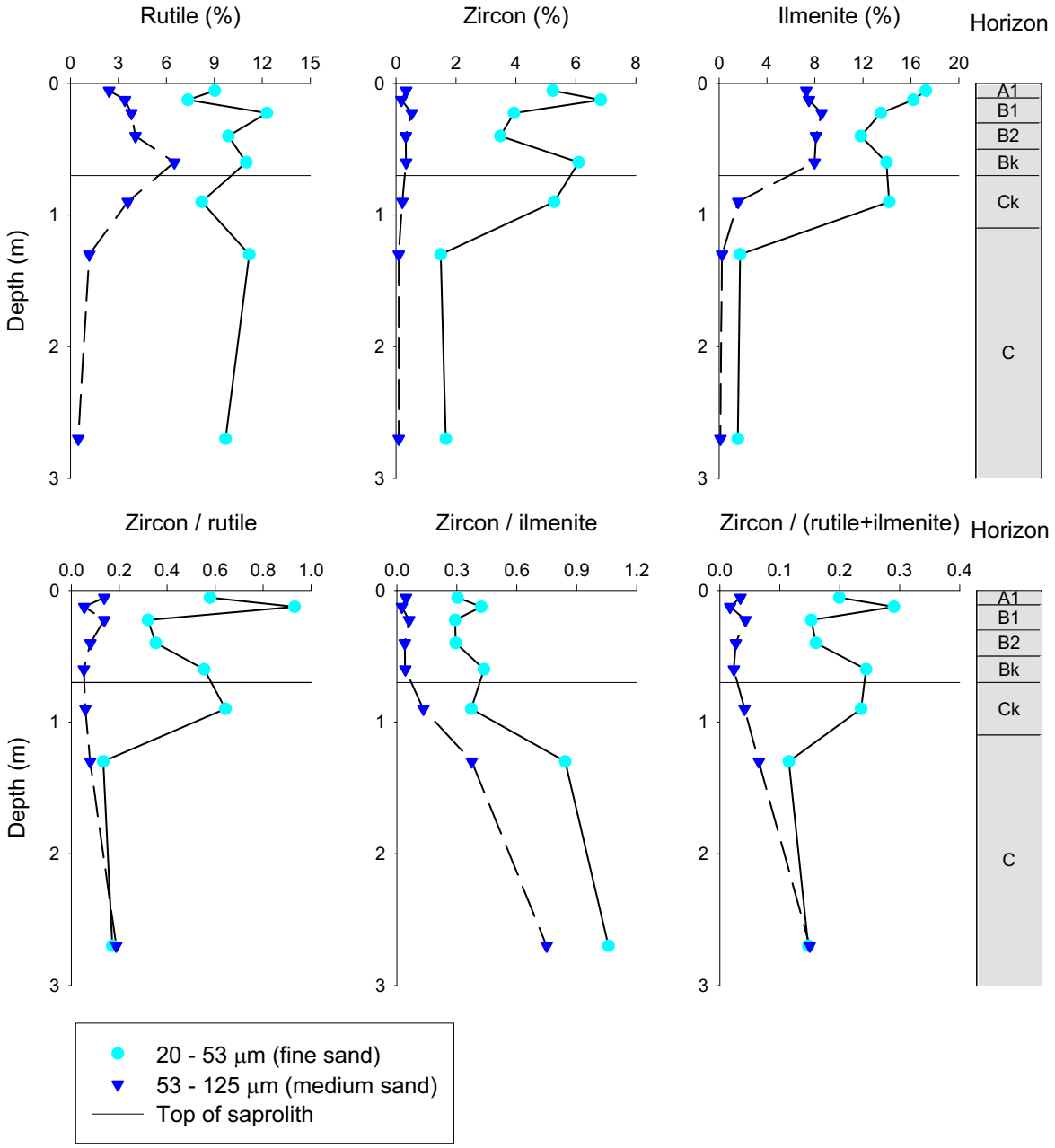

Figure 6.32: Zircon, rutile and ilmenite grain counts of sand fractions and associated ratios by profile depth.

Elemental assays may be substituted for mineral counts and offer a more rapid solution, although the source of an element is not always restricted to a single mineral. For example Ti may be present within rutile, anatase, and ilmenite (Brimhall & Dietrich, 1987; Chadwick *et al.*, 1990; Fitzpatrick & Chittleborough, 2002). Size fraction assays of Zr and Ti were completed on the clay-sized, fine, and medium sand fractions by XRF and included in the bulk sample assays by ICP-OES. These assays and associated ratios are shown in Figure 6.33.

Concentration of Ti in the size fractions is higher and more variable than in the bulk sample. The sand fractions have similar dispersion patterns through the pedolith with a decrease in concentration at the base (WD3-05), followed by a significant elevation towards the base of the saprolith. In the fine sand however, the Ti concentration is approximately 1500 ppm higher through the pedolith and increases to 4195 ppm at the base of the saprolith. Highest variation is in the clay-sized fraction, which decreases from 6,293 ppm at the top of the pedolith to 3,895 ppm at the base, before increasing to > 10,000 ppm for the lower two saprolith samples (WD3-07 & WD3-08).

The Zr dispersion pattern is relatively uniform for the bulk and all size fractions through the pedolith. In the fine sand fraction however, the Zr concentration is approximately five times higher. This is illustrated in Figure 6.33 where the Zr concentrations have been scaled down by 10 in order to plot them on the same axis as the other size fractions. At the top of the saprolith, Zr concentrations are similar to those in the pedolith. At the base of the saprolith, in the clay-sized and fine sand fractions however, there is a significant increase in Zr.

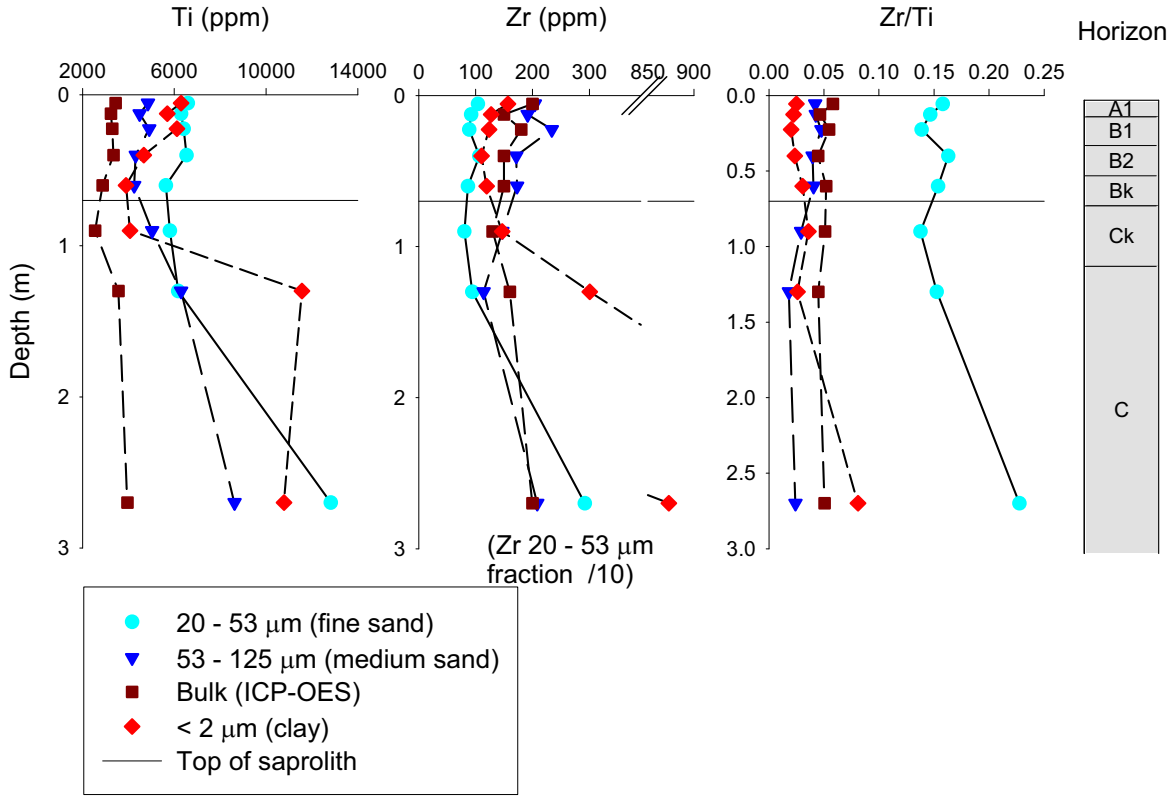

Figure 6.33: Plot of Ti and Zr concentrations as determined by XRF for the clay, fine and medium sand fractions, and by ICP-OES for the bulk samples. Note: Values for Zr in the 20-53 µm fraction have been divided by 10.

The Zr/Ti ratios for each size fractions and the bulk samples have minimal variation through the profile, especially when compared with the zircon, rutile and ilmenite ratios Table 6.12. Variations in the mineral ratios are lower in the medium than the fine sand fraction. The combined zircon / (rutile + ilmenite) ratio has the lowest variation in both sand fractions, but it does not match the low variations of the Zr/Ti ratios. Variation of the medium sand fraction is also very low for the Zr/Ti ratio (±0.007); however, the lowest variation is for the bulk material (±0.003).

Ratios of grain size, particularly the non-clay fractions, have been used to test for textural uniformity through the profile (Barshad, 1964; Raad & Protz, 1971; Evans, 1978; Asady & Whiteside, 1982; Cremeens & Mokma, 1986; Beshay & Sallam, 1995; Schaetzl, 1998; Tsai & Chen, 2000). This is based on the idea that in the coarser fractions, weathering is reduced and there is a higher content of more resistant minerals such as quartz, compared with clay-sized and silt fractions. The fine sand/silt, medium sand/fine sand, and coarse sand/medium sand, ratios for Profile 2 are plotted in Figure 6.34 and the variations are summarised in Table 6.13.

Concentrations through the profile are relatively uniform for all the sand fractions with a < 10% difference between samples (Table 6.8). An exception is at the base of the saprolith between samples WD3-07 and WD3-08 for the medium and coarse sand fractions where there is a > 10% decrease for the medium sand and equivalent increase for the coarse sand.

Table 6.12: Comparison of mean ± 2SE (n = 8) for Zr/Ti, and zircon, rutile, and ilmenite ratios.

Size Fraction	zircon/ rutile	zircon/ ilmenite	zircon/ (rutile+ilmenite)	Zr/Ti
Bulk	–	–	–	0.050 ±0.003
< 2 μm (clay-sized)	–	–	–	0.033 ±0.013
20–53 μm (fine sand)	0.460 ±0.370	0.502 ±0.403	0.193 ±0.142	0.160 ±0.019
53–125 μm (medium sand)	0.099 ±0.077	0.184 ±0.214	0.050 ±0.045	0.035 ±0.007

Table 6.13: Summary of mean ±2SE (n=8) for the sand fraction ratios.

Size fraction ratio	Mean ±2SE (n=8) Full profile	Mean ±2SE (n=6), to Ck horizon (WD3-06)
53 -125 μm (medium sand) / 20 – 53 μm (fine sand)	2.56 ±1.84	2.30 ±1.89
20 – 53 μm (fine sand) / 2 – 20 μm (silt)	1.16 ±0.91	0.85 ±0.70
125 – 2,000 μm (coarse sand) / 53 -125 μm(medium sand)	3.64 ±2.86	2.91 ±2.40

The sand fraction ratios gradually decrease through the profile up to the top of the saprolith, where they increase significantly. Variations in the size fraction ratios are significantly higher than those in the mineral and element ratios presented in Table 6.12. The increased sand content of the lower saprolith samples (WD3-07 & WD3-08, see Figure 6.23) appears to have a negative effect on the ratios of the size fractions, however, if the two samples are removed from the calculations the standard error is reduced, but still larger than the variance in the grain and element ratios (Table 6.13).

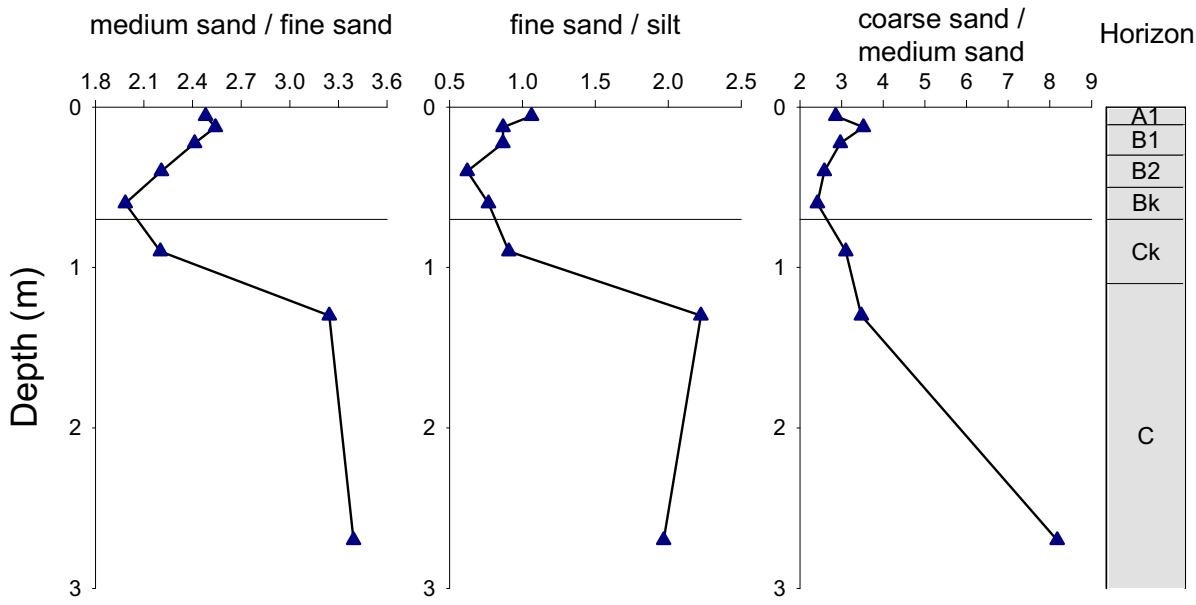

Figure 6.34: Ratios of sand and silt fractions plotted by profile depth.

Several of the elemental assays and grain counts have significant variations in samples WD3-07 and WD3-08 from those in the overlying samples. These samples are at the base of the saprolith and warrant further discussion. The two samples are of a weathered biotite gneiss that has few pedologic features, hence the samples were more rock than soil. The impact of this is most significant within the size fractions where the clay-sized and silt fractions are < 2 and 3% respectively. This is potentially a true reflection of the samples, however, the initial separation process of lightly crushing the material to break up the peds may not have been as efficient on the more consolidated lithic fragments. The particle size distribution is therefore likely to be inaccurate for the saprolith samples (WD3-07 & WD3-08). There is also an increased risk of analytical errors due to the small sample sizes.

The data presented above do not indicate the presence of a discontinuity within Profile 2, hence the material appears to have developed *in-situ* from the underlying biotite gneiss (WD3-08). Mass balance calculations, as described in Section 3.5.1 can therefore be applied to sample data obtained from this profile with sample WD3-08 as the parent material.

6.6.2. Mass balance calculations for Profile 2

From the analysis in Section 6.6.1 it is concluded that the parent material of Profile 2 is uniform. It is therefore feasible to undertake the mass balance calculations detailed in Section 3.5.1 on the samples. The first stage of this analysis requires the calculation of any volume change (strain) within the weathered material and requires the selection of an immobile element.

The extremely low variation throughout the profile (pedolith and saprolith) in the Zr/Ti ratios (Table 6.12) is an indication that the profile has formed from uniform material without unconformities (Barshad, 1964; Beshay & Sallam, 1995).

Relative to the mineral counts and size fraction assays, elemental ratios are more representative of the value since the samples have undergone less preparation, and therefore have a lower risk of introduced analytical errors. Zirconium and Ti are candidates for selection as the immobile element for further mass balance calculations on the data from

Profile 2. Both Zr and Ti have been used in previous research as immobile elements (e.g. Smith & Wilding, 1972; Jersak, 1991; Beshay & Sallam, 1995; Jersak *et al.*, 1995). It has been shown however, that Ti can be mobile in the weathering environment (Sudom & Arnaud, 1971; Smith & Wilding, 1972; Smeck & Wilding, 1980; Fitzpatrick & Chittleborough, 2002). This view was supported by FESEM observations of rutile and ilmenite in the heavy mineral fractions, which showed that many of the grains had dissolution features and were highly etched (Figure 6.11 D, E, & F, and Figure 6.24 C, D, & E). The data presented above also shows that Ti has more variation through the profile compared with Zr, possibly because a proportion is contained within ilmenite. Therefore Zr is chosen as the preferred immobile element for the mass balance calculations presented here.

The lowest saprolith sample (WD3-08) is taken as the representative parent material for Profile 2. This is based on the above ratio data and also because many of the element assays discussed in Section 6.5.4 have similar concentrations in the lower saprolith samples (WD3-07 & WD3-08), suggesting that they are representative of an homogeneous parent material.

The volumetric (strain) changes that have occurred due to soil forming processes for Profile 2, along with the physical properties used to derive them, are shown in Figure 6.35. The strain ($\varepsilon_{Zr,w}$) was calculated using equation 3.8 with Zr as the immobile element and assay values from sample WD3-08 as the parent material.

The bulk density (ρ_b) decreases up the profile from the initial parent material value, resulting in an increasing trend up the profile in the bulk density ratio (ρ_p / ρ_w). The highest bulk density ratio is at the top of the B1 horizon (WD3-02). The profile is generally depleted in Zr for both absolutely (weight %) and relative to parent Zr concentration (enrichment factor $C_{Zr,w} / C_{Zr,p}$). At the top of the profile the Zr concentration is the same as the parent material. There is a deviation from the Zr trend at the top of the B1 horizon (WD3-02), which has a lower concentration than its surrounding samples.

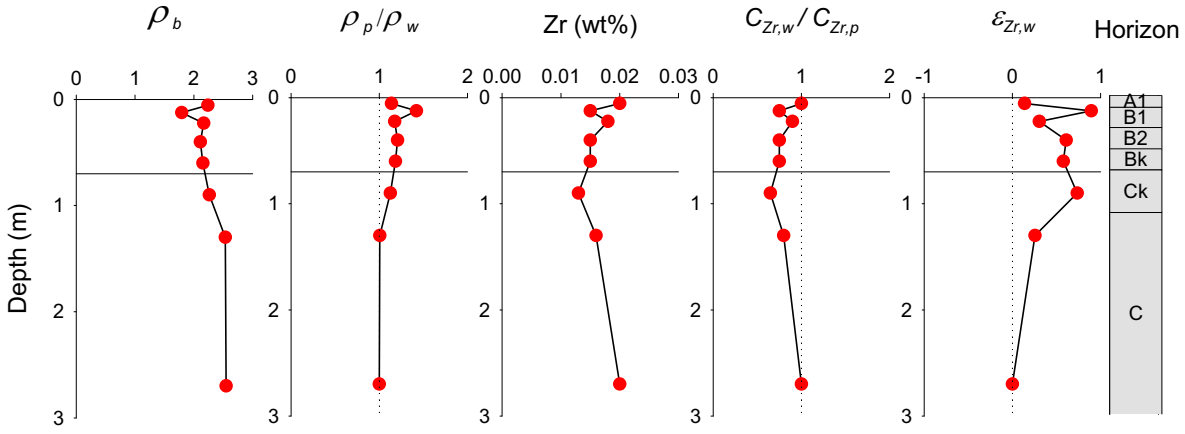

Figure 6.35: Depth plots of bulk density (ρ_b), bulk density ratio (ρ_p / ρ_w), Zr concentration, enrichment factor ($C_{Zr,w} / C_{Zr,p}$), and strain ($\varepsilon_{Zr,w}$) for Profile 2.

The top of the B1 horizon has the highest positive strain value of 0.89 or 89% dilation. This is due to the high bulk density ratio and low Zr concentration. These values do not fit with the general trend of the profile as measured in the other samples and may therefore indicate a discontinuity in the profile. This is possibly an analytical error caused by the small sample size. Sample WD3-02 was collected from a total thickness of only 4 cm. This sample could be removed from the dataset and instead use sample WD3-03 to represent the complete B1

horizon. This would mean ignoring potentially valuable data and so the sample has been retained and treated as valid. The last point to note is that despite the high dilation of 89%, the small thickness represented by this sample, which is used in overall mass calculations, negates this large increase. In the following discussion the values calculated from this sample are considered carefully and not discussed where they are extreme.

Positive strain ($\varepsilon_{Zr,w}$), or dilation, has occurred throughout the profile with values in excess of 0.58 (58%) in the B2, Bk and Ck horizons (Figure 6.35). These horizons coincide with the highest clay-sized and $CaCO_3$% content (Table 6.8 & Table 6.10). The higher clay-sized content may give rise to mechanical movement through shrink–swell processes. Above the B2 horizon the amount of dilation decreases to 31 and 14% for the B1 and A1 horizons respectively.

Dilation may be due to changes in bulk density and/or additions to the profile. It is not possible to determine the direction of dilation from mass balance equations, however, it is most likely to be vertical (Jersak *et al.*, 1995). If this assumption is made then an estimate of the original profile thickness prior to soil development can be calculated from the strain. The change in mass, and hence the original mass can be estimated by rearranging equations 3.2 and 3.3 so that:

$$\Delta M = \rho_w V_w \left(1 - \frac{C_{Zr,w}}{C_{Zr,p}} \right) \qquad [6.1]$$

Figure 6.36 illustrates the results of these calculations for a 1 cm^2 column through the profile. Dilation of the original profile is equivalent to approximately 45 cm in thickness with a material gain in total mass of ~73 g. These gains are significant given the erosional landscape position of the profile and therefore show that there as been an overall enrichment in material despite the loss of material through erosion.

Elemental flux changes, or percentage gains and losses were calculated using the mass transport function (equation 3.7) and from this, actual mass changes for each horizon (equation 3.12), and the total profile (equation 3.13) were determined. A table of these results is included in Appendix 7. The mass changes of the major and trace elements are discussed in the following sections.

6.6.3. Major element mass changes for Profile 2

The estimated dilation and mass gains in the profile (Figure 6.36) suggest large additions to the profile. The majority of major elements support this with only Al, K and Mg having an overall material loss (Table 6.14). The largest mass flux gains are Ca, especially in the B2, Bk and Ck horizons with gains of 1,096, 2,656 and 3,336% respectively, which equates to a total material gain for a cm^2 column through the profile of ~148 g (Figure 6.37). In absolute mass terms the gain in Si (~161 g) is slightly higher than Ca, but the gains are more evenly spread throughout the profile. The Si weight percent and enrichment factor suggests a loss of material in the B2, Bk, and Ck horizons where Ca had its largest gains, but when corrected for density and volume changes there are material gains in these horizons of 28, 12, and 26% respectively (Figure 6.37).

Mass flux gains are also apparent for Fe, Na, and Mn (Table 6.14). The percentage Fe increase was between 61 and 98%, apart from the A1 horizon where the gain was 37%. The

highest gain was in the B2 horizon. Although Na had an overall mass gain it had a material loss in the B2 and Bk horizons. The main gains of Na were in the Ck and C horizons.

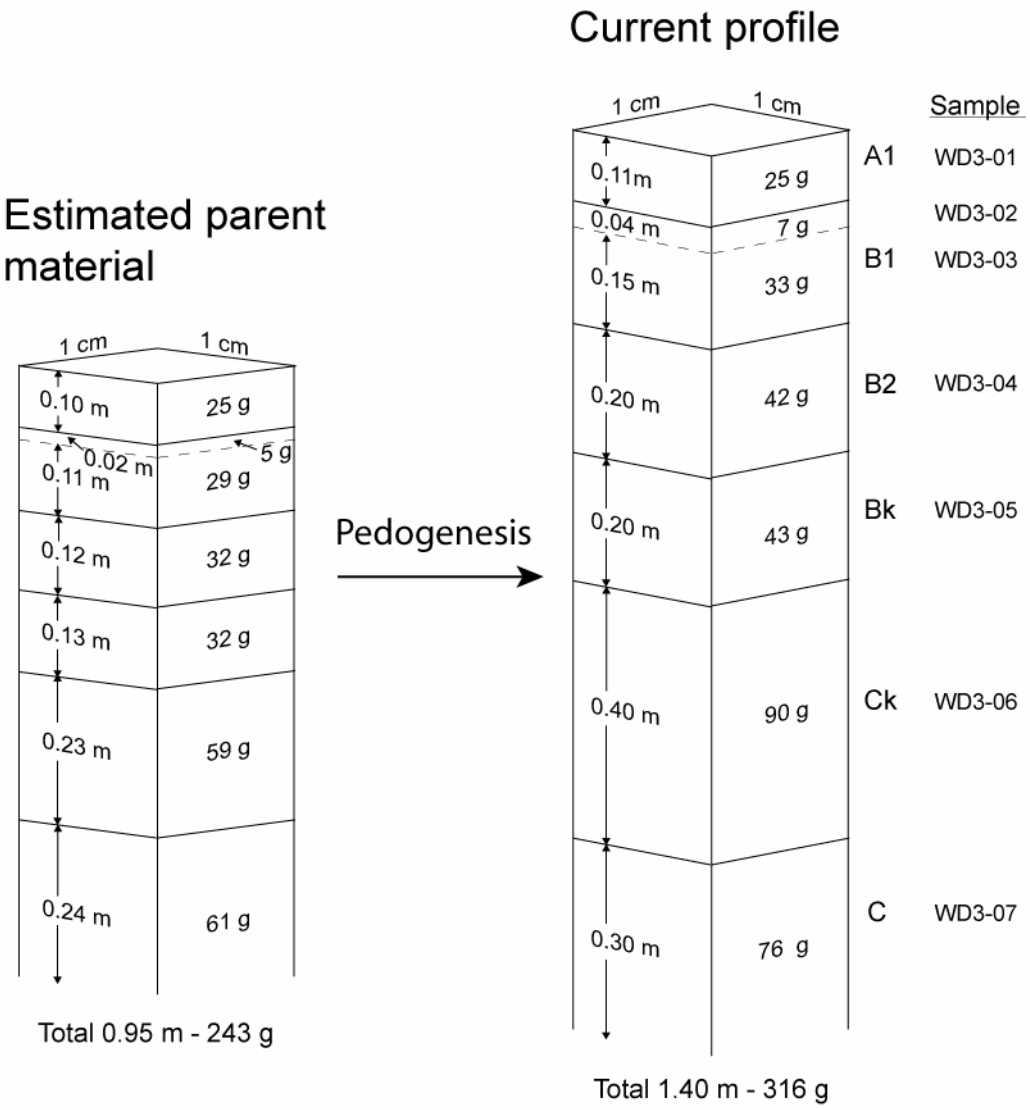

Figure 6.36: Estimates of original profile depth and mass calculated from volumetric changes and Zr concentrations.

The largest material loss (130 g) through the profile was K with a loss of >69% in all horizons apart from the C horizon (42%). The only other major element to have a significant loss through the profile was Al (-11.49 g). Despite the overall loss of Al there was a gain of 5.8 g in the C horizon and only a minor loss in the B2 horizon of 0.11 g (Figure 6.37 and Table 6.14).

The material increase through the profile is reflected in the elemental gains. Whereas some of these gains may be through enrichment due to the loss of elements such as K, the large increases, especially in the Bk and Ck horizons are due to the addition of material derived from an external source. These additions and/or enrichments are discussed further in Section 6.8.

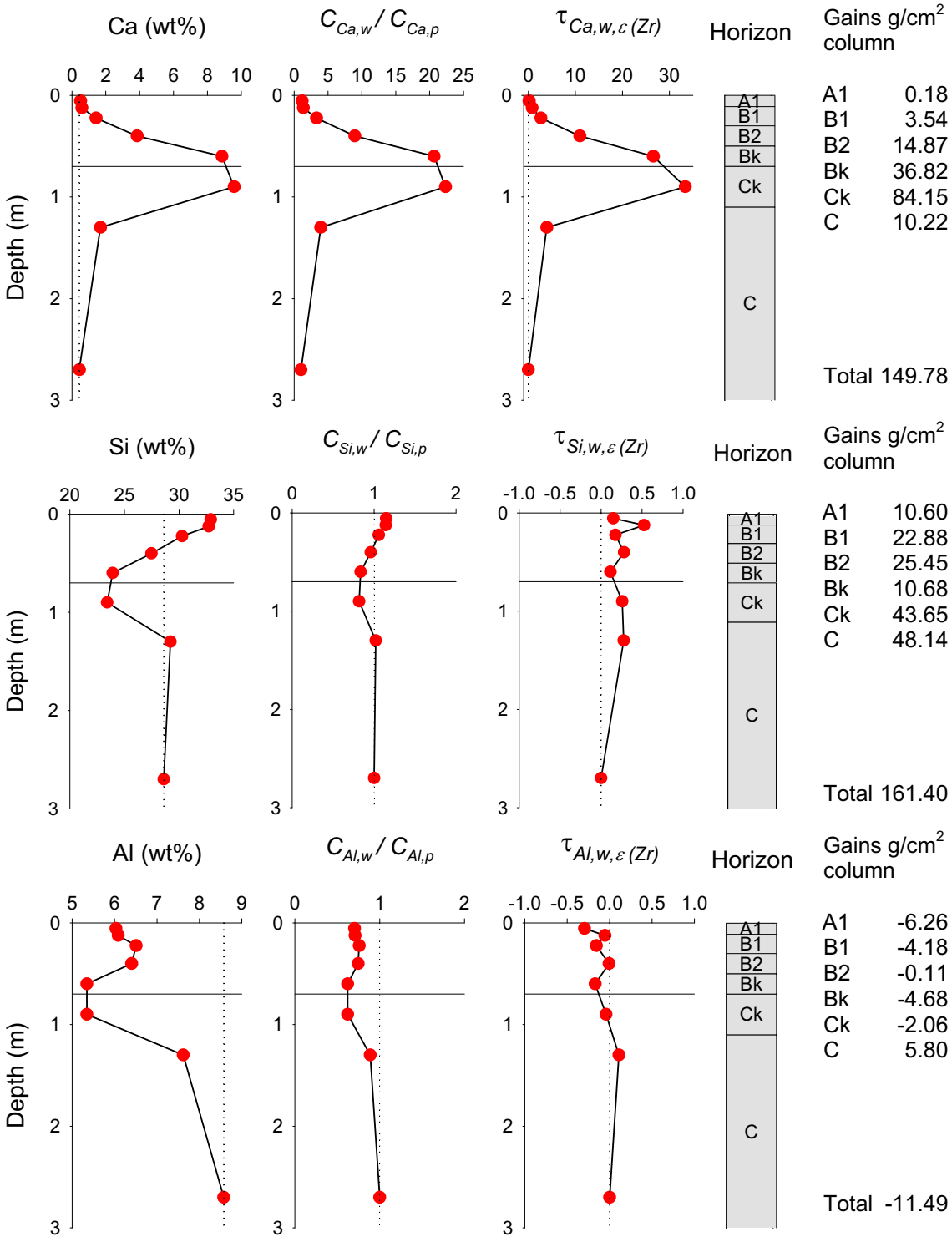

Figure 6.37: Depth plots of selected major element concentrations, enrichment factor ($C_{Zr,w}/C_{Zr,p}$), transport function ($\tau_{El,w,\varepsilon(Zr)}$), and mass flux changes for Profile 2.

Table 6.14: Major element mass flux gains or losses by horizon and in order of maximum gain/loss.

Input / Enrichment (g/cm^2)	Horizon	Loss (g/cm^2)
Si(10.6), Fe(2.4), Ca(0.2), Mn(1.1), Na(0.4)	**A1**	K(16.0), Al(6.3), Mg(1.5)
Si(22.9), Fe(6.1), Ca(3.5), Na(0.6), Mn(0.3),	**B1**	K(21.5), Al(4.2), Mg(1.1)
Si(25.5), Ca(14.9), Fe(8.1), Mg(0.4), Mn(0.3)	**B2**	K(19.1), Na(0.6), Al(0.1)
Ca(36.8), Si(10.7), Fe(6.1), Mn(0.2)	**Bk**	K(20.0), Al(4.7), Na(0.3), Mg(0.0)
Ca(84.2), Si(43.6), Fe(11.2), Na(6.4), Mn(3.6), Mg(0.7)	**Ck**	K(32.6), Al(2.1)
Si(48.1), Ca(10.2), Na(11.1), Fe(9.7), Al(5.8), Mg(1.5), Mn(0.3)	**C**	K(20.5)

6.6.4. Trace and rare earth element mass changes for Profile 2

Flux changes for the majority of trace elements are generally between ±20%. Where elements show an overall loss there is at least one horizon, typically the C and / or Ck that have been enriched. Of particular interest in this study are those elements associated with Au mineralisation.

The Au concentration and enrichment factor for the profile suggests that there has been a loss of Au through the pedolith and enrichment at the top of the saprolith (Figure 6.38). The transport function (τ) supports the enrichment in the saprolith, but values also show a slight enrichment in the B2 horizon. The highest loss of Au was at the surface (-0.79 or 79%). Losses in the remainder of the profile were only ~14% in the B1 and B2 horizon and 5% in the Bk horizon. The concentration, enrichment factor and flux of Ag shows a general loss throughout the profile of approximately 50% (Figure 6.38).

One of the largest percentage gains is for As with increases in excess of 100% for all horizons apart from the A1 horizon (25%) (Figure 6.39). The highest gains were in the lower horizons (B2, Bk, & Ck) and top of the saprolith with values > 330%.

In absolute mass gains, Cu had an overall increase of 1 g for the cm^2 column, although this is misleading since there was a loss of material for all soil horizons (Figure 6.39). The increase in the saprolith of 169 and 306% in the Ck and C horizons respectively, also coincides with high concentrations compared with the soil samples, which emphasises / exaggerates the difference. In the upper soil horizons (A1 & B1) the Cu losses are > 69%, which drop to a still relatively high > 40% loss in the B2 and Bk horizons.

Other elements that have large losses through the profile are Ba, Cr, Cs, Mo, Rb, Sc, Th, Tl, U, and Zn. Of these elements, Ba, Mo, Rb, U, and Zn, have losses > 50% for most if not all horizons. In the Ck and C horizons Zn has a percentage gain of 10 and 79% respectively, which is a similar profile enrichment and loss pattern as Cu.

The REEs show a general increasing gain in transport function value from the LREEs to HREEs through the profile (Figure 6.40). There are also distinct patterns for where these gains occur within the soil profile. All of the REEs have gains in the saprolite. In the C horizon these range from 5% in the LREEs to 500% in the HREEs. A similar pattern is present in the Ck horizon, but the range, from 60% in the LREEs to 200% in the HREEs is significantly less. Gains and losses in the pedolith are best described by splitting the REEs into three groups, LREEs, MREEs, and HREEs.

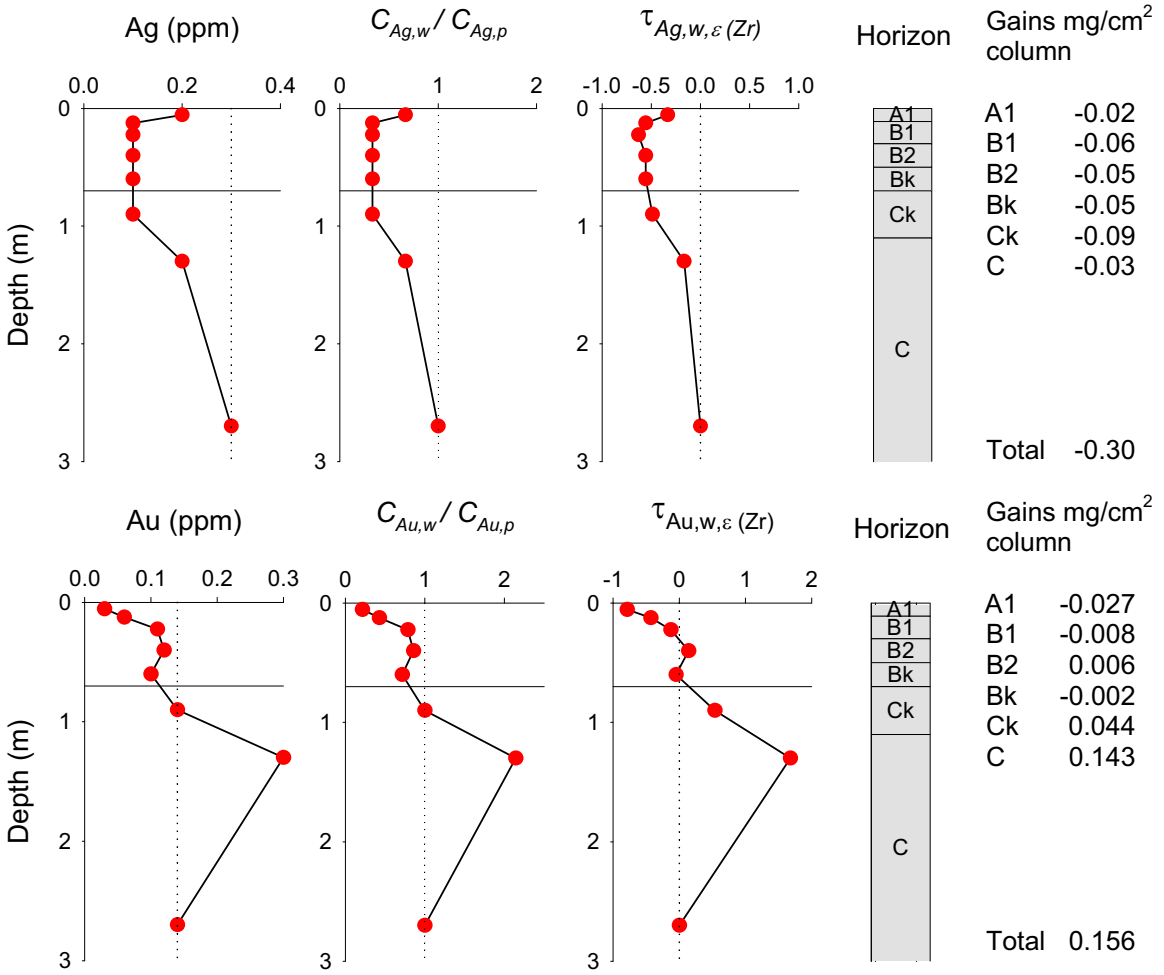

Figure 6.38: Depth plots of concentration, enrichment factor ($C_{Zr,w}/C_{Zr,p}$), transport function ($\tau_{El,w,\varepsilon(Zr)}$), and flux changes for Au and Ag in Profile 2.

There has been a loss of the LREEs throughout the profile with the highest losses towards the surface (Figure 6.40). Theses losses range from 5% in the B2 and Bk horizons and increase to 33% in the A1 horizon. This trend continues into the MREEs except that the losses gradually reduce to become gains starting with the deeper samples and lighter elements. Hence by Dy and Ho, only gains have occurred. The exception to this trend is Eu, which has a loss throughout the profile of 10 to 33% in the B2 and A1 horizons respectively. The HREE fluxes are all positive with gains as high as 70% (Yb) in the B2 horizon (Figure 6.40) and 20% (Tm) in the A1 horizon.

6.7. Gold morphology in the White Dam profiles

In addition to the analytical results presented above, time was spent in trying to locate and view the Au both *in-situ* and in the particle separates as described in Section 3.5.7. The results were disappointing especially with the thin sections of the impregnated (*in-situ*) samples. Despite searching using both manual and automatic techniques, no Au was located on these samples. This indicated that the Au was extremely fine and likely to be evenly dispersed throughout the sample. Although this condition is a hindrance to physical observations it is a benefit in exploration since it negates the nugget effect that is typical in Au assays.

Due to the separation method by gravity settling (Section 3.5.2.2) and the high density of Au (19.3 g.cm^{-3}) compared with most silicate minerals (~2.7 g.cm^{-3}), the size of the Au particles within the silt fraction were actually from 0.6 – 6 µm. This size difference added to the difficulty of locating the small grains against the larger silt particles (Figure 6.41C).

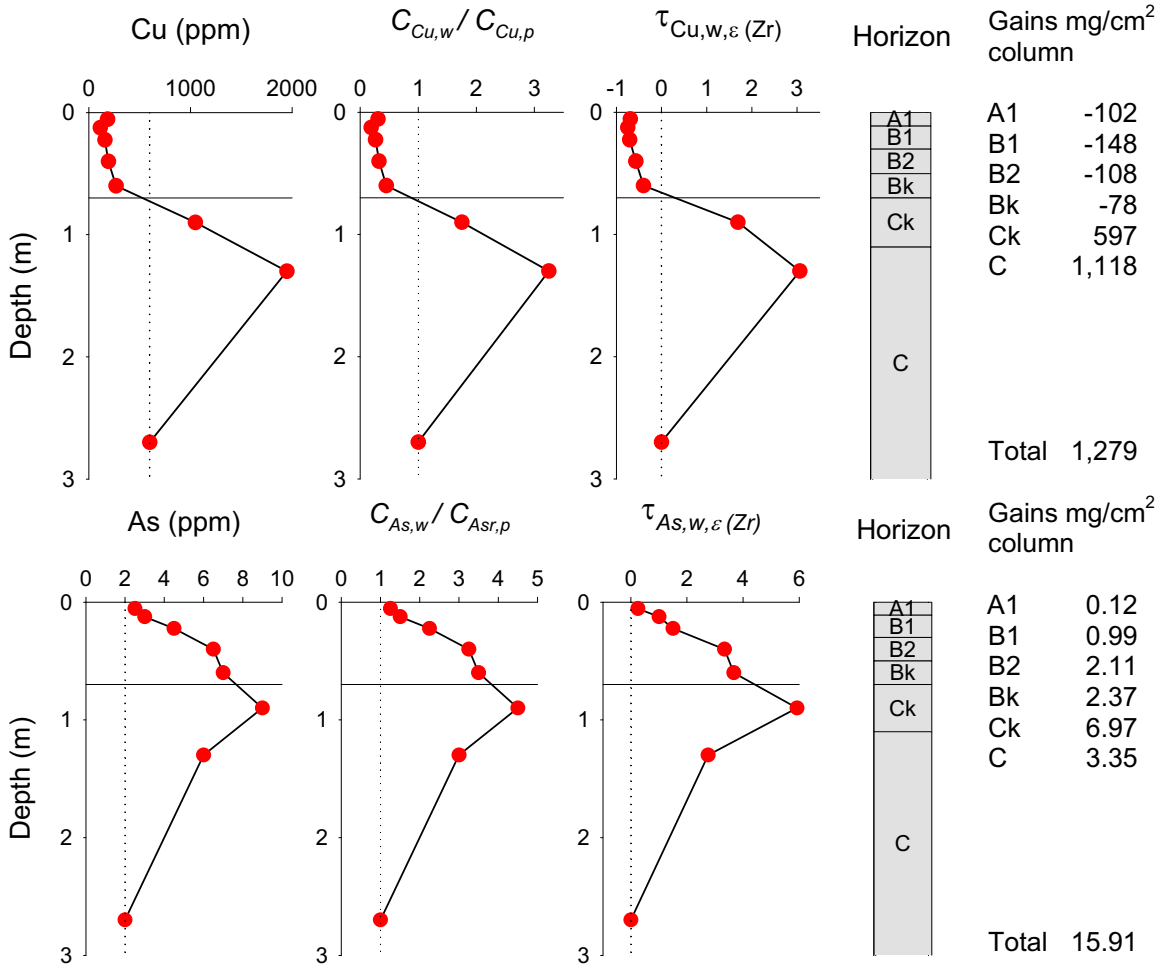

Figure 6.39: Depth plots of concentration, enrichment factor ($C_{Zr,w}/C_{Zr,p}$), transport function ($\tau_{El,w,\varepsilon(Zr)}$), and flux changes for Cu and As in Profile 2.

To improve the chances of locating Au grains, the heavy mineral separates were used from the density separation procedure (Section 3.5.5). Hence the samples placed in the FESEM only had those minerals that had densities > ~2.9 g.cm^{-3}. Although this removed most silicate minerals, biotite, with a density > 2.9 g.cm^{-3}, was not removed and made up a large proportion of the minerals on the prepared mounting stubs. Despite these issues, Au grains were located in the silt fraction of Profile 1, which had the highest Au concentrations through most of the profile (Figure 6.15 and Figure 6.28). Several grains were located in the saprolith samples and one grain was located in the B2 horizon.

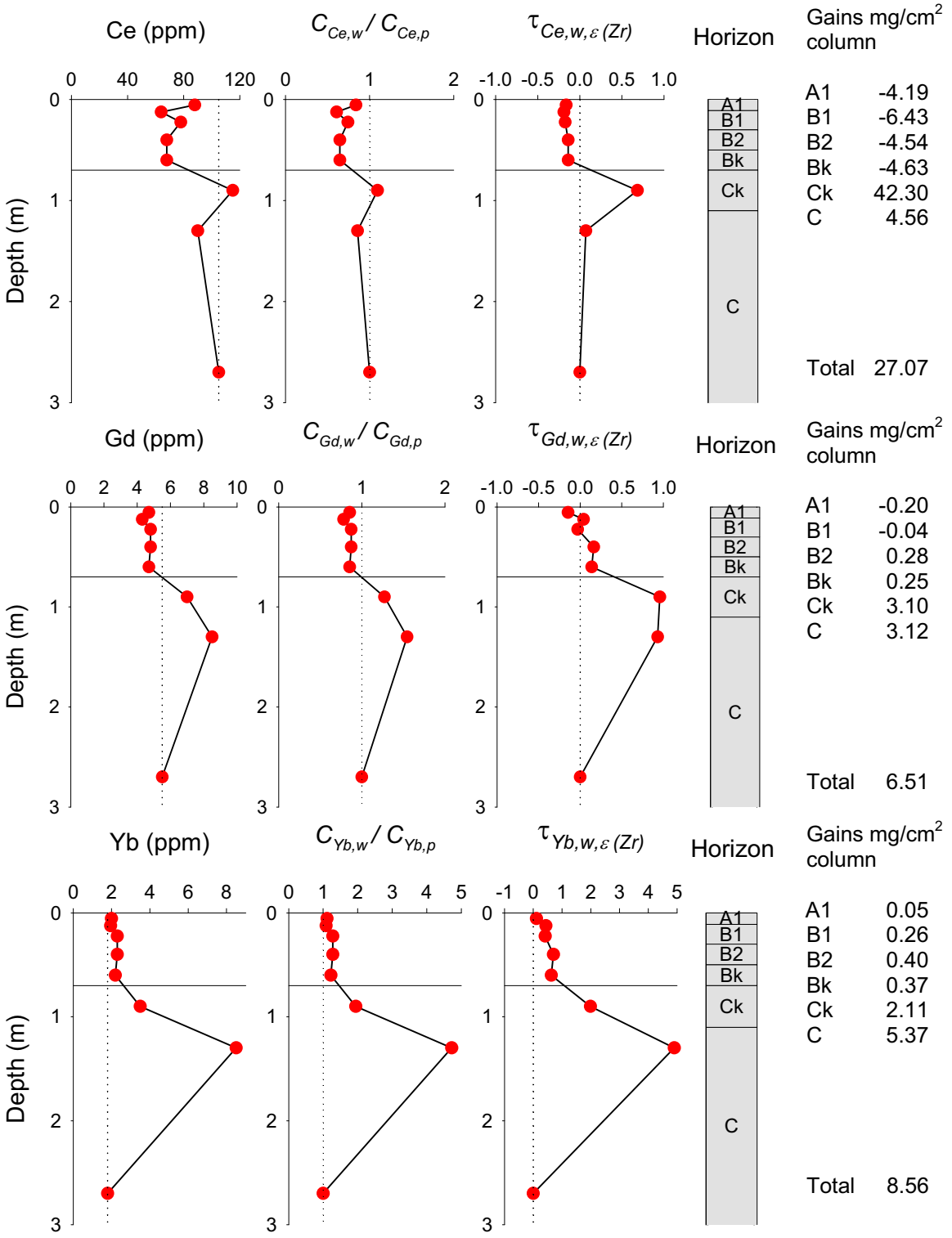

Figure 6.40: Depth plots of concentration, enrichment factor ($C_{Zr,w}/C_{Zr,p}$), transport function ($\tau_{El,w,\varepsilon(Zr)}$), and flux changes for Ce (LREE), Gd (MREE) and Yb (HREE) in Profile 2.

The morphology of Au grains within the saprolith tended to be smooth, rounded and about 1 µm in diameter (Figure 6.41A, B, & D). Many of the grains were obscured by, or possibly imbedded within the larger biotite grains (Figure 6.41A). This fits with previously described Au and biotite associations at White Dam, although the size of the observed Au grains is considerably smaller than the Au platelets described for the oxide zone of up to 165 µm

(Cordon, 1998; Croxford, 1998; Cooke, 2003). This suggests that during pedogenesis the Au has been altered through weathering processes, or mobilised in solution and reprecipitated.

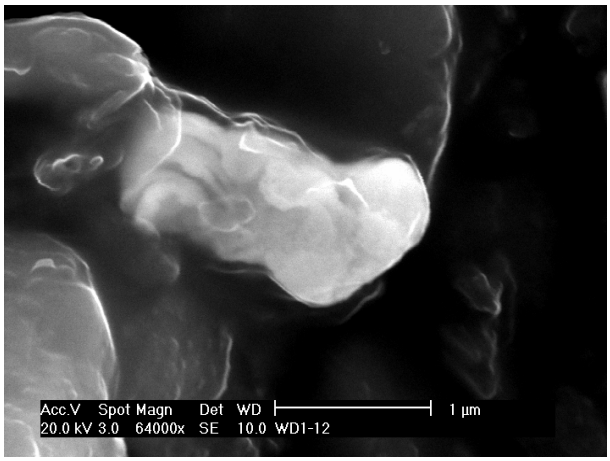

A. Gold grain from base of saprolith that is partially covered by and possibly associated with biotite

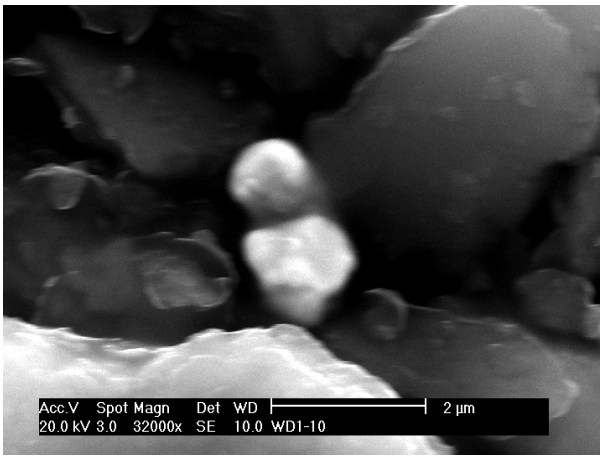

B. Free angular Au grain amongst larger biotite grains from saprolite

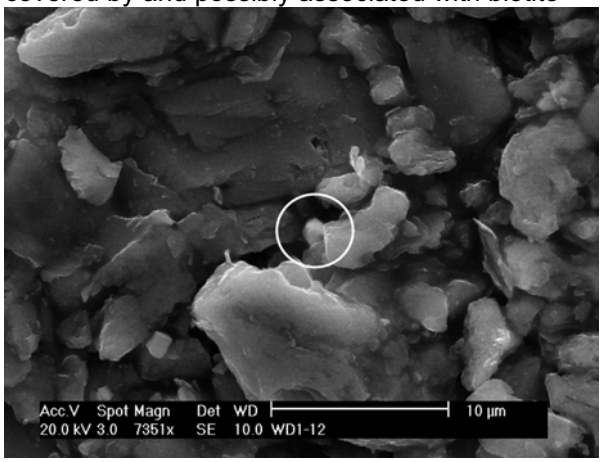

C. Small Au grain (circled) amongst larger biotite grains

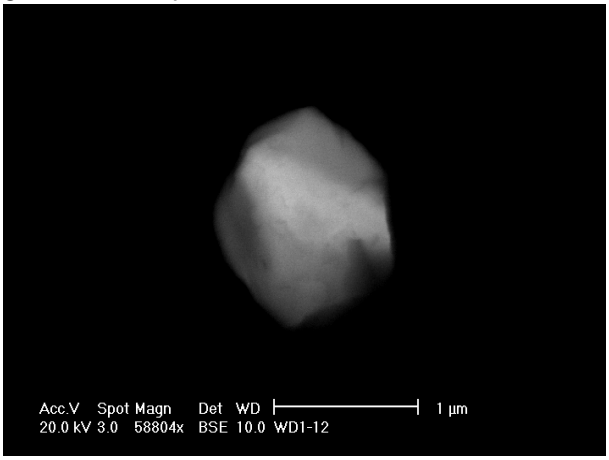

D. Backscatter electron image of Au grain in microphotograph C.

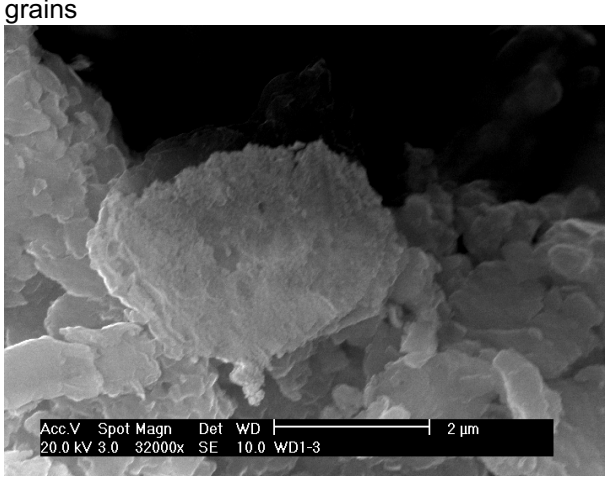

E. Relatively large Au grain and the only one found in the pedolith samples, from the B2 horizon

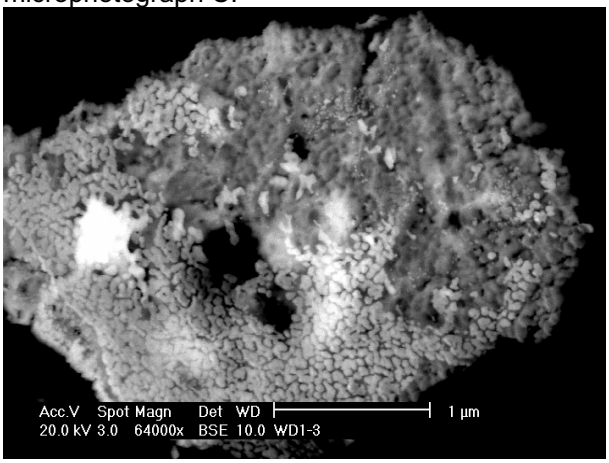

F. Backscatter electron image of the Au grain in E. The brighter areas have a purer Au signature

Figure 6.41: FESEM microphotographs of Au grains from Profile 1. Morphology of Au particle in F, suggests possible microbial involvement.

There are differences in morphology between the saprolith samples and the one from the B2 horizon. The single Au grain located within the B2 horizon was larger (~3 µm) than the

saprolith samples and had a nodular surface texture (Figure 6.41E & F). This suggests that the Au was precipitated from solution. The texture of this particle is similar in appearance to SEM micrographs of microbiota growing on a Au pellet by Reith & McPhail (2006), although the individual structures are significantly smaller. It is therefore possible that the Au within the pedolith was concentrated and precipitated through microbial activity. It is impossible to justify this statement on a single grain and based solely on morphology.

6.8. Synthesis: Formation of the White Dam profiles and implications for gold mobility

Analytical techniques and observations of the White Dam profiles reported above reveal a complex history of denudation and pedogenesis. Despite this complexity, several features and trends have emerged that help to define their history. In this section these trends are discussed with reference to their relationships, especially their relevance to Au and regolith carbonate association. The main features discussed are:

1) The large dilation / expansion of Profile 2.

2) Increasing development of interstratified illite and smectite, from phlogopite and non-interstratified smectite in the saprolith.

3) The major accumulation of Ca in the B2, Bk and Ck horizon of Profile 2.

4) Variation in major element flux changes through the profile, including: a major loss of K; minor loss of Al; a gain in Si and Fe; and variable Mg and Na gain or loss by horizon.

5) The Au loss from the A1, B1 and Bk horizons with gains in the remaining horizons, in relation to Au concentrations in the size fractions.

6) Similarities between the compositions of the two profiles, notwithstanding their transported and *in-situ* regolith settings.

Expansion of the saprolith and soil horizons may be due to a variety of factors including: addition of water during chemical weathering (hydrolysis); increased void space due to biological and/or physical weathering processes; and the addition of transported materials (Nahon, 1991; Schaetzl & Anderson, 2005). Evidence at White Dam supports all of these processes. Increasing void space is demonstrated by lower bulk density values, which decrease up the profiles towards the surface (Table 6.5 & Table 6.10). Both profiles have relatively high bulk densities in the A1 horizon, which is probably the result of compaction by vehicles or animals rather than any pedological process. Changes in the clay minerals and element fluxes also support expansion and are discussed in more detail below. These properties indicate profiles that have been extensively altered from their original parent material.

The type of clay in the profile is at least partly dependent on the parent rock and can be an indicator of the parent material (Ollier, 1984). At the base of Profile 2, kaolin, smectite and illite (phlogopite) are co-dominant, and sum to 60% of the clay minerals. Phlogopite is a primary mineral similar in appearance to biotite, which, along with other micas, can weather to form smectite, and likewise feldspars to kaolin (Schaetzl & Anderson, 2005). The underlying and assumed parent material, quartz-feldspar-biotite gneiss is therefore the most likely source of these minerals. Above the basal sample, but still in the C horizon (sample

WD3-07), illite becomes a trace mineral and smectite with a very clean non-stratified signal becomes dominant. Above this horizon and continuing to the surface increased weathering results in an inter-stratification of illite and smectite, a common feature of clay minerals (Eggleton, 2008).

Weathering of the rock-forming silicate minerals leads to the formation of clays with the release of soluble ions, including K^+, Na^+, Ca^{2+}, and Mg^{2+} into the environment (Ollier, 1984; Paton *et al.*, 1995). Whereas these ions are typically leached from the system, Fe becomes oxidised and remains in the profile as Fe-oxides or hydroxides (Ollier, 1984). Flux changes in these elements at White Dam indicate gains in Ca and Fe, loss of K, and mixed gains and losses for Na and Mg, through Profile 2. Other major element flux changes for Profile 2 are in Si and Mn gains and a loss of Al apart from in the C horizon where Al shows a mass gain (Table 6.14).

The highly weathered C horizon maintains a high degree of parent structure and has had a moderate volume change (Figure 6.35). Major elements in this horizon are enriched apart from K, but even K has its lowest percentage loss in this horizon. Major elements that show losses and minor gains through the profile have their highest percentage gains in this horizon (Al, K, Mg, & Na), whereas elements that have gains through most of the profile tend to have their lowest gains (Ca, Fe, Mn, & P). The exception is Si with a relatively uniform gain of between 12 and 28%. These results, including the dominant presence of clean smectite in the clay fraction, indicates that the degree of weathering is significantly less in this horizon and that the geochemistry is largely controlled by the parent material. When converted to absolute mass gains or losses these percentage variations are not always reflected in the same way. For example, K has its lowest loss of 42% in the C horizon with the overlying horizons showing > 70% loss, but when the absolute mass is compared, a loss of 42 g/cm^2 for the C horizon is not dissimilar to those values for the profile, which range from 16 to 33 g/cm^2 (Table 6.14).

Above the C horizon and into the base of the pedolith are the highly calcareous Ck, Bk and B2 horizons. The regolith carbonates are mostly powdery accumulations in the form of mottles, and some rhizomorphs. Calcite forms a large part of the groundmass as accumulations of small birefringent crystals or crystallitic b-fabric, which also fills many of the voids (Figure 6.7B), particularly in the Bk and Ck horizons. The high $CaCO_3$ content of these horizons (Ck – 17.5%, Bk – 18.6%, & B2 – 9.13%, Table 6.10), large volume expansion (Ck – 74%, Bk – 58%, and B2 – 61%, Figure 6.35), and high Ca gains of >1,000, >2,600, and >3,300% for the B2, Bk, and Ck horizons respectively are indicative of the large accumulations of Ca. The Sr isotope values for both White Dam profiles indicate that at least 90% of the Ca is from an extrinsic source (Section 4.2.3). This equates to a Ca addition of approximately 135 g/cm^2 column for the profile and 122 g/cm^2 column for the B2, Bk, and Ck horizons.

Quantitative estimates of Ca input from atmospheric sources are scarce, but some very broad estimates can be determined. Rainwater in southern Australia contains an average 3.2 kg/ha/yr (3.2 μg/cm^2/yr) Ca (Hill, 2004). Since the last glacial maximum total dust deposition of between 31.4 to 43.8 t/km^2/yr (3.14 to 4.38 mg/cm^2/yr) has been estimated for northern NSW and central Queensland, although a conservative 50% of this amount is expected to be added to the soil with the remainder being lost (McTainsh & Lynch, 1996; Cattle *et al.*, 2002; Hesse & McTainsh, 2003). The amount of Ca deposited in this way is not well quantified and estimates of the Ca content in dust varies from 1 to 25% (Butler, 1956; Pye & Tsoar, 1987; Pecsi, 1990). Assuming a dust retention rate of 50% and a Ca content of 10%, the dust contribution equates to approximately 150 to 219 μg/cm^2/yr, which would provide the

estimated 135g/cm^2 of Ca added to Profile 2 in 0.6 to 0.9 million years. This is well within the proposed period of regolith carbonate accumulation (Figure 5.8). It is also a maximum age, given that increased deposition rates during glacial maxima of between 2 to 5 times the current rate have been suggested (Mahowald *et al.*, 1999; Hesse & McTainsh, 2003). An age of < 150,000 years is therefore feasible given higher deposition and retention rates.

The formation of soil horizons may be the result of additions and removals to and from the system. The loss from one horizon, eluviation, is typically matched by accumulation, (illuviation) in another. The existence or lack of cutans around grains and voids is evidence of these processes (Schaetzl & Anderson, 2005). The translocation of components in this way requires good drainage (Brewer, 1964). Petrological observations on samples from the White Dam profiles (Sections 6.4.1 and 6.5.1) located clay cutans around many of the larger grains through both profiles. In the carbonate-rich horizons cutans are greatly reduced, and in some case only partially surround grains. Very few cutans were on the surfaces of smaller grains, voids and channels. This indicates that water moving through the profile, particularly along channels has relocated the clays. In the carbonate-rich horizons calcite has filled many of the voids and reduced water flow (Figure 6.20C). The cutans observed in these horizons are therefore likely to be relict features that formed prior to calcite precipitation.

Continuing calcite precipitation in the regolith carbonate zones will eventually lead to the formation of an impermeable indurated carbonate (calcrete) horizon (Gile *et al.*, 1966; Milnes, 1992). This will influence on the overall profile development and greatly slow down, and possibly stop, movement of material through this part of the profile. It also means that material within these horizons prior to induration is trapped.

The main difference between the Ck and overlying Bk horizon is the degree of weathering. Primary structures are still observable in the Ck horizon, although very friable, whereas in the Bk horizon and above, all evidence of original rock fabric has been destroyed. This horizon therefore marks a significant change in mineralogy, geochemistry, and physical properties: Primary minerals, apart from quartz, are greatly reduced (Table 6.7); most elements have either flux losses or gains to levels that in general are repeated throughout the pedolith; and the clay-sized fraction is greatly increased (Figure 6.23 and Table 6.8).

Within the saprolith the major elements are generally elevated. This enrichment is likely the result of movement of material from the overlying horizons. There is also less leaching in the saprolith and lower pedolith horizons due to reduced permeability caused by calcite precipitation in the voids and channels, and flocculation of clays because of the cation effect. The enrichment may also be due to the removal of other components. The only major element with a significant loss in the saprolith is K, which also has losses from all horizons. The K, sourced from the feldspars and micas, is leached from the system either directly in solution or via plant uptake.

The overall enrichment of several elements through the profile, the large volumetric expansion, and minor elemental losses indicates that there has been significant external input. There are two potential sources for this material: atmospheric, as proposed for Ca and described above, or lateral downslope movement. Because the profile is in an erosional setting, the expectation is that the profile should have collapsed; i.e. material should have been removed. The appearance that this is false may be misleading. It is likely that material is migrating down slope, but this process does not start at Profile 2. Hence, while material may be transported down slope from the profile, the same process will be adding material from up slope. The profile expansion and element increase may indicate that this setting is a sediment

transit zone and addition of material may be faster than removal during the development of this profile.

Parent material for Profile 2 was shown to be the underlying saprolite, which consists of a quartz-feldspar-biotite gneiss. The gneiss is host to mineralisation and contains abundant pegmatites (Cooke, 2003). Profile 1 is sited above one such pegmatite, but rather than forming *in-situ*, Profile 1 has formed within transported material. Whereas smectite and illite are co-dominant in Profile 2, in Profile 1 smectite is dominant with only minor illite. This is reflecting a higher degree of weathering, which in part may be due to transportation processes as well as pedogenesis. Hence more of the illite has broken down to form smectite.

The similarities in the properties of Profile 1 compared with those of Profile 2 suggest that it has developed in material derived from the same gneiss. Hence it has formed in locally derived material that has most likely moved down slope. This means that although mass balance calculations could not be undertaken on Profile 1 because of the disconformities, the results from Profile 2 are likely to apply to Profile 1. Although Profile 2 is located upslope, it is not currently supplying material to Profile 1 because of a shallow drainage depression that separates the two profiles (Figure 6.3). This may be a relatively recent change and does not mean that material was not deposited in the past.

Mass balance calculations reveal that Au has been lost from the A1, B1, and Bk horizons with minor enrichment in the B2 horizon and significant enrichment in the saprolith (Figure 6.38). This matches the bulk sample Au concentrations with the highest values in the saprolith. In the clay-sized and silt fractions, Au concentrations were generally higher than their bulk equivalents with subtle differences between the fractions (Figure 6.28). In the clay-sized fraction the highest Au concentrations are in the saprolith, whereas in the silt fraction the highest values are in the pedolith. This may be misleading due to the high density of Au and the separation method, which relied on a particle density of 2.6 $g.cm^{-3}$, resulting in finer Au particles in the coarser size fractions (see Section 6.7).

The location for Profile 2 is off the main mineralization zone (Figure 6.3), which is reflected in the low Au concentration of the assigned parent material at the base of the profile. The high values in the B2, Ck, and C horizons are therefore due to the translocation of Au from the A1, B1, and Bk horizons that had Au losses, and / or the addition of material through lateral movement. In either instance, the mobility of Au in this system is demonstrated. It is unclear whether the Au was transported as particles or in solution, given that attempts to locate and characterise the Au were inconclusive (Section 6.7).

The highest Au concentrations are from the saprolith of Profile 1, with all size fractions containing >500 ppb, apart from clay-sized with about 300 ppb (Figure 6.15). This spread of Au reflects the size of the oxidised / near surface Au described as small platelets up to ~60 μm in diameter with occasional larger grains to 165 μm (Cordon, 1998; Croxford, 1998; Cooke, 2003). Although lower concentrations of Au are present in the saprolith of Profile 2 the spread within the fractions is similar. In the pedolith the higher Au concentrations of both profiles is in the silt and clay-sized fractions, which indicates that the larger Au particles of the saprolith are breaking down into smaller particles.

Previous research has indicated a correlation between Au and Ca, although this has been restricted to the top of the profile in most cases (Lintern, 1989; Lintern & Butt, 1993; Lintern, 1997; Lintern & Butt, 1998b; Smee, 1998; Lintern & Sheard, 1999a; Okujeni *et al.*, 2005; Lintern *et al.*, 2006). At White Dam there are variations in the Au dispersion through the

profiles between the size fractions, but there is no correlation between Au and Ca. The Ca content of the size fractions was not determined, but in the bulk samples the concentrations peak in the regolith carbonate horizons (Figure 6.37). Gold tends to increase down the profile to the top of the regolith carbonate in the B2 horizon, drop slightly in the Bk, and then rise once in the saprolith (Figure 6.38). The increased Au content at the top of the regolith carbonate suggests that future sampling should be from this location. In most instances samples have been collected from the top of the indurated zone due in part to the difficulty in breaking through this material with hand tools. Hence it may be fortuitous that samples have generally been collected from the most Au enriched zone.

Additional elements associated with mineralisation at White Dam are Cu and Mo from a stockwork of pyrite, chalcopyrite and molybdenite veins (McGeough & Anderson, 1998; Cooke, 2003). In the pedolith Cu and Mo have had similar losses of between 60 and 75% from the surface to the B2 horizon and about 40% in the Bk horizon (Figure 6.39). Although these elements have been leached from the pedolith, Cu has been enriched in the Ck and C horizon by ~170 and ~300% respectively. Weathering of the sulphide minerals releases these elements into the regolith where they are leached from the system. Although not documented as part of mineralisation, Ag also has large losses from the profile of around 50%.

The decrease in Au concentration in the Bk horizon is why there is no correlation between Au and Ca in Profile 2. It is unclear why this drop in concentration occurs, but it may relate to variation in permeability. In the B1, B2, and C horizons there is a large proportion of interconnected pore space that provide plenty of opportunities for colloid transport form higher up the profile. Movement of clay from higher horizons may flocculate when it reaches the Ca enriched Bk horizon because of the cation effect (Ca^{2+}) and electrolyte concentration ($CaCO_3$). This results in a denser horizon with less interconnected pores. Hence subsequent illuviation of silt sized particles (e.g. Au) will deposit higher in the profile since they are unable to permeate into the Bk horizon.

The presence of rhizomorphs in the calcareous horizons and root activity in the saprolite is evidence of vegetation processes occurring in the profile (Figure 6.7C & D). The detection of Au and Cu in *Atriplex vesicaria* (bladder saltbush) over mineralisation (Brown & Hill, 2004) highlights that vegetation is involved in the translocation of these elements. The single Au particle from the pedolith has a morphology suggesting possible microbial involvement (Section 6.7). Hence there is a definite biotic role in the development of the White Dam profile, including the formation of regolith carbonates and distribution of Au, but how much the biota is a control of the Au and Ca association is unknown.

6.9. Conclusion

The research presented in this chapter illustrates the complexity of Profile 2, which appears to be a relatively straightforward *in-situ* developed profile with its position on an erosional rise suggesting that material is lost over time. Instead, mass balance calculations have revealed that, rather than material being eroded, there has been significant input, especially Ca. Based on the rate of Ca addition a minimum age of about 150,000 years is proposed for the development of Profile 2. The addition of Ca explains the formation of regolith carbonates and raises questions about Au association, which is intrinsically derived.

The lack of a direct correlation between Au and Ca compared with other areas where the regolith carbonates are generally more developed or indurated suggests that the relationship may develop over time. Hence the more indurated the carbonate, the more it correlates with Au. For this to occur Au has to be added to the carbonate horizons, which is unlikely since

increased induration will reduce permeability and therefore restrict Au movement. This aspect of regolith carbonate formation and Au association is discussed further in the next chapter.

Chapter 7

Synthesis

7.1. Introduction

The aim of this research is to identify methods to improve the use of regolith carbonates in Au exploration, and ways that Au-in-calcrete anomalies can be constrained. The research here is designed and presented in a modular structure that investigated aspects of regolith carbonate formation and relationships with Au, ranging between continental, local landscape and profile scales.

The first module (Chapter 4) determined the source of Ca within regolith carbonates from southern Australia. The hypothesis for this module was:

> *the Ca is from an extrinsic marine source; therefore any association between Au and Ca is due to similar processes rather than the same process.*

Results from Sr isotope analysis of regolith carbonates demonstrated that > 90% of the Ca is derived from an extrinsic source. The research also revealed that continual mixing of Ca inland maintains a homogeneous mixture that results in uniform $^{87}Sr/^{86}Sr$ ratios between 0.712 and 0.717. Analysis of Profile 2 at White Dam provided additional evidence of an extrinsic Ca source with Ca enrichment in excess of 1,000% in the B2, Bk and Ck horizons. The high Ca input means that there can be no direct association with locally derived Au. This hypothesis is therefore confirmed.

In the second module (Chapter 5) a known Au-in-calcrete anomaly extending over mineralised and barren bedrock was investigated. Geochemical analysis and regolith-landform mapping was undertaken to test the hypothesis that:

> *Au-in-calcrete anomalies include contributions from Au and associated elements laterally transported from mineralised areas by physical and chemical landscape processes.*

Through the use of regolith-landform mapping at Tunkillia, the Au-in-calcrete anomaly was shown to follow palaeo- and contemporary drainage systems. The majority of elements associated with the mineralisation area, including many that are typically considered immobile, have been transported along drainage systems toward the north of the area. The precise form of the mobile Au was not determined, but movement as free Au, bound to clay minerals or within regolith carbonate nodules, is proposed. Evidence supports the proposed hypothesis and demonstrates how Au-in-calcrete anomalies are influenced by landscape processes.

In the third module (Chapter 6), two regolith carbonate profiles proximal to mineralisation were investigated using a variety of pedological techniques.

> *Au is mobilised, either chemically or physically, in association with clay minerals and the clay-size fraction. Precipitation of regolith carbonates fills void space and reduces permeability. This acts as a barrier to Au movement and immobilises the*

clay minerals (and Au). Ongoing dissolution and re-precipitation of the carbonates leads to increased Au concentrations.

Analysis of the White Dam profiles revealed that Au was mostly in the finer fractions and enriched at the top of the regolith carbonate and at the top of the saprolith. Other horizons from White Dam are Au depleted. Clay-sized material is mobile through both profiles, but its mobility becomes restricted in the regolith carbonate horizons due to infilling of void spaces by precipitated calcite and flocculation of clays because of the cation effect, which reduces porosity and permeability in this part of the profile. Given this information it is not possible to confirm how Au is mobilised, although calcite precipitation and flocculation of clay will greatly reduce its mobility through the profile. If the build-up of regolith carbonates was enriching the Au concentrations, then higher Au concentrations within the Ck horizon (rather than initially above it) would be expected. It is therefore unlikely that Au is mobilised by the dissolution and re-precipitation of carbonate alone. This third hypothesis is therefore only partially confirmed and requires further investigation.

Validation of the hypotheses acted as a guide to this research project, which has led to a better understanding of Au-in-calcrete formation. In the next section, results from the three modules are combined to demonstrate the formation of a Au-in-calcrete anomaly, and what happens when it is further exposed to landscape processes.

7.2. Pedological, geochemical, and geomorphological evolution of Au-in-calcrete

The rapid adoption of regolith carbonate sampling by mineral exploration companies and the limited research on this medium, has resulted in a poor and at best anecdotal framework and understanding of Au-in-calcrete systematics. Results from this study have the potential to address some of these shortcomings. One aspect of interest to both research and industry is the evolution of the regolith carbonate profile and how it relates to Au mineralisation.

Regolith carbonate profiles have been well described in the scientific literature (e.g. Gile *et al.*, 1966; Goudie, 1973; Read, 1974; Bachman & Machette, 1977; Arakel, 1982; Goudie, 1983; Milnes & Hutton, 1983; Machette, 1985; Phillips & Milnes, 1988; Gile, 1993; Paquet & Ruellan, 1997; Alonso-Zarza *et al.*, 1998b; Hill *et al.*, 1998a; McQueen *et al.*, 1999). A major benchmark was the work of Gile *et al*. (1966), that proposed a model describing the evolution of a regolith carbonate profile, which has since become widely recognised and supported. Some further refinements of the model, including the addition of extra stage, have been made by Bachman & Machette (1977) and Machette (1985).

The Gile *et al.* (1966) model is based on regolith carbonate morphology variations, reflecting the degree of carbonate accumulation in the profile. Stage I represents the start of carbonate accumulation and is recognised by rhizomorphic, small nodular, and powdery carbonate accumulations that are mostly within the B horizon. These morphologies are the result of carbonates that have been deposited on the surface, and eluviated from here to infiltrate the profile and accumulate on grain and void surfaces, and around roots. Continued accumulation of carbonates leads to stage II, where coated grains start to coalesce, voids are infilled and powdery carbonates start to become indurated. Nodule and rhizomorph structures are within the indurated material. Stage III consists of many infilled voids and cemented nodules and the beginning of an indurated horizon. The final stage (stage IV) of Gile *et al.* (1966) is a completely indurated horizon with the possibility of overlying laminations.

Bachman & Machette (1977) added two more stages to represent further carbonate addition to the profile, and reactions due to the impermeable indurated horizon created in stage IV. Their stage V consists of a well developed laminated upper surface with scattered pisoliths. The change from downward to lateral movement of water results in the build up of laminations and precipitation of carbonate coats grains, and forms pisoliths and nodules on or just above the indurated hardpan horizon. Stage VI is due to long term, periodic drying and wetting of the indurated horizon. This causes it to swell and crack, creating irregular shaped fragments that either litter the surface or become re-cemented into a brecciated zone.

The source of Ca in regolith carbonates is largely extrinsic (Quade *et al.*, 1995; Capo & Chadwick, 1999; Chiquet *et al.*, 1999; Naiman *et al.*, 2000; Hamidi *et al.*, 2001; Van Der Hoven & Quade, 2002; Lintern *et al.*, 2006). Results from Sr isotope analysis and mass balance calculations presented in this study support this extrinsic source for regolith carbonates and regionally demonstrates this for southern and central Australia.

Despite the abundant knowledge on the evolution of regolith carbonate profiles presented above, very little of this has been applied to mineral exploration programs, in particular in understanding the formation of Au-in-calcrete anomalies. This study aims to rectify this omission and draw these two research pathways closer together.

Systematic variation in Au concentration occurs in the profiles at White Dam, where Au was enriched at the top of and immediately above the regolith carbonate zones. According to the regolith carbonate evolution model of Gile *et al.* (1966), the White Dam profile is at stage II. At this stage the main location of carbonate precipitation is therefore alongside but not associated with Au accumulation.

Profiles beyond stage II were not specifically investigated in detail in this study, but a re-evaluation of previously described Au-in-calcrete profiles revealed some results that can be related to regolith carbonate evolution stages subsequent to the White Dam profiles. The only previous Au-in-calcrete studies that have related Au to profile morphology, mineralogy, and elemental chemistry are Hill *et al.* (1998a), McQueen *et al.* (1999) and Hill (2000). These studies include three profiles that, like White Dam, are also from the Curnamona Province. The profiles from Broken Hill at the Pinnacles (the "Marnpi" profile), Limestone Station and Corona represent stage III of Gile *et al.* (1966), and stages V and VI of Bachman & Machette (1977) respectively.

As with the White Dam profile there is a systematic variation in Au concentration through these profiles. The highest Au concentrations in all profiles are at the top of the regolith carbonate horizons. In terms of morphology, the highest Au concentrations are associated with carbonate nodules overlying laminated regolith carbonates (Hill *et al.*, 1998a; McQueen *et al.*, 1999; Hill, 2000). It is apparent that Au becomes enriched at the top of the regolith carbonate horizon following stage II of the profile formation and remains concentrated throughout all further stages as the profile accretes upwards in the profile. Laminar carbonates are typically void of skeletal grains, but clay-sized particles and organic matter, possibly from downward moving water and root activity, form darker coloured layers as they become engulfed by the developing laminations (Gile *et al.*, 1966).

The results in this study from Tunkillia support an additional stage (stage VII), which forms after a fully developed profile is exposed to erosion. Firstly the unconsolidated material, including carbonate nodules, is transported downslope. This is followed by the transport of indurated carbonate "blocks" that break free from the consolidated profile. The transported

material is re-deposited downslope and in some instances may be integrated into an existing or developing profile.

Stage VII explains how the Tunkillia Au-in-calcrete anomaly may have formed. The highest Au concentrations are at the top of the regolith carbonate and are the first parts of the profile to be eroded. As this eroded material moves downslope and laterally through the landscape, it transports any Au that is entrapped within it. Later incorporation of this material into new and evolving regolith carbonate profiles will therefore include anomalous Au-in-calcrete values, but they may be sited over bedrock that may not necessarily host mineralisation. Should a Au enriched regolith carbonate profile overlying a mineralisation source be fully eroded, all indication of the underlying mineralisation may be removed and instead transported laterally, hence the "true" Au-in-calcrete anomaly is destroyed. Later burial and further accumulation of regolith carbonates may completely obscure any prior Au-in-calcrete anomaly.

This stage may also explain why there is no anomaly along the "Tunkillia East" drainage pathway and the higher Au concentrations in the samples from "Area 191" (Figure 5.18). It is possible that many of the regolith carbonates in the Tunkillia area have been near or at the surface and affected by erosion and breakup of the profile. The extensive areas of calcrete lag, and aeolian nature of the overlying soils is evidence of previous exposure. The lower Au concentrations from samples at "Area 223" may be due to the removal of the "Au-in-calcrete", which is now located downslope and along the palaeo- and contemporary drainage pathway of "Tunkillia Central". Hence, the true "Area 223" anomaly has been dispersed down slope with only remnants of it remaining beneath the dunes and partially exposed in dune swales.

The sequence of profile evolution described above can be summarised diagrammatically in a new model for Au-in-calcrete formation (Figure 7.1). The model incorporates the Au results from this study and previous work in the region by Hill *et al.* (1998a), McQueen *et al.* (1999) and Hill (2000) with the evolution stages proposed by Gile *et al.* (1966) and Bachman & Machette (1977). A major assumption of the model is that Au is dispersed and mobile within the regolith prior to evolution of the regolith carbonate profile. This is a valid assumption, given that regolith carbonates as described above, form by overprinting existing profiles. It is the mobility of Au in the regolith and variations of permeability in reaction to regolith carbonate formation in the profile, which controls the Au concentrations.

Prior to regolith carbonate accumulation, a general soil/regolith profile depending on local substrate and site conditions is assumed. For the regions considered in this study, this typically consists of a thin A horizon with some organic matter above a clay enriched B horizon. The depth and composition of the profile is not specifically relevant given that the Ca is externally derived and will overprint pre-existing material. Similarly the profile may have developed within transported or *in-situ* material.

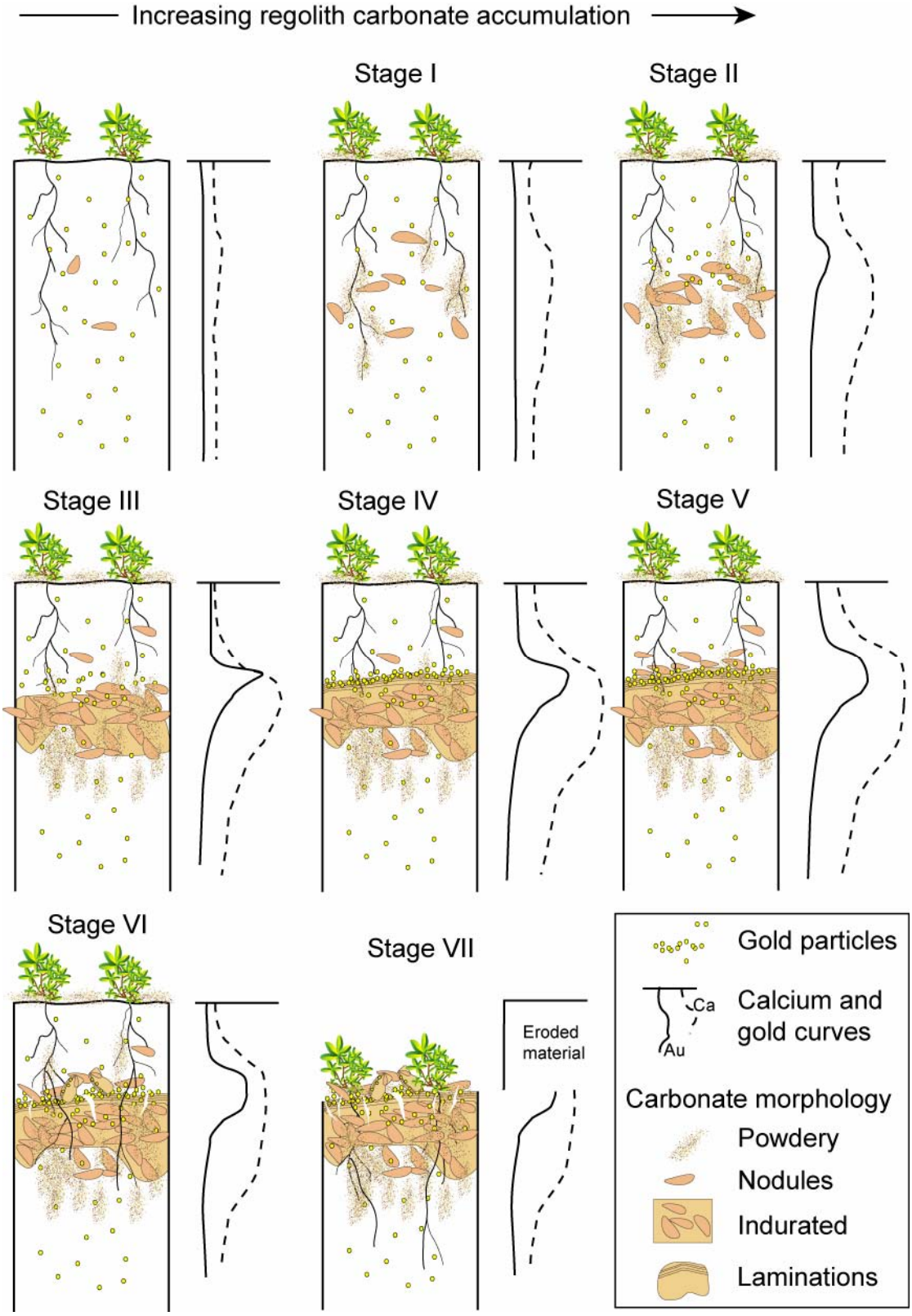

Figure 7.1: Proposed model of Au-in-calcrete anomaly formation.

During stage I, rhizomorphs and thin carbonate coatings start forming around grain and void surfaces. This initial development has minimal impact to the overall profile permeability and Au mobility and accumulation is maintained, therefore remaining dispersed throughout the profile. In stage II, permeability is significantly reduced as continuing carbonate accumulation

starts to cement grains and nodules, and fill voids (Figure 6.7F). Clay and silt-sized material (including Au) that was previously free to move down through the profile, becomes trapped and enriched at the top of the developing regolith carbonate. Continual carbonate accumulation further reduces permeability until stage IV where a fully indurated horizon results in a near impermeable barrier. Any Au within this impermeable horizon is now trapped either physically or chemically by the regolith carbonates. Gold migrating down the profile continues to collect at the top of the regolith carbonate with some Au becoming entrapped as the regolith carbonate becomes more indurated, and laminations start forming. As the regolith carbonate profile evolves to stage V, Au continues to collect at the top, resulting in greater concentrations being incorporated into the expanding laminations and nodules forming above the hardpan. The profile is now considered fully developed with a significant Au enrichment at the top of the regolith carbonate horizon, which if sampled within close proximity to mineralisation would best represent an anomalous Au-in-calcrete.

In stage VI, cracks start to develop in the indurated part of the profile, forming large blocky fragments. Depending on local circumstances these blocks may remain in place and be re-cemented. Alternatively, erosion may cause these blocks, along with any overlying nodules to be transported. Gold trapped within this upper horizon material will also be transported. This is the newly proposed stage VII.

In the light of this model, a re-evaluation of previously described profiles indicates previously unrecognised support, of the systematic variation of Au through the regolith carbonate profile (e.g. Lintern & Butt, 1993; Lintern, 1997; Lintern & Butt, 1998b; Lintern & Sheard, 1999a; Okujeni *et al.*, 2005; Lintern *et al.*, 2006). The majority of these illustrate a Au enrichment at the top of the carbonate horizon, but it is not always discussed in terms of profile development or Au / carbonate association. An exception is Lintern & Butt (Lintern & Butt, 1998a) where significant Au in the top 0.5 m of the carbonate profile was suggested to be the result of physical processes, independently acting on Au and carbonate accumulations. An example in which they claimed there was no Au enrichment at the top of the carbonate horizon is seen in Lintern & Butt (1993; 1998b), even though the data that they presented showed otherwise. A selection of plots from Lintern & Butt (1993; 1998b), of Au and Ca concentrations through soil profiles at Bounty and Zuleika Sands Au deposits in Western Australia are shown in Figure 7.2. These plots illustrate that highest Au concentrations are at the top, or just above, peak Ca concentration in profiles, which are at various stages of regolith carbonate formation.

The recognition of Au enrichment at the top of regolith carbonates and the adoption of this model has major implications for Au exploration. The model shows that individual vertical profiles contain significant and systematic Au variation. The variation within the profile can be equivalent to the difference between geochemical background and anomalous values. Therefore the sample position within the profile is an important consideration. Sampling programs to date have mostly collected material from the top of the regolith profile because it is the easiest part of the profile to sample. It is somewhat fortuitous that this is the zone of highest Au concentration.

Another consideration when sampling regolith carbonates is the status or stage of the profile evolution. The evolution stage, apart from stage VII, is not critical in terms of what morphology is sampled, so long as the sample is collected from near the top or just above the regolith carbonate horizon. This was demonstrated with samples collected from White Dam and Tunkillia. What does need to be considered is the Au concentration with respect to sample morphology. Although not investigated fully in this study, lower Au concentrations

may be expected in the less developed stages I and II. The concern therefore, is the assignment of a single anomalous Au cut-off value by exploreres, when it may be different depending on the sample type. The completeness of the profile is the most important consideration, since at stage VII the profile may give a blind response (anomaly removed) or false anomaly if transported (Figure 7.3). Identification of an eroded profile that has been buried, possibly with additional regolith carbonate overprinting, is difficult due to the fragmented nature of the material. This is made more difficult when digging up samples, or auger sampling profiles that are not visible.

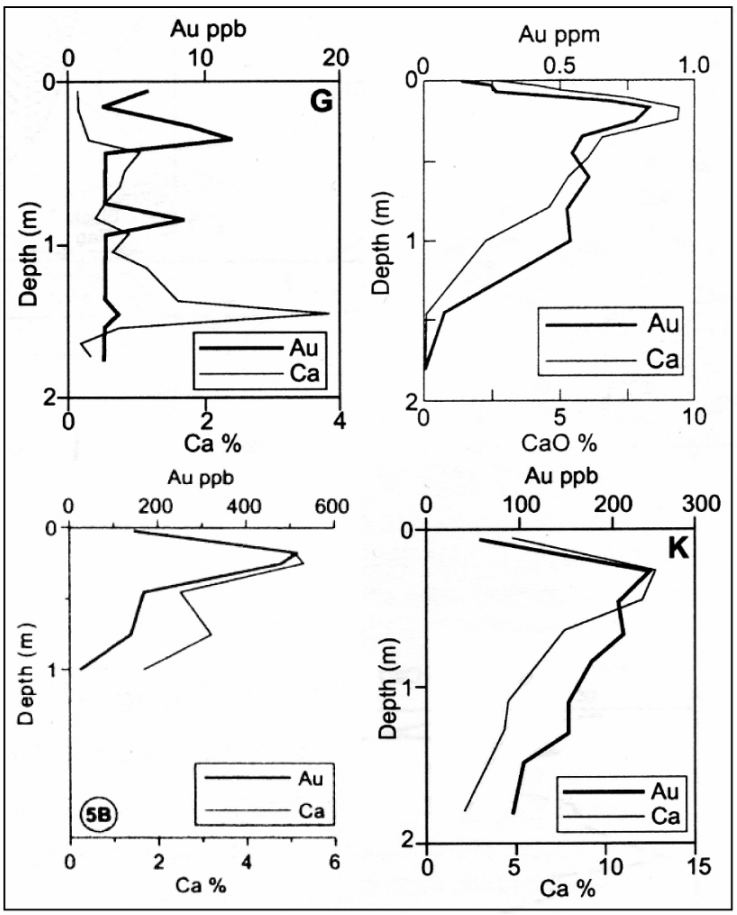

Figure 7.2: Soil depth profile plots from Bounty and Zuleika Sands Au deposits showing Au enrichment aligned with, or just above the high Ca concentration zone, even when Ca is very low (plot G) (from Lintern & Butt, 1993; 1998b).

One aspect that has not been investigated in this research, but warrants further investigation is the state of Au in the profile prior to regolith carbonate formation. The proposed model is based on the assumption that Au is dispersed throughout a regolith profile that has been exposed to regolith forming processes since the Late Palaeozoic. The question is therefore asking what the original state, mobility, and concentration of Au was in the profile, prior to regolith carbonate formation? Another aspect that requires further investigation is the interaction of the clay and Au with respect to regolith carbonate evolution. The build up of regolith carbonate in the profile causes clay to flocculate. Hence, clay moving down the profile through eluviation, concentrates toward the top, and just above the regolith carbonate horizon. It is unclear how this process affects the Au, but given that Au is enriched in the same position as the clay, then a physical or chemical association is likely. It may be that Au in regolith carbonate has a stronger association with clay than regolith carbonate evolution.

The answer to these questions may have important implications to the development of Au-in-calcrete and the proposed model.

7.3. Conclusion

Based on the research presented in this study, the geochemical dispersion pathways of Au and Ca within the regolith are independent until regolith carbonates start to precipitate in the profile. As carbonate precipitation increases, permeability is reduced. This causes Au and Ca to become physically and maybe chemically unified, thus forming Au-in-calcrete. Therefore, Au – Ca association is one of coincidence that is due to similar, but independent Ca and Au reactions to the physical, chemical and biological processes active in the regolith.

Geochemical results offer no clear identification as to whether a Au-in-calcrete anomaly is over mineralised or barren bedrock. The best surficial clues are gained by understanding and interpreting landscape processes. This is best done through the use of regolith-landform maps, which can be easily constructed from information gathered whilst sampling, along with aerial satellite images.

In central and southern Australia regolith carbonates are widespread, easily identifiable, and typically enriched in Au when near mineralisation. This makes them an ideal sampling medium for Au exploration. This study has revealed that the ideal regolith carbonate sampling material is from the top of the regolith horizon, independent of morphology type. A proposed formation model illustrates how this is Au enrichment at the top of the profile occurs and explains the formation of true, transported and blind anomalies (Figure 7.1 & Figure 7.3).

The research has linked applied knowledge of Au-in-calcrete from its use as a sampling medium by exploration companies with knowledge of regolith carbonates and their formation. Although a definitive solution has not been found that will confirm a Au-in-calcrete anomaly is overlying mineralisation, the research does provide reasons why these anomalies may occur over barren bedrock. The research has also shown that regolith-landform mapping can be a first step in improving the targeting of Au mineralisation from a spatially extensive Au-in-calcrete anomaly, as found at Tunkillia.

Mineral deposits are becoming more difficult to locate due to the majority of exposed and near surface deposits possibly located. It is a requirement therefore that mineral exploration companies become “smarter” in their sampling methodology. The aim of most exploration companies when sampling, is to obtain the greatest number of samples for minimal cost. This is not necessarily the most economical method in the long term. As shown in this study, interpretation of sample geochemistry can be improved through the use of additional information gathered at the time of sample location, such as the regolith-landform setting and pedology. For instance, recognition that the Au-in-calcrete anomaly at Tunkillia was following palaeo- and contemporary drainage may have resulted in faster location of the deposit and reduced drilling into barren bedrock.

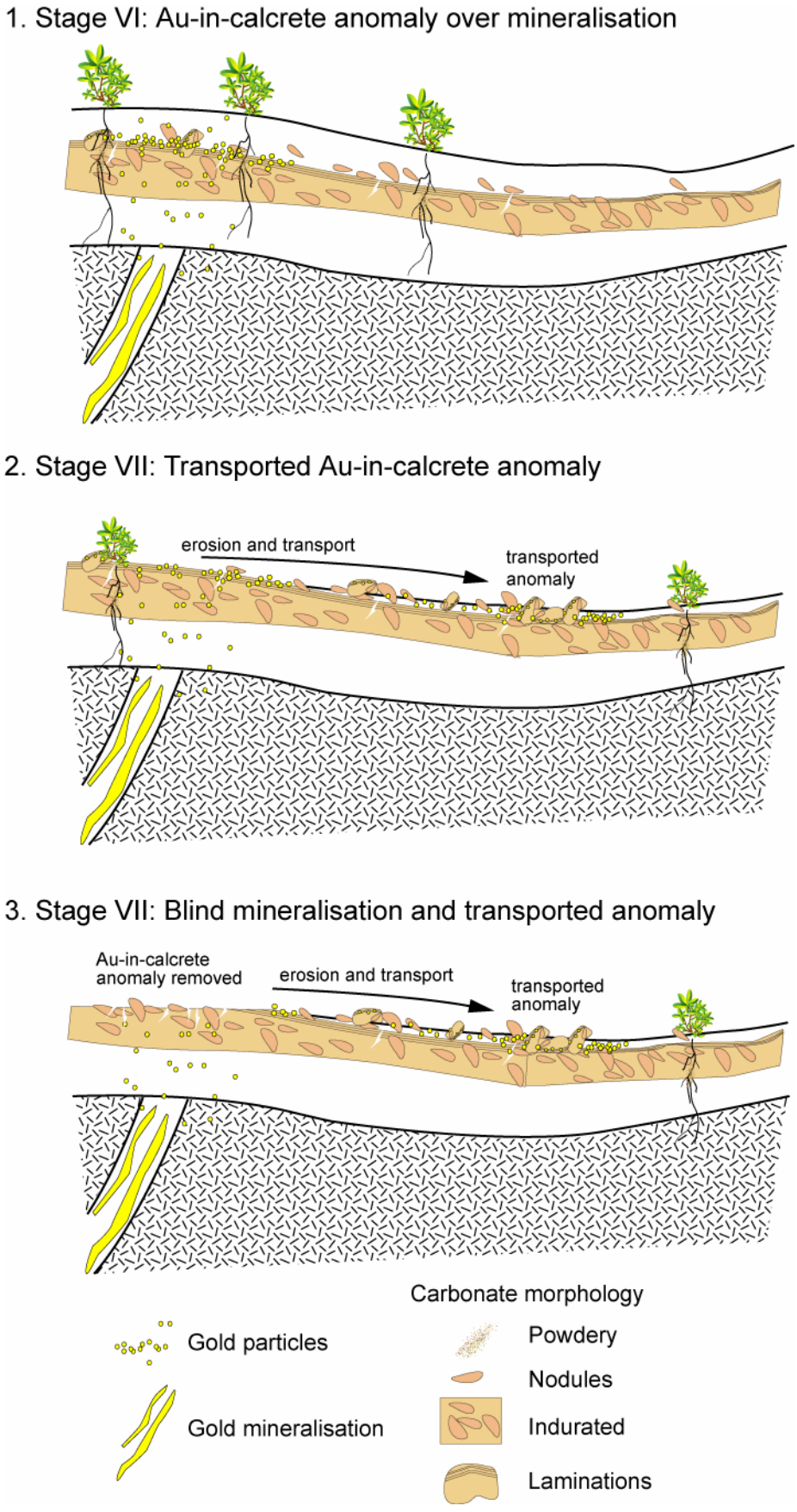

Figure 7.3: Model of blind and transported Au-in-calcrete anomaly formation. Later burial of the removed anomaly (step 3) would obscure evidence of underlying mineralisation.

References

ALLEN B. L. & HAJEK B. F. 1989. Mineral occurrence in soil environments. *In:* DIXON J. B. and WEED S. B., ed. *Minerals in soil environments*, pp. 199-278. Soil Science Society of America, Madison, WI.

ALLEY N. F. 1977. Age and origin of laterite and silcrete duricrusts and their relationship to episodic tectonism in the mid-north of South Australia. *Journal of the Geological Society of Australia* **24,** 107-116.

ALLISON L. E. & MOODIE C. D. 1965. Carbonate. *In:* BLACK C. A., ed. *Methods of soil analysis: Pt 2 Chemical and microbiological properties*, pp. 1379-1396. American Society of Agronomy-Soil Science Society of America, Madison, Wisconsin.

ALONSO-ZARZA A. M. 1999. Initial stages of laminar calcrete formation by roots: examples from the Neogene of central Spain. *Sedimentary Geology* **126,** 177-191.

ALONSO-ZARZA A. M., SANZ M. E., CALVO J. P. & ESTEVEZ P. 1998a. Calcified root cells in Miocene pedogenic carbonates of the Madrid Basin: evidence for the origin of Microcodium b. *Sedimentary Geology* **116,** 81-97.

ALONSO-ZARZA A. M., SILVA P. G., GOY J. L. & ZAZO C. 1998b. Fan-surface dynamics and biogenic calcrete development: Interactions during ultimate phases of fan evolution in the semiarid SE Spain (Murcia). *Geomorphology* **24,** 147-167.

ANAND R. R., PHANG C., WILDMAN J. E. & LINTERN M. J. 1997. Genesis of some calcretes in the southern Yilgarn Craton, Western Australia; implications for mineral exploration. *Australian Journal of Earth Sciences* **44,** 87-103.

ANAND R. R., PHANG C., WILDMAN J. E. & LINTERN M. J. 1998. Genesis of some calcretes in the southern Yilgarn craton, Western Australia: implications for mineral exploration - Reply. *Australian Journal of Earth Sciences* **45,** 179-182.

ANDERHALT R. & SWENSON L. 2006. Applications for automated particle analysis. *Microscopy today* **14,** 22-26.

ARAKEL A. V. 1982. Genesis of calcrete in Quaternary soil profiles, Hutt and Leeman lagoons, Western Australia. *Journal of Sedimentary Petrology* **52,** 109-125.

ARAKEL A. V. 1988. Carnotite mineralization in inland drainage areas of Australia. *Ore Geology Reviews* **3,** 289-311.

ARAKEL A. V. & MCCONCHIE D. 1982. Classification and genesis of calcrete and gypsite lithofacies in paleodrainage systems of inland Australia and their relationship to carnotite mineralization. *Journal of Sedimentary Petrology* **52,** 1149-1170.

ASADY G. H. & WHITESIDE E. P. 1982. Composition of a Conover-Brookston map unit in southeastern Michigan. *Soil Science Society of America Journal* **46,** 1043-1047.

ASHLEY P. M., CONOR C. H. H. & SKIRROW R. G. 1998. Geology of the Olary Domain, Curnamona Province, South Australia. Field guidebook to Broken Hill Exploration Initiative excursion 13 - 15 October 1998, pp. 53. Primary Industries and Resources, South Australia.

BACHMAN G. O. & MACHETTE M. N. 1977. *Calcic soils and calcretes in the southwestern United States*. U. S. Geological Survey Open-File Report 77-794, 163 pp.

BAIRD A. J. 1997. Overland flow generation and sediment mobilisation by water. *In:* THOMAS D. S. G., ed. *Arid zone geomorphology: Process, form and change in drylands*, pp. 165-184. John Wiley & Sons Ltd, Chichester.

BAKER W. E. 1978. The role of humic acid in the transport of gold. *Geochimica et Cosmochimica Acta* **42,** 645-649.

BALDOCK J. A. & SKJEMSTAD J. O. 1999. Soil organic carbon/soil organic matter. *In:* PEVERILL K. I., SPARROW L. A. and REUTER D. J., ed. *Soil analysis: an interpretation manual*CSIRO, Melbourne.

BAMBA O., PARISOT J. C., GRANDIN G. & BEAUVAIS A. 2002. Ferricrete genesis and supergene gold behaviour in Burkina Faso, West Africa. *Geochemistry - Exploration, Environment, Analysis* **2,** 3-14.

BANFIELD J. F. & EGGLETON R. A. 1989. Apatite replacement and rare earth mobilization, fractionation, and fixation during weathering. *Clays and Clay Minerals* **37,** 113-127.

BANNER J. L. 2004. Radiogenic isotopes: systematics and applications to earth surface processes and chemical stratigraphy. *Earth-Science Reviews* **65,** 141-194.

BARSHAD I. 1964. Chemistry of soil development. *In:* BEAR F. E., ed. *Chemistry of the soil*, pp. 1-70. Reinhold, New York.

BATJES N. H. 1996. Total carbon and nitrogen in the soils of the world. *European Journal of Soil Science* **47,** 151-163.

BATJES N. H. & SOMBROEK W. G. 1997. Possibilities for carbon sequestration in tropical and subtropical soils. *Global Change Biology* **3,** 161-173.

BECKMANN G. G. 1983. Development of old landscapes and soils. *In:* ANONYMOUS, ed. *Soils, an Australian viewpoint*, pp. 51-71. CSIRO, Melbourne, Australia.

BENBOW M. C. 1983. Tertiary stratigraphy and weathering events, western margin of the Gawler Craton, South Australia. *In:* ANONYMOUS, ed. *Sixth Australian geological convention; Lithosphere dynamics and evolution of continental crust.*, pp. 217-218. Geological Society of Australia, Sydney, N.S.W., Australia.

BENBOW M. C., CALLEN R. A., BOURMAN R. P. & ALLEY N. F. 1995. Deep weathering, ferricrete and silcrete. *In:* DREXEL J. F. and PREISS W. V., ed. *The geology of South Australia. Volume 2. The Phanerozoic*, pp. 201-207. South Australia. Geological Survey. Bulletin 54.

BENEDETTI M. & BOULEGUE J. 1991. Mechanism of gold transfer and deposition in a supergene environment. *Geochimica et Cosmochimica Acta* **55,** 1539-1547.

BENTON R. Y. 1994. A petrological, geochemical and isotopic investigation of granitoids from the Olary province of South Australia - implications for Proterozoic crustal growth, p. 68. University of Adelaide, Honours (*unpublished*).

BERMAN Y. S., BOTOVA M. M., BOCHEK L. I. & PLESHAKOV A. P. 1978. The natural series gold-silver. *Geochemistry International* **15,** 42-50.

BESHAY N. F. & SALLAM A. S. 1995. Evaluation of some methods for establishing uniformity of profile parent materials. *Arid Soil Research and Rehabilitation* **9,** 63-72.

BIERLEIN F. P., ASHLEY P. M. & PLIMER I. R. 1995. Sulphide mineralisation in the Olary Block, South Australia. *Mineralium Deposita* **30,** 424-438.

BIERLEIN F. P., ASHLEY P. M. & SECCOMBE P. K. 1996a. Origin of hydrothermal Cu-Zn-Pb mineralisation in the Olary Block, South Australia: evidence from fluid inclusions and sulphur isotopes. *Precambrian Research* **79,** 281-305.

BIERLEIN F. P., FOSTER D. A. & PLIMER I. R. 1996b. Tectonthermal implications of laser 40Ar/39Ar ages of sulphide-bearing veins and their host rocks in the Willyama Supergroup, South Australia. *Mineralogy and Petrology* **58,** 1-22.

BIRD M. I. & CHIVAS A. R. 1988. Oxygen isotope dating of the Australian regolith. *Nature (London)* **331,** 513-516.

BIRD M. I. & CHIVAS A. R. 1989. Stable-isotope geochronology of the Australian regolith. *Geochimica et Cosmochimica Acta* **53,** 3239-3256.

BIRD M. I. & CHIVAS A. R. 1993. Geomorphic and palaeoclimatic implications of an oxygen-isotope chronology for Australian deeply weathered profiles. *Australian Journal of Earth Sciences* **40,** 345-358.

BLACKBURN G. & MCLEOD S. 1983. Salinity of atmospheric precipitation in the Murray-Darling drainage division, Australia. *Australian Journal of Soil Research* **21,** 411-434.

BLAKE G. R. & HARTGE K. H. 1986. Bulk density. *In:* KLUTE A., ed. *Methods of soil analysis: Pt 1 Physical and mineralogical methods*, pp. 363-375. American Society of Agronomy-Soil Science Society of America, Madison, Wisconsin.

BLATT H. & TRACY R. J. 1996. *Petrology: Igneous, Sedimentary, and metamorphic*. W. H. Freeman and Company, New York, 529 pp.

BLUM J. D. 1997. The effect of Late Cenozoic glaciation and tectonic uplift on silicate weathering rates and the marine $^{87}Sr/^{86}Sr$ record. *In:* RUDDIMAN W. F., ed. *Tectonic uplift and climate change*, pp. 259-288. Plenum Press, New York.

BLUM J. D. & EREL Y. 1997. Rb-Sr isotope systematics of a granitic soil chronosequence: The importance of biotite weathering. *Geochimica et Cosmochimica Acta* **61,** 3193-3204.

BONWICK C. M. 1997. Discovery of the Challenger Gold Deposit: Implications for future exploration on the Gawler Craton, pp. 7.1-7.16 in *New Generation Gold Mines '97. Case histories of discovery*. Australian Mineral Foundation, Adelaide.

BOURMAN R. P. 1993a. Modes of ferricrete genesis: Evidence from southeastern Australia. *Zeitschrift fur Geomorphologie* **37,** 77-101.

BOURMAN R. P. 1993b. Perennial problems in the study of laterite: A review. *Australian Journal of Earth Sciences* **40,** 387-401.

BOWELL R. J., FOSTER R. P. & GIZE A. P. 1993a. The mobility of gold in tropical rain forest soils. *Economic Geology* **88,** 999-1016.

BOWELL R. J., GIZE A. P. & FOSTER R. P. 1993b. The role of fulvic acid in the supergene migration of gold in tropical rain forest soils. *Geochimica et Cosmochimica Acta* **57,** 4179-4190.

BOWLER J. M. 1976. Aridity in Australia: age, origins and expressions in aeolian landforms and sediments. *Earth-Science Reviews* **12,** 279-310.

BOYLE R. W. 1974. Element associations in mineral deposits and indicator elements of interest in geochemical prospecting (revised), pp. 40. Geological Survey of Canada, Paper 74-45.

BOYLE R. W. 1979. *The geochemistry of gold and its deposits (together with a chapter on geochemical prospecting for the element)*. Geological Survey of Canada, Bulletin 280, Ottawa, 584 pp.

BOYLE R. W., ALEXANDER W. M. & ASLIN G. E. M. 1975. Some observations on the solubility of gold. *Geological Survey of Canada Paper* **75-24,** 1-6.

BRANTLEY S. L., GOLDHABER M. B. & RAGNARSDOTTIR K. V. 2007. Crossing disciplines and scales to understand the critical zone. *Elements* **3,** 307-314.

BREWER R. 1964. *Fabric and mineral analysis of soils*. John Wiley & Sons, New York, 470 pp.

BRIMHALL G. H., ALPERS C. N. & CUNNINGHAM A. B. 1985. Analysis of supergene ore-forming processes and ground-water solute transport using mass balance principles. *Economic Geology and the Bulletin of the Society of Economic Geologists* **80,** 1227-1256.

BRIMHALL G. H., CHADWICK O. A., LEWIS C. J., COMPSTON W., WILLIAMS I. S., DANTI K. J., DIETRICH W. E., POWER M. E., HENDRICKS D. & BRATT J. 1992. Deformational mass transport and invasive processes in soil evolution. *Science* **255,** 695-702.

BRIMHALL G. H. & DIETRICH W. E. 1987. Constitutive mass balance relations between chemical composition, volume, density, porosity, and strain in metasomatic hydrochemical systems; results on weathering and pedogenesis. *Geochimica et Cosmochimica Acta* **51,** 567-587.

BRIMHALL G. H., LEWIS C. J., AGUE J. J., DIETRICH W. E., HAMPEL J., TEAGUE T. & RIX P. 1988. Metal enrichment in bauxites by deposition of chemically mature aeolian dust. *Nature (London)* **333,** 819-824.

BRIMHALL G. H., LEWIS C. J., FORD C. R. B., BRATT J., TAYLOR G. & WARIN O. 1991. Quantitative geochemical approach to pedogenesis; importance of parent material reduction, volumetric expansion, and eolian influx in lateritization. *Geoderma* **51; 1-4,** 51-91.

BROOKE B. 2001. The distribution of carbonate eolianite. *Earth-Science Reviews* **55,** 155-164.

BROOKS R. R. 1995. The nature, structure, and environment of microorganisms. *In:* BROOKS R. R., DUNN C. E. and HALL G. E. M., ed. *Biological systems in mineral exploration and processing*, pp. 159-175. Ellis Horwood Ltd., London.

BROWN A. D. & HILL S. M. 2003. Litter dams: A new method of mapping surface dispersion vectors at the White Dam prospect, Curnamona Craton, SA. *In:* ROACH I. C., ed. *Advances in Regolith*, pp. 24-28. CRC LEME.

BROWN A. D. & HILL S. M. 2004. Regolith-landform maps are an essential tool for interpreting regolith geochemistry: The White Dam, SA, experience. *In:* ROACH I. C., ed. *Regolith 2004*, pp. 37-41. CRC LEME.

BROWN A. D. & HILL S. M. 2005. White Dam Au-Cu Prospect, Curnamona Province, South Australia. *In:* BUTT C. R. M., ROBERTSON I. D. M., SCOTT K. M. and CORNELIUS M., ed. *Regolith expressions of Australian ore system*, pp. 392-394. CRC LEME, Perth.

BRUAND A. & DUVAL O. 1999. Calcified fungal filaments in the petrocalcic horizon of Eutrochrepts in Beauce, France. *Soil Science Society of America Journal* **63,** 164-169.

BUDD A., WYBORN L. & BASTRAKOVA I. 1998. Exploration significance of the Hiltaba Suite, South Australia. *AGSO Research Newsletter* **29,** 1-4.

BULLOCK P., FEDEROFF N., JONGERIUS A., STOOPS G., TURSINA T. & BABEL U. 1985. *Handbook for soil thin section description*. Waine Research Publications, Wolverhampton, 152 pp.

BURFORD E. P., HILLIER S. & GADD G. M. 2006. Biomineralization of fungal hyphae with calcite ($CaCO_3$) and calcium oxelate mono- and dihydrate in carboniferous limestone microcosms. *Geomicrobiology Journal* **23,** 599-611.

BUSCHE F. D. 1989. Using plants as an exploration tool for gold. *Journal of Geochemical Exploration* **32; 1-3,** 199-209.

BUTLER B. E. 1956. Parna - an aeolian clay. *Australian Journal of Science* **18,** 145-151.

BUTT C. R. M. 1987. The dispersion of gold in the weathered zone, Yilgarn Block, Western Australia, pp. 27-53 in *Meaningful sampling in gold exploration*. Australian Institute of Geoscientists, Bulletin no. 7, Perth.

CALLAHAN J. 1987. A nontoxic heavy liquid and inexpensive filters for separation of mineral grains. *Journal of Sedimentary Petrology* **57,** 765-766.

CANADELL J., JACKSON R. B., EHLERINGER J. R., MOONEY H. A., SALA O. E. & SCHULZE E. D. 1996. Maximum rooting depth of vegetation types at the global scale. *Oecologia* **108,** 583-595.

CAPO R. C. & CHADWICK O. A. 1999. Sources of strontium and calcium in desert soil and calcrete. *Earth and Planetary Science Letters* **170,** 61-72.

CAPO R. C., STEWART B. W. & CHADWICK O. A. 1998. Strontium isotopes as tracers of ecosystem processes: theory and methods. *Geoderma* **82,** 197-225.

CARLISLE D. 1983. Concentration of uranium and vanadium in calcretes and gypcretes. *In:* WILSON R. C. L., ed. *Residual deposits; surface related weathering processes and materials*, pp. 185-195. Geological Society of London, London.

CASTANIER S., LE METAYER LEVREL G. & PERTHUISOT J. P. 1999. Ca-carbonates precipitation and limestone genesis - the microbiogeologist point of view. *Sedimentary Geology* **126,** 9-23.

CATTLE S. R., MCTAINSH G. H. & WAGNER S. 2002. Aeolian dust contributions to soil of the Namoi Valley, northern NSW, Australia. *Catena (Giessen)* **47,** 245-264.

CHADWICK O. A., BRIMHALL G. H. & HENDRICKS D. M. 1990. From a black to a gray box; a mass balance interpretation of pedogenesis. *Geomorphology* **3; 3-4,** 369-390.

CHEN X. Y., LINTERN M. J. & ROACH I. C. 2002. *Calcrete: characteristics, distribution and use in mineral exploration*. Cooperative Research Centre for Landscape Environments and Mineral Exploration (CRC LEME), Canberra, Australia, 160 pp.

CHIQUET A., MICHARD A., NAHON D. & HAMELIN B. 1999. Atmospheric input vs in situ weathering in the genesis of calcretes: An Sr isotope study at Galvez (Central Spain). *Geochimica et Cosmochimica Acta* **63,** 311-323.

CHUBB A. J. 1999. The geology of the White Dam area, Bulloo Creek Station, Olary, South Australia, p. 131. University of New England, Honours Thesis (*unpublished*).

CLARKE G. L., BURG J. P. & WILSON C. J. L. 1986. Stratigraphic and structural constraints on the Proterozoic tectonic history of the Olary Block, South Australia. *Precambrian Research* **34,** 107-137.

COLIN F. 1997. The behaviour of gold in the lateritic alteroshere. *In:* PAQUET H. and CLAUER N., ed. *Soils and sediments; mineralogy and geochemistry.*, pp. 139-156. Springer, Berlin, Federal Republic of Germany.

COLIN F., LECOMTE P. & BOULANGE B. 1989. Dissolution features of gold particles in a lateritic profile at Dondo Mobi, Gabon. *Geoderma* **45,** 241-250.

COLIN F. & VIEILLARD P. 1991. Behaviour of gold in the lateritic equatorial environment: weathering and surface dispersion of residual gold particles, at Dondo Mobi, Gabon. *Applied Geochemistry* **6,** 279-290.

COLIN F., VIEILLARD P. & AMBROSI J. P. 1993. Quantitative approach to physical and chemical gold mobility in equatorial rainforest lateritic environment. *Earth and Planetary Science Letters* **114,** 269-285.

CONKLIN A. R. 2005. *Introduction to soil chemistry: analysis and instrumentation*. John Wiley & Sons, Inc., Hoboken, New Jersey, 218 pp.

CONOR C. H. H. 2000. Definition of major sedimentary and igneous units of the Olary Domain, Curnamona Province. *MESA Journal* **19,** 51-56.

CONOR C. H. H. 2004. Geology of the Olary Domain, Curnamona Province, South Australia, pp. 87. Department of Primary Industries and Resources, South Australia.

CONOR C. H. H. 2006a. Lithostratigraphy of the Olary and Mulyugarie domains - 2006, pp. 26-33 in *Broken Hill Exploration Initiative: Abstracts for the September 2006 conference*, edited by KORSCH R. J. and BARNES R. G. Geoscience Australia, Record 2006/21.

CONOR C. H. H. 2006b. Lithostratigraphy-related mineralisation of the Olary and Mulyungarie domains, pp. 22-25 in *Broken Hill Exploration Initiative: Abstracts for the September 2006 conference*, edited by KORSCH R. J. and BARNES R. G. Geoscience Australia, Record 2006/21.

CONOR C. H. H. & FANNING C. M. 2001. Geochronology of the Woman-in-White amphibolite, Olary Domain. *MESA Journal* **20,** 41-43.

COOK N. J., WOOD SCOTT A. & ZHANG Y. 1992. Transport and fixation of Au, Pt and Pd around the Lac Sheen Cu-Ni-PGE occurrence in Qubec, Canada. *Journal of Geochemical Exploration* **46,** 187-228.

COOKE A. 2003. White Dam - an exciting new gold project in the Curnamona Province. *MESA Journal* **31,** 46-47.

CORDON E. L. 1998. An investigation into the genesis of mineralisation at the White Dam prospect, Olary Block, South Australia, p. 64. The University of Adelaide, Honours Thesis (*unpublished*).

COTTON S. A. 1997. *Chemistry of precious metals*. Blackie Academic & Professional, London, 374 pp.

COX R. 1975. Geochemical soil surveys in exploration for nickel-copper sulphides at Pioneer, near Norseman, Western Australia. *In:* ELLIOTT I. L. and FLETCHER W. K., ed. *Geochemical exploration 1974*, pp. 437-460. Elsevier, Amsterdam.

CRAIG M. A. 2005. Regolith-landform mapping, the path to best practice. *In:* ANAND R. R. and DE BROEKERT P., ed. *Regolith landscape evolution across Australia*, pp. 53-61. CRCLEME, Perth.

CREMEENS D. L. & MOKMA D. L. 1986. Argillic horizon expression and classification in the soils of two Michigan Hydrosequences. *Soil Science Society of America Journal* **50,** 1002-1007.

CROCKER R. L. 1946. Post-Miocene climatic and geologic history and its significance in relation to the genesis of the major soil types of South Australia. *Council for Scientific and Industrial Research (CSIR) Bulletin* **193,** 56pp.

CROMACK K., JR., SOLLINS P., TODD R. L., FOGEL R., TODD A. W., FENDER W. M., CROSSLEY M. E. & CROSSLEY D. A., JR. 1977. The role of oxalic acid and bicarbonate in calcium cycling by fungi and bacteria: some possible implications for soil animals. *Ecology Bulletin* **25,** 246-252.

CROXFORD N. J. W. 1998. White Dam, Olary Block, South Australia, The Petrology of drill core samples from DDH WD15, WD16 and WD17, pp. 100. Rockco Mineralogy and Petrology Services, Brisbane.

CULLERS R., CHAUDHURI S., KILBANE N. & KOCH R. 1979. Rare-earths in size fractions and sedimentary rocks of Pennsylvanian-Permian age from the mid-continent of the USA. *Geochimica et Cosmochimica Acta* **43,** 1285-1301.

DALY S. J., FANNING C. M. & FAIRCLOUGH M. C. 1998. Tectonic evolution and exploration potential of the Gawler Craton, South Australia. *AGSO Journal of Australian Geology and Geophysics* **17,** 145-168.

DEAN J. A. 1992. *Lange's handbook of chemistry*. McGraw-Hill, New York pp.

DELANEY T. A. & FLETCHER W. K. 1993. Size distribution of gold in some soils associated with selected gold mineralisation in Canada and the United States of America. *Journal of Geochemical Exploration* **48,** 309-327.

DHU T., HEINSON G. S. & JOSEPH J. 2003. The hydraulic and electrical fractal dimension of regolith. *In:* ROACH IAN C., ed. *Advances in regolith; proceedings of the CRC LEME regional regolith symposia 2003.*, pp. 95-99. Cooperative Research Centre for Landscape Environments and Mineral Exploration. Bentley, West. Aust., Australia. 2003.

DIXON J. C. 1998. Need for an international concensus on calcareous paleosol classification. *Quaternary International* **51-52,** 11-12.

DONER H. E. & GROSSL P. R. 2002. Carbonates and evaporites. *In:* DIXON J. B. and SCHULZE D. G., ed. *Soil mineralogy with environmental applications*, pp. 199-228. Soil Science Society of America, Madison, USA.

DREW M. C. 1990. Root function, development, growth and mineral nutrition. *In:* LYNCH J. M., ed. *The rhizosphere*John Wiley & Sons Ltd., Chichester, England.

DUNN C. E. 1995a. A field guide to biogeochemical prospecting. *In:* BROOKS R. R., DUNN C. E. and HALL G. E. M., ed. *Biological systems in mineral exploration and processing*, pp. 345-369. Ellis Horwood Ltd., London.

DUNN C. E. 1995b. Introduction to biogeochemical prospecting. *In:* BROOKS R. R., DUNN C. E. and HALL G. E. M., ed. *Biological systems in mineral exploration and processing*, pp. 233-242. Ellis Horwood Ltd., London.

DUNN C. E., COKER W. B. & ROGERS P. J. 1991. Reconnaissance and detailed geochemical surveys for gold in eastern Nova Scotia using plants, lake sediment, soil and till. *Journal of Geochemical Exploration* **40,** 143-163.

DURAND N., AHMAD S. M., HAMELIN B., GUNNELL Y. & CURMI P. 2006. Origin of Ca in South Indian calcretes developed on metamorphic rocks. *Journal of Geochemical Exploration* **88,** 275-278.

EDGECOMBE D. 1997. Challenger gold deposit; exploration case history. *MESA Journal* **4,** 8-11.

EGGLETON R. A. 2001. *The regolith glossary; surficial geology, soils and landscapes*. Cooperative Research Centre for Landscape Evolution and Mineral Exploration, Canberra, 144 pp.

EGGLETON R. A. 2008. Regolith mineralogy. *In:* SCOTT K. M. and PAIN C. F., ed. *Regolith science*, pp. 45-72. CSIRO Publishing, Melbourne.

EGLI M. & FITZE P. 2000. Formulation of pedologic mass balance based on immobile elements: A revision. *Soil Science* **165,** 437-443.

EHRLICH H. L. 1996. How microbes influence mineral growth and dissolution. *Chemical Geology* **132,** 5-9.

EHRLICH H. L. 1998. Geomicrobiology: its significance for geology. *Earth-Science Reviews* **45,** 45-60.

ELBERSEN G. W. W., DAVIES G. R., VAN R. L. P. & JANSSEN R. P. T. 1999. Quantification of the incorporation of atmospheric CO (sub 2) in calcic horizons. *In:* LAL R., KIMBLE JOHN M., ESWARAN H. and STEWART B. A., ed. *Global climate change and pedogenic carbonates*, pp. 87-95. Lewis Publishers, Boca Raton, FL, United States.

ERICKSON R. L., MARRANZINO A. P., ODA U. & JANES W. W. 1964. *Geochemical exploration near the Getchell Mine Humboldt County, Nevada*. U. S. Geological Survey Bulletin 1198-A, Washington, 26 pp.

ESWARAN H., REICH P. F., KIMBLE J. M., BEINROTH F. H., PADMANABHAN E. & MONCHAROEN P. 1999. Global carbon stocks. *In:* LAL R., KIMBLE J., M., ESWARAN H. and STEWART B. A., ed. *Global climate change and pedogenic carbonates*, pp. 15-25. Lewis Publishers, Boca Raton, FL.

EVANS L. J. 1978. Quantification and pedological processes. *In:* MAHANEY W. C., ed. *Quaternary soils*, pp. 361-378. Geo Abstracts, Norwich.

EXCO RESOURCES. 2006. Annual Report 2006, pp. 68. Exco Resources, (available online from www.excoresources.com.au), Perth.

FAURE G. & MENSING T. M. 2005. *Isotopes: principles and applications*. John Wiley & Sons, Inc., Hoboken, N.J, 897 pp.

FERRIS G. 1996. The Yarlbrinda Shear Zone - a new exploration focus for the western Gawler Craton. *MESA Journal* **3,** 29-31.

FERRIS G. 1998. Calcrete sampling within Pureba Conservation Park. *MESA Journal* **8,** 12-14.

FERRIS G. & SCHWARZ M. 2003. Proterozoic gold province of the central Gawler Craton. *MESA Journal* **30,** 4-12.

FERRIS G. & WILSON M. 2004. Tunkillia Project; Proterozoic shear-zone-hosted gold mineralisation within the Yarlbrinda shear zone. *MESA Journal* **35,** 6-12.

FERRIS G. M. 2001. *The geology and geochemistry of granitoids in the Childara region, west Gawler Craton, South Australia; implications for the Proterozoic tectonic history of the western Gawler Craton, and development of lode-style gold mineralisation at Tunkillia* pp.

FERRIS G. M. & FAIRCLOUGH M. C. 2007. Explanatory notes for the CHILDARA 1:250 000 Geological Map, pp. 64. Department of Primary Industries and Resources. Report Book 2007/8, South Australia.

FERRIS G. M. & SCHWARZ M. 2004. Definition of the Tunkillia Suite, western Gawler Craton. *MESA Journal* **34,** 32-41.

FERRIS G. M., SCHWARZ M. P. & HEITHERSAY P. 2002. The geological framework, distribution and controls of Fe-oxide Cu-Au mineralisation in the Gawler Craton, South Australia. Part 1; Geological and tectonic framework. *In:* PORTER T. M., ed. *Hydrothermal iron oxide copper gold & related deposits: A global perspective, volume 2*, pp. 9-31. PGC Publishing, Adelaide.

FETZER W. G. 1934. Transportation of gold by organic solutions. *Economic Geology* **29,** 599-604.

FIDLER R. 2007. Reduce, reuse, recycle: The Gawler calcrete reanalysis project. *In:* COOPER B. J. and KEELING J. L., ed. *5th Sprigg Symposium, Regolith, Mineral Deposits and Environment*, pp. 62-66. Geological Society of Australia Abstracts, No. 87, Adelaide.

FITZPATRICK R. W. & CHITTLEBOROUGH D. J. 2002. Titanium and zirconium minerals. *In:* DIXON J. B., SCHULZE D. G. and AMONETTE JAMES E., ed. *Soil mineralogy with environmental applications*, pp. 667-690. Soil Science Society of America, Madison, Wis.

FLINT D. J. & PARKER A. J. 1993. Willyama Inliers. *In:* DREXEL J. F., PREISS W. V. and PARKER A. J., ed. *The geology of South Australia; Volume 1, The Precambrian*, pp. 82-93. Geological Survey of South Australia, Adelaide.

FODEN J., BAROVICH K., JANE M. & O'HALLORAN G. 2001. Sr-isotopic evidence for late Neoproterozoic rifting in the Adelaide Geosyncline at 586 Ma: implications for a Cu ore forming fluid flux. *Precambrian Research* **106,** 291-308.

FORBES B. G. & PREISS W. V. 1987. Stratigraphy of the Burra Group. *In:* PREISS W. V., ed. *The Adeldaide Geosyncline-late Proterozoic stratigraphy, sedimentation, palaeontology and tectonics*, pp. 73-123. Geological Survey of South Australia.

FREEMAN H. S. R. 1995. A geochemical and isotopic study of mafic and intermediate rocks in the Olary province, South Australia - magma series discrimination and geochronological framework, p. University of Adelaide, Honours (*unpublished*).

FREISE F. W. 1931. The transportation of gold by organic underground solutions. *Economic Geology* **26,** 421-431.

FREYSSINET P., LAWRANCE L. M. & BUTT C. R. M. 1990. Geochemistry and morphology of gold in lateritic profiles in savanna and semi-arid climates. *Chemical Geology* **84,** 61-63.

FREYSSINET P., LECOMTE P. & EDIMO A. 1989a. Dispersion of gold and base metals in the Mborguene lateritic profile, East Cameroun. *Journal of Geochemical Exploration* **32,** 99-116.

FREYSSINET P., ZEEGERS H. & TARDY Y. 1989b. Morphology and geochemistry of gold grains in lateritic profiles of southern Mali. *Journal of Geochemical Exploration* **32,** 17-31.

GARDNER G. J., MORTLOCK A. J., PRICE D. M., READHEAD M. L. & WASSON R. J. 1987. Thermoluminescence and radiocarbon dating of Australian desert dunes. *Australian Journal of Earth Sciences* **34,** 343-357.

GARNETT D. L., REA W. J. & FUGE R. 1982. Geochemical exploration techniques applicable to calcrete-covered areas. *In*, ed. *Proceedings; Twelfth congress of the Council of Mining and Metallurgical Institutions; Vol. 2.*, pp. 945-955. S. Afr. Inst. Min. Metall., Marshalltown, South Africa.

GATELLIER J. P. & DISNAR J. R. 1990. Kinetics and mechanism of the reduction of Au(III) to Au(0) by sedimentary organic materials. *Organic Geochemistry* **16,** 631-640.

GEE G. W. & BAUDER J. W. 1986. Particle-size analysis. *In:* KLUTE A., ed. *Methods of soil analysis: Pt 1 Physical and mineralogical methods*, pp. 383-411. American Society of Agronomy-Soil Science Society of America, Madison, Wisconsin.

GEE G. W. & OR D. 2002. Particle-size analysis. *In:* DANE J. H. and TOPP G. C., ed. *Methods of soil analysis: Pt 4 Physical methods*, pp. 255-293. Soil Science Society of America Inc., Madison, Wisconsin.

GIBBONS L. 1997. Regolith study at the Old Well gold prospect, Tarcoola district, Gawler Craton, p. 37. The University of Adelaide, Honours Thesis (*unpublished*).

GIBBS R. J., MATTHEWS M. D. & LINK D. A. 1971. The relationship between sphere size and settling velocity. *Journal of Sedimentary Petrology* **41,** 7-18.

GILE L. H. 1993. Carbonate stages in sandy soils of the Leasburg surface, southern New Mexico. *Soil Science* **156,** 101-110.

GILE L. H., PETERSON F. F. & GROSSMAN R. B. 1966. Morphological and genetic sequences of carbonate accumulation in desert soils. *Soil Science* **101,** 347-360.

GILKES R. J. 1999. Don't forget the biological part of the regolith. *AIG Bulletin* **30,** 35-55.

GLASS A. D. M. 1989. *Plant nutrition: An introduction to current concepts*. Jones and Bartlett, Boston, 234 pp.

GLEN R. A., DALLMEYER R. D. & BLACK L. P. 1992. Isotopic dating of basin inversion - The Palaeozoic Cobar Basin, Lachlan Orogen, Australia. *Tectonophysics* **214,** 249-268.

GOODHEW P. J., HUMPHREYS J. & BEANLAND R. 2001. *Electron microscopy and analysis*. Taylor & Francis, London, 251 pp.

GOUDIE A. 1972. On the definition of calcrete deposits. *Zeitschrift fuer Geomorphologie* **16,** 464-468.

GOUDIE A. 1973. *Duricrusts in Tropical and Subtropical Landscapes*. Clarendon Press; Oxford Research Studies in Geography, 174 pp.

GOUDIE A. S. 1983. Calcrete. *In:* GOUDIE A. S. and PYE K., ed. *Chemical sediments and geomorphology; precipitates and residua in the near-surface environment*, pp. 93-131. Acad. Press, London, United Kingdom.

GRAUSTEIN W. C., CROMACK K., JR. & SOLLINS P. 1977. Calcium oxalate: occurrence in soils and effect on nutrient and geochemical cycles. *Science* **198,** 1252-1254.

GRAY D. & LINTERN M. 1994. The solubility of gold in soils from semi-arid areas of Western Australia. *Exploration and Mining Research News / CSIRO Division of Exploration and Mining* **1,** 8-9.

GRAY D. J., BUTT C. R. M. & LAWRANCE L. M. 1992. The geochemistry of gold in lateritic terrains. *In:* BUTT C. R. M. and ZEEGERS H., ed. *Regolith exploration geochemistry in tropical and subtropical terrains.*, pp. 461-482. Elsevier, Amsterdam-Oxford-New York, International.

GRAY D. J. & LINTERN M. J. 1998. Chemistry of gold in soils from the Yilgarn Craton, Western Australia, pp. 209-221 in *The state of the regolith. Proceedings of the second Australian conference on landscape evolution and mineral exploration*, edited by EGGLETON R. A. Geological Society of Australia Special Publication, Brisbane.

GRAY D. J., LINTERN M. J. & LONGMAN G. D. 1990. *Chemistry of gold in some Western Australian soils*. CSIRO Division of Exploration Geoscience Report 126R (Reissued as CRC LEME Open File Report 68, Cooperative Research Centre for Landscape Evolution and Mineral Exploration (CRCLEME), Perth,1999), 62 pp.

GRAY D. J., LINTERN M. J. & LONGMAN G. D. 1998. Readsorption of gold during selective extraction - observations and potential solutions. *Journal of Geochemical Exploration* **61,** 21-37.

GRAY D. J. & PIRLO M. C. 2004. Geochemistry of groundwaters at Tunkillia; similarities and differences to Yilgarn Craton groundwaters. *In:* ROACH IAN C., ed. *Regolith 2004;*

proceedings of the CRC LEME regional regolith symposia 2004., pp. 103-106. Cooperative Research Centre for Landscape Environments and Mineral Exploration. Bentley, West. Aust., Australia. 2004.

GRAY D. J. & PIRLO M. C. 2005. *Hydrogeochemistry of the Tunkillia gold prospect, South Australia*. Cooperative Research Centre for Landscape Evolution and Mineral Exploration. Open file report 194, Perth, Australia, 92 pp.

GRIMES D. J., FICKLIN W. H., MEIER A. L. & MCHUGH J. B. 1995. Anomalous gold, antimony, arsenic, and tungsten in ground water and alluvium around disseminated gold deposits along the Gretchell Trend, Humboldt County, Nevada. *Journal of Geochemical Exploration* **52,** 351-371.

GUEDRIA A., TRICHET J. & WILHELM E. 1989. Behaviour of lead and zinc in calcrete-bearing soils around Bou Grine, Tunisia; its application to geochemical exploration. *Journal of Geochemical exploration* **32; 1-3,** 117-132.

HAMIDI E. M., COLIN F., MICHARD A., BOULANGE B. & NAHON D. 2001. Isotopic tracers of the origin of Ca in a carbonate crust from the Middle Atlas, Morocco. *Chemical Geology* **176,** 93-104.

HAMIDI E. M., NAHON D., MCKENZIE J. A., MICHARD A., COLIN F. & KAMEL S. 1999. Marine Sr (Ca) input in Quaternary volcanic rock weathering profiles from the Meditterranean coast of Morrocco: Sr isotopic approach. *Terra Nova* **11,** 157-161.

HAND M., REID A. & JAGODZINSKI L. 2007. Tectonic framework and evolution of the Gawler Craton, southern Australia. *Economic Geology* **102,** 1377-1395.

HARVEY N., BELPERIO A. P. & BOURMAN R. P. 2001. Late Quaternary sea-levels, climate change and South Australian coastal geology. *In:* GOSTIN V. A., ed. *Gondwana to greenhouse; Australian environmental geoscience*Geological Society of Australia, Sydney.

HAWKES H. E. & WEBB J. S. 1962. *Geochemistry in mineral exploration*. Harper & Row, New York pp.

HENDRICKX M., SLATER K., CRISP A., DEAN A., VANDENBERG L. & SMITH J. 2000. *Palaeoproterozoic stratigraphy of the Tanami region: regional correlations and relation to mineralisation-preliminary results*. Northern Territory Geological Survey, Record 2000-013 pp.

HESSE P. P., MAGEE J. W. & VAN DER KAARS S. 2004. Late Quaternary climates of the Australian arid zone: a review. *Quaternary International* **118-119,** 87-102.

HESSE P. P. & MCTAINSH G. H. 2003. Australian dust deposits: modern processes and the Quaternary record. *Quaternary Science Reviews* **22,** 2007-2035.

HILL L. J. 2004. Geochemical and biogeochemical dispersion and residence in landscapes of western New South Wales, p. 376. Australian National University, Ph.D. (*unpublished*).

HILL S. M. 2000. The regolith and landscape evolution of the Broken Hill block, Australia, p. 476. Australian National University, Ph.D. (*unpublished*).

HILL S. M., EGGLETON R. A. & TAYLOR G. 2003. Neotectonic disruption of silicified palaeovalley systems in an intraplate, cratonic landscape: regolith and landscape evolution of the Mulculca range-front, Broken Hill Domain, New South Wales. *Australian Journal of Earth Sciences* **50,** 691-707.

HILL S. M. & HILL L. J. 2003. Some important plant characteristics and assay overviews for biogeochemical surveys in western New South Wales. *In:* ROACH IAN C., ed. *Advances in regolith*, pp. 187-192. CRC LEME.

HILL S. M., MCQUEEN K. G. & FOSTER K. A. 1998a. Regolith carbonate accumulations in western and central NSW: characteristics and potential as an exploration sampling medium, pp. 191-206 in *Regolith 98, Australian regolith & mineral exploration: New*

approaches to an old continent, edited by TAYLOR G. M. and PAIN C. F., WMC Conference centre, Kalgoorlie, Western Australia.

HILL S. M., TAYLOR G. & MCQUEEN K. G. 1998b. Genesis of some calcretes in the southern Yilgarn craton, Western Australia: implications for mineral exploration - Discussion. *Australian Journal of Earth Sciences* **45,** 177-178.

HILL S. M., TAYLOR G., MCQUEEN K. G., ANAND R. R., PHANG C., WILDMAN J. E. & LINTERN M. J. 1998c. Genesis of some calcretes in the southern Yilgarn Craton, Western Australia; implications for mineral exploration; discussion and reply. *Australian Journal of Earth Sciences* **45,** 177-182.

HONG H. 2000. Behaviour of gold in the weathered mantle at Shewushan, Hubei, China. *Journal of Geochemical Exploration* **68,** 57-68.

HONG H., SUN Z., FU Z. & MIN X. 2003. Adsorption of $AuCL_4^-$ by kaolinites: Effect of pH, Temperature and kaolinite crystallinity. *Clays and Clay Minerals* **51,** 493-501.

HOU B., FRAKES L. A., SANDIFORD M., WORRALL L., KEELING J. L. & ALLEY N. F. 2008. Cenozoic Eucla Basin and associated palaeovalleys, southern Australia - Climatic and tectonic influences on landscape evolution, sedimentation and heavy mineral accumulation. *Sedimentary Geology* **203,** 112-130.

HOUGH R., REDDY S., HITCHEN G., VAUGHAN D., ANAND R., HART R. & SAUNDERS M. 2006. Supergene gold at the Golden Virgin Pit, Parker Range, Western Australia. *In:* FITZPATRICK R. W. and SHAND P., ed. *Regolith 2006 - Consolidation and dispersion of ideas*, pp. 154-155. CRC LEME, Perth, Western Australia.

HUTTON J. T. & DIXON J. C. 1981. The chemistry and mineralogy of some South Australian calcretes and associated soft carbonates and their dolomitisation. *Journal of the Geological Society of Australia* **28,** 71-79.

IOGLOBAL. 2007. ioGAS Exploratory data analysis, pp. ioGlobal http://www.ioglobal.net, Perth.

ISBELL R. F. 1996. *The Australian soil classification*. CSIRO Publishing, Collingwood, Victoria, 143 pp.

JAILLARD B., GUYON A. & MAURIN A. F. 1991. Structure and composition of calcified roots, and their identification in calcareous soils. *Geoderma* **50,** 197-210.

JAMES N. P., BOREEN T. D., BONE Y. & FEARY D. A. 1994. Holocene carbonate sedimentation on the west Eucla Shelf, Great Australian Bight: a shaved shelf. *Sedimentary Geology* **90,** 161-177.

JARVIS A., REUTER H. I., NELSON E. & GUEVARA E. 2006. *Hole-filled seamless SRTM data V3*, [Online, accessed 23/01/2008], International Centre for Tropical Agriculture (CIAT). http://srtm.csi.cgiar.org

JEAN G. E. & BANCROFT G. M. 1985. An XPS and SEM study of gold deposition at low temperatures on sulphide mineral surfaces: Concentration of gold by adsorption/reduction. *Geochimica et Cosmochimica Acta* **49,** 979-987.

JENNY H. & LEONARD C. D. 1934. Functional relationships between soil properties and rainfall. *Soil Science* **38,** 363-398.

JERSAK J., AMUNDSON R. & BRIMHALL G., JR. 1995. A mass balance analysis of podzolization; examples from the northeastern United States. *Geoderma* **66,** 15-42.

JERSAK J. M. 1991. Quantification of chemical and physical changes occurring during the pedogenic processes of podzolization: Examples from Northeastern United States, p. 272. University of California, PhD Thesis (*unpublished*).

JONES B. 1988. The influence of plants and micro-organisms on diagenesis in caliche; example from the Pleistocene Ironshore Formation on Cayman Brac, British West Indies. *Bulletin of Canadian Petroleum Geology* **36,** 191-201.

JOYCE A. S. 1984. *Geochemical exploration*. Australian Mineral Foundation Inc, Glenside, South Australia, 184 pp.

KABANOV P., ANADON P. & KRUMBIEN W. E. 2008. *Microcodium*: An extensive review and a proposed non-rhizogenic biologically induced origin for its formation. *Sedimentary Geology* **205,** 79-99.

KABATA-PENDIAS A. & PENDIAS H. 2001. *Trace elements in soils and plants. 3 ed*. CRC Press. Boca Raton, FL, United States. Pages: 413. 2001. pp.

KEELING J. 2004. Metal ion dispersion through transported cover at Moonta, South Australia. *In:* ROACH I. C., ed. *Regolith 2004; proceedings of the CRC LEME regional regolith symposia 2004*, pp. 161-165. CRC LEME.

KLAPPA C. F. 1978. Biolithogenesis of Microcodium: elucidation. *Sedimentology* **25,** 489-522.

KLAPPA C. F. 1980. Rhizoliths in terrestrial carbonates: classification, recognition, genesis and significance. *Sedimentology* **27,** 613-629.

KLEIN C. & HURLBUT C. S., JR. 1999. *Manual of mineralogy. 21st ed, rev.* John Wiley & Sons, New York, 681 pp.

KNOX G. J. 1977. Caliche profile formation, Saldanha Bay (South Africa). *Sedimentology* **24,** 657-674.

KOSIR A. 2004. *Microcodium* revisited: Root calcification products of terrestrial plants on carbonate-rich substrates. *Journal of Sedimentary Research* **74,** 845-857.

KRAUSKOPF K. B. 1951. The solubility of gold. *Economic Geology* **46,** 858-870.

KRUPP R. E. & WEISER T. 1992. On the stability of gold-silver alloys in the weathering environment. *Mineralium Deposita* **27,** 268-275.

KUNZE G. W. & DIXON J. B. 1986. Pretreatment for mineralogical analysis. *In:* KLUTE A., ed. *Methods of soil analysis: Pt 1 Physical and mineralogical methods*, pp. 91-100. American Society of Agronomy-Soil Science Society of America, Madison, Wisconsin.

LAING B. 1996. Stratigraphic subdivision of the Willyama Supergroup - Olary domain, South Australia. *MESA Journal* **2,** 39-48.

LAKIN H. W., CURTIN G. C. & HUBERT A. E. 1974. *Geochemistry of gold in the weathering cycle*. U. S. Geological Survey Bulletin 1330, Washington, 80 pp.

LAMPLUGH G. W. 1902. Calcrete. *Geological Magazine* **9,** 575.

LANE R. & WORRALL L. 2002. Interpretation of airborne electromagnetic data: Summary report on the Tunkillia workshop, pp. 78. Geoscience Australia.

LAU I. C. 2004. Regolith-Landform and mineralogical mapping of the White Dam Prospect, eastern Olary Domain, South Australia, using integrated remote sensing and spectral techniques, p. 428. The University of Adelaide, Phd Thesis (*unpublished*).

LAWRANCE L. M. & GRIFFIN B. J. 1994. Crystal features of supergene gold at Hannan South, Western Australia. *Mineralium Deposita* **29,** 391-398.

LECOMTE P. & COLIN F. 1989. Gold dispersion in a tropical rainforest weathering profile at Dondo Mobi, Gabon. *Journal of Geochemical Exploration* **34,** 285-301.

LEDIN M. 2000. Accumulation of metals by microorganisms - processes and importance for soil systems. *Earth-Science Reviews* **51,** 1-31.

LENGKE M. F. & SOUTHAM G. 2005. The effect of thiosulfate-oxidizing bacteria on the stability of the gold-thiosulfate complex. *Geochimica et Cosmochimica Acta* **69,** 3759-3772.

LEVINSON A. A. 1974. *Introduction to exploration geochemistry*. Applied publishing Ltd., Calgary, Alberta, 612 pp.

LIBBY W. G. & DE LAETER J. R. 1998. Biotite Rb-Sr age evidence for Early Palaeozoic tectonism along the cratonic margin in southwestern Australia. *Australian Journal of Earth Sciences* **45,** 623-632.

LIDE D. R. 2004. *CRC Handbook of chemistry and physics*. CRC Press, Boca Raton, FL, 2616 pp.

LINDSAY W. L., VLEK P. L. G. & CHIEN S. H. 1989. Phosphate Minerals. *In:* DIXON J. B. and WEED S. B., ed. *Minerals in soil environments*, pp. 1089-1130. Soil Science Society of America, Madison, WI, United States.

LINTERN M. J. 1989. *Study of the distribution of gold in soils at Mt Hope, Western Australia*. CSIRO Division of Exploration Geoscience Report 24R (Reissued as CRC LEME Open File Report 65, Cooperative Research Centre for Landscape Evolution and Mineral Exploration (CRCLEME), Perth,1999), 36 pp.

LINTERN M. J. 1997. Calcrete sampling for gold exploration. *MESA Journal* **5,** 5-8.

LINTERN M. J. 2001. Exploration for gold using calcrete; lessons from the Yilgarn Craton, Western Australia. *Geochemistry - Exploration, Environment, Analysis* **1,** 237-252.

LINTERN M. J. 2002. Calcrete sampling for mineral exploration. *In:* CHEN X. Y., LINTERN M. J. and ROACH I. C., ed. *Calcrete: Characteristics, distribution and use in mineral exploration*, pp. 31-109. Cooperative Research Centre for Landscape Environments and Mineral Exploration, Belconnen, ACT.

LINTERN M. J. & BUTT C. R. M. 1993. Pedogenic carbonate; an important sampling medium for gold exploration in semi-arid areas. *Exploration Research News / CSIRO Division of Exploration Geoscience* **7,** 7-11.

LINTERN M. J. & BUTT C. R. M. 1998a. *The distribution of gold and other elements in soils at Mulline, Western Australia*. Cooperative Research Centre for Landscape Evolution and Mineral Exploration. Open File Report 47, Perth, 58 pp.

LINTERN M. J. & BUTT C. R. M. 1998b. Gold exploration using pedogenic carbonate (calcrete), pp. 200-208 in *The state of the regolith. Proceedings of the second Australian conference on landscape evolution and mineral exploration*, edited by EGGLETON R. A. Geological Society of Australia Special Publication 20, Brisbane.

LINTERN M. J., BUTT C. R. M. & SCOTT K. M. 1997. Gold in vegetation and soil; three case studies from the goldfields of southern Western Australia. *Journal of Geochemical exploration* **58,** 1-14.

LINTERN M. J. & SHEARD M. J. 1999a. Regolith geochemistry and stratigraphy of the Challenger gold deposit. *MESA Journal* **14,** 9-14.

LINTERN M. J. & SHEARD M. J. 1999b. *Regolith studies related to the Challenger gold deposit, Gawler Craton, South Australia*. Cooperative Research Centre for Landscape Evolution and Mineral Exploration. Wembley, West, Aust., Australia, 85 pp.

LINTERN M. J., SHEARD M. J. & CHIVAS A. R. 2006. The source of pedogenic carbonate associated with gold-calcrete anomalies in the western Gawler Craton, South Australia. *Chemical Geology* **235,** 299-324.

LOISY C., VERRECCHIA E. P. & DUFOUR P. 1999. Microbial origin for pedogenic micrite associated with a carbonate paleosol (Champagne, France). *Sedimentary Geology* **126,** 193-204.

LOWREY J. R. 2007. Plant biogeochemical expression of Au-mineralisation buried by an aeolian dunefield: Tunkillia, South Australia, p. 116. The University of Adelaide, Honours thesis (*unpublished*).

LOWREY J. R. & HILL S. M. 2006. Plant biogeochemistry of Au-mineralisation burried by an aeolian dunefield: Tunkillia, SA. *In:* FITZPATRICK R. W. and SHAND P., ed. *Regolith 2006 - Consolidation and dispersion of ideas*, pp. 217-220. CRC LEME, Perth, Western Australia.

MACHETTE M. N. 1985. Calcic soils of the southwestern United States. *In:* WEIDE D. L. and FABER M. L., ed. *Soils and Quaternary geology of the Southwestern United States*, pp. 1-21. Geological Society of America (GSA), Boulder, CO, United States.

MAHOWALD N., KOHFELD K., HANNSSON M., BALKANSKI Y., HARRISON S. P., PRENTICE I. C., SCHULZ M. & RODHE H. 1999. Dust sources and deposition during the last glacial maximum and current climate: A comparison of model results with paleodata from ice cores and marine sediments. *Journal of Geophysical Research* **104,** 15895-15916.

MANN A. W. 1984. Mobility of gold and silver in lateritic weathering profiles: Some observations from Western Australia. *Economic Geology* **79,** 38-49.

MANN A. W. & HORWITZ R. C. 1979. Groundwater calcrete deposits in Australia; some observations from Western Australia. *Journal of the Geological Society of Australia* **26,** 293-303.

MANN S. 1992. Bacteria and the Midas touch. *Nature (London)* **357,** 358-360.

MARJORIBANKS R. W. 1997. *Geological methods in mineral exploration and mining*. Chapman & Hall, London, 115 pp.

MARSHALL C. E. & HASEMAN J. F. 1942. The quantitative evaluation of soil formation and development by heavy mineral studies: A grundy silt loam profile. *Soil Science society of America Journal* **7,** 448-453.

MARTIN A. R. 1997. The discovery of gold mineralisation at Tunkillia in the Gawler Craton, pp. 8.1- 8.8 in *New generation gold mines '97 case histories of discovery, conference proceedings*. Australian Mineral Foundation, Perth, Western Australia.

MCCONNAUGHEY T. A. & WHELAN J. F. 1997. Calcification generates protons for nutrient and bicarbonate uptake. *Earth-Science Reviews* **42,** 95-117.

MCDONALD R. C. & ISBELL R. F. 1990. Soil profile. *In:* MCDONALD R. C., ISBELL R. F., SPEIGHT J. G., WALKER J. and HOPKINS M. S., ed. *Australian soil and land survey: field handbook*, pp. 103-152. Inkata Press, Melbourne.

MCDONALD R. C., ISBELL R. F., SPEIGHT J. G., WALKER J. & HOPKINS M. S. 1990. *Australian soil and land survey: field handbook*. Inkata Press, Melbourne, 198 pp.

MCGEOUGH M. & ANDERSON J. 1998. Discovery of the White Dam Au-Cu mineralisation, pp. 69-71 in *Broken Hill Exploration Initiative: Abstracts of papers presented at fourth annual meeting in Broken Hill, October 19-21, 1998*, edited by GIBSON G. M. Australian Geological Survey Organisation, Record 1998/25.

MCGILLIS J. L. 1967. The silver content of caliche on alluvial fans as a regional guide to areas of silver and gold mineralization in the Basin and Range Province, p. 30. University of Nevada, MSc Thesis (*unpublished*).

MCHUGH J. B. 1988. Concentration of gold in natural waters. *Journal of Geochemical Exploration* **30,** 85-94.

MCKENZIE N., JACQUIER D., ISBELL R. & BROWN K. 2004. *Australian soils and landscapes: an illustrated compendium*. CSIRO Publishing, Collingwood, Australia, 416 pp.

MCLENNAN S. M. 1989. Rare earth elements in sedimentary rocks: Influence of provenance and sedimentary processes. *In:* LIPIN B. R. and MCKAY G. A., ed. *Reviews in Mineralogy V. 21 Geochemistry and mineralogy of rare earth elements*, pp. 169-200. Mineralogical Society of America, Washington.

MCQUEEN K. G., HILL S. M. & FOSTER K. A. 1999. The nature and distribution of regolith carbonate accumulations in southeastern Australia and their potential as a sampling medium in geochemical exploration. *Journal of Geochemical Exploration* **67,** 67-82.

MCTAINSH G. H. 1989. Quaternary aeolian dust processes and sediments in the Australian region. *Quaternary Science Reviews* **8,** 235-253.

MCTAINSH G. H. & LYNCH A. W. 1996. Quantitative estimates of the effect of climate change on dust storm activity in Australia during the last glacial maximum. *Geomorphology* **17,** 263-271.

MILNES A. R. 1992. Calcrete. *In:* MARTINI I. P. and CHESWORTH W., ed. *Weathering, soils & Paleosols.*, pp. 309-347. Elsevier, Amsterdam.

MILNES A. R. & HUTTON J. T. 1983. Calcretes in Australia. *In:* ANONYMOUS, ed. *Soils, an Australian viewpoint*, pp. 119-162. CSIRO, Melbourne, Australia.

MINEYEV G. G. 1976. Organisms in the gold migration-accumulation cycle. *Geochemistry International* **13,** 164-168.

MINOTAUR EXPLORATION LTD. 2007. 2007 Annual Report, pp. 69. Minotaur Exploration Ltd, (available online from http://www.minotaurexploration.com.au/), Adelaide, South Australia.

MOON C. J. 2006. Exploration geochemistry. *In:* MOON C. J., WHATELEY M. K. G. and EVANS A. M., ed. *Introduction to mineral exploration*, pp. 155-178. Blackwell Publishing, Malden, MA.

MORRIS B. J. & FLINTOFT M. W. 1999. Calcrete sampling of the Hawks Nest Prospect; highlighting the mineral potential. *MESA Journal* **15,** 5-7.

MOSSMAN D. J. & DYER B. D. 1985. The geochemistry of Witwatersrand-type gold deposits and the possible influence of ancient prokaryotic communities on gold dissolution and precipitation. *Precambrian Research* **30,** 303-319.

MUNSTERMAN D. & KERSTHOLT S. 1996. Sodium polytungstate, a new non-toxic alternative to bromoform in heavy liquid separation. *Review of Palaeobotany and Palynology* **91,** 417-422.

MURRAY-WALLACE C. V. 2002. Pleistocene coastal stratigraphy, sea-level highstands and neotectonism of the southern Australian passive continental margin - a review. *Journal of Quaternary Science* **17,** 469-489.

MYERS J. S. 1993. Precambrian history of the West Australian Craton and adjacent Orogens. *Annual Review of Earth and Planetary Sciences* **21,** 453-485.

NAHON D. & TARDY Y. 1992. The ferruginous laterites. *In:* BUTT C. R. M. and ZEEGERS H., ed. *Regolith exploration geochemistry in tropical and subtropical terrains.*, pp. 41-55. Elsevier, Amsterdam-Oxford-New York, International.

NAHON D. B. 1991. *Introduction to the petrology of soils and chemical weathering*. John Wiley and Sons, New York, 313 pp.

NAIMAN Z., QUADE J. & PATCHETT P. J. 2000. Isotopic evidence for eolian recycling of pedogenic carbonate and variations in carbonate dust sources throughout the Southwest United States. *Geochimica et Cosmochimica Acta* **64,** 3099-3109.

NAKATA P. A. 2003. Advances in our understanding of calcium oxalate crystal formation and function in plants. *Plant Science* **164,** 901-909.

NANSON G. C., CHEN X. Y. & PRICE D. M. 1995. Aeolian and fluvial evidence of changing climate and wind patterns during the past 100 ka in the western Simpson Desert, Australia. *Palaeogeography Palaeoclimatology Palaeoecology* **113,** 87-102.

NESBITT H. W. & YOUNG G. M. 1989. Formation and diagenesis of weathering profiles. *Journal of Geology* **97,** 129-147.

NETTERBERG F. 1967. Discussion on the nomenclature of soil carbonates. *Australian Journal of Science* **29,** 224-225.

NETTERBERG F. & CAIGER J. H. 1983. A geotechnical classification of calcretes and other pedocretes. *In:* WILSON R. C. L., ed. *Residual deposits; surface related weathering processes and materials.*, pp. 235-243. Geological Society of London, London, United Kingdom.

NORRISH K. & ROSSER H. 1983. Mineral phosphate. *In*, ed. *Soils: An Australian viewpoint*, pp. 335-361. CSIRO, Melbourne.

OKUJENI C. D., ACKON P., BAUGAARD W. & LANGA N. 2005. Controls of element dispersion in aeolian sand and calcrete-dominated regolith associated with gold mineralization in the Kraaipan greenstone belt, South Africa. *Geochemistry - Exploration, Environment, Analysis* **5,** 223-231.

OLLIER C. 1984. *Weathering*. Longman, London, 270 pp.

ONG H. L. & SWANSON V. E. 1969. Natural organic acids in the transportation, deposition, and transportation of gold. *Quarterly of the Colorado School of Mines* **64,** 395-425.

PAGE R. W., CONOR C. H. H., STEVENS B. P. J., GIBSON G. M., PREISS W. V. & SOUTHGATE P. N. 2005. Correlation of Olary and Broken Hill Domains, Curnamona Province: Possible relationship to Mount Isa and other north Australian Pb-Zn-Ag-bearing successions. *Economic Geology* **100,** 663-676.

PAIN C., CHAN R., CRAIG M., GIBSON D., KILGOUR P. & WILFORD J. 2007. *RTMAP regolith database field book and users guide (second edition)*. CRCLEME Open File Report 231, Perth, WA, 97 pp.

PAQUET H. & RUELLAN A. 1997. Calcareous epigenetic replacement (epigenie) in soils and calcrete formation. *In:* PAQUET H. and CLAUER N., ed. *Soils and sediments; mineralogy and geochemistry.*, pp. 21-48. Springer, Berlin.

PARKER A. J. 1990. Gawler Craton and Stuart Shelf; regional geology and mineralisation. *In:* HUGHES F. E., ed. *Geology of the mineral deposits of Australia and Papua New Guinea; Volume 2.*, pp. 999-1008. Australasian Institute of Mining and Metallurgy, Melbourne, Victoria, Australia.

PARKER A. J., PREISS W. V. & RANKIN L. R. 1993. Geological framework. *In:* DREXEL J. F., PREISS W. V. and PARKER A. J., ed. *The geology of South Australia; Volume 1, The Precambrian.*, pp. 9-31. Geological Survey of South Australia, Adelaide, South Aust., Australia.

PATON T. R., HUMPHREYS G. S. & MITCHELL P. B. 1995. *Soils: A new global view*. UCL Press, London, 213 pp.

PATON T. R. & WILLIAMS M. A. J. 1972. The concept of laterite. *Annals of the Association of American Geographers* **62,** 42-56.

PECSI M. 1990. Loess is not just the accumulation of dust. *Quaternary International* **7/8,** 1-21.

PHILLIPS S. E. & MILNES A. R. 1988. The Pleistocene terrestrial carbonate mantle on the southeastern margin of the St Vincent Basin, South Australia. *Australian Journal of Earth Sciences* **35,** 463-481.

PHILLIPS S. E., MILNES A. R. & FOSTER R. C. 1987. Calcified filaments; an example of biological influences in the formation of calcrete in South Australia. *Australian Journal of Soil Research* **25,** 405-428.

PHILLIPS S. E. & SELF P. G. 1987. Morphology, crystallography and origin of needle-fibre calcite in Quaternary pedogenic calcretes of South Australia. *Australian Journal of Soil Research* **25,** 429-444.

PILLANS B. 2005. Geochronology of the Australian regolith. *In:* ANAND R. R. and DE BROEKERT P., ed. *Regolith landscape evolution across Australia*, pp. 41-52. CRC LEME, Perth.

PILLANS B. 2007. Pre-Quaternary landscape inheritance in Australia. *Journal of Quaternary Science* **22,** 439-447.

PLEWINSKY B. & KAMPS R. 1984. Sodium Metatungstate, a New Medium for Binary and Ternary Density Gradient Centrifugation. *Makromolekulare Chemie-Macromolecular Chemistry and Physics* **185,** 1429-1439.

PREISS W. V. & CONOR C. H. H. 2001. Origin and nomeclature of the Willyama Inliers, Curnamona Province. *MESA Journal* **21,** 47-49.

PUDDEPHATT R. J. 1978. *The chemistry of gold*. Elsevier, Amsterdam pp.

PYE K. & TSOAR H. 1987. The mechanics and geological implications of dust transport and deposition in deserts with particular reference to loess formation and dune sand diagenesis in the northern Negev, Israel. *In:* FROSTICK L. E. and REID I., ed. *Desert sediments; ancient and modern*, pp. 139-156. Geological Society of London, London.

QUADE J., CHIVAS A. R. & MCCULLOCH M. T. 1995. Strontium and carbon isotope tracers and the origins of soil carbonate in South Australia and Victoria. *Palaeogeography Palaeoclimatology Palaeoecology* **113,** 103-117.

RAAD A. T. & PROTZ R. 1971. A new method for the identification of sediment stratification in soils of the Blue Springs Basin, Ontario. *Geoderma* **6,** 23-41.

RAN Y., FU J., RATE A. W. & GILKES R. J. 2002. Adsorption of Au(I, III) complexes on Fe, Mn oxides and humic acid. *Chemical Geology* **185,** 33-49.

RAYMENT G. E. & HIGGINSON F. R. 1992. *Australian laboratory handbook of soil and water chemical methods*. Inkata Press, Melbourne, 330 pp.

READ J. F. 1974. Calcrete Deposits and Quaternary Sediments, Edel Province, Shark Bay, Western Australia. *In*, ed. *Evolution and Diagenesis of Quaternary Carbonate Sequences, Shark Bay, Western Australia.*, pp. 250-282. American Association of Petroleum Geologists, Tulsa, OK, United States.

RECH J. A., QUADE J. & HART W. S. 2003. Isotopic evidence for the source of Ca and S in soil gypsum, anhydrite and calcite in the Atacama Desert, Chile. *Geochimica et Cosmochimica Acta* **67,** 575-586.

REEVES C. C., JR. 1970. Origin, classification, and geologic history of caliche on the southern High Plains, Texas and eastern New Mexico. *Journal of Geology* **78,** 352-362.

REID N., HILL S. M. & LEWIS D. M. 2008. Spinifex biogeochemical expressions of buried gold mineralisation: The great mineral exploration penetrator of transported regolith. *Applied Geochemistry* **23,** 76-84.

REITH F. & MCPHAIL D. C. 2006. Effect of resident microbiota on the solubilization of gold in soil from the Tomakin Park Gold Mine, New South Wales, Australia. *Geochimica et Cosmochimica Acta* **70,** 1421-1438.

REITH F. & MCPHAIL D. C. 2007. Mobility and microbially mediated mobilization of gold and arsenic in soils from two gold mines in semi-arid and tropical Australia. *Geochimica et Cosmochimica Acta* **71,** 1183-1196.

REITH F., ROGERS S. L., MCPHAIL D. C. & WEBB D. 2006. Biomineralization of gold: Biofilms on bacterioform gold. *Science* **313,** 233-236.

RETALLACK G. J. 2001. *Soils of the past an introduction to paleopedology*. Blackwell Science Ltd., Oxford, 404 pp.

RETALLACK G. J. 2005. Pedogenic carbonate proxies for amount and seaonality of precipitation in paleosols. *Geology (Boulder)* **33,** 333-336.

ROALDSET E. 1973. Rare earth elements in Quarternary clays of the Numedal area, southern Norway. *Lithos* **6,** 349-372.

ROBERTSON R. S., PREISS W. V., CROOKS A. F., HILL P. W. & SHEARD M. J. 1998. Review of the Proterozoic geology and mineral potential of the Curnamona Province in South Australia. *AGSO Journal of Australian Geology and Geophysics* **17,** 169-182.

ROBINSON-COOK S. E. 1986. Heavy liquid separation with Na-metatungstate, pp. 8 in *Open File Report 242*. New Mexico Bureau of Mines and Mineral Resources, Socorro, NM, United States.

ROLLINSON H. R. 1993. *Using geochemical data: Evaluation, presentation, interpretation*. Longman Group, Harlow UK pp.

ROWNTREE D. 1981. *Statistics without tears: A primer for non-mathematicians*. Penguin Books, London, 199 pp.

ROYER L. D. 1999. Depth to pedogenic carbonate horizon as a paleoprecipitation indicator? *Geology (Boulder)* **27,** 1123-1126.

RYABININ A. I., ROMANOV A. S., KHATAMOV S. & KHAMIDOVA R. 1974. Gold in ocean waters. *Geochemistry International* **11,** 118-122.

SANDIFORD M. 2003. Neotectonics of southeastern Australia: Linking the Quaternary faulting record with seismicity and *in situ* stress. *In:* HILLIS R. R. and MULLER R. D., ed. *Evolution and dynamics of the Australian plate*, pp. 107-119. Geological Society of Australia Special Publication **22** and Geological Society of America Special Paper **372**, Sydney.

SANTOS M. C. D., ST. ARNAUD R. J. & ANDERSON D. W. 1986. Quantitative evaluation of pedogenic changes in Boralfs (gray Luvisols) of east central Saskatchewan. *Soil Science Society of America Journal* **50,** 1013-1019.

SANTOSH M. & OMANA P. K. 1991. Very high purity gold from lateritic weathering profiles of Nilambur, southern India. *Geology (Boulder)* **19,** 746-749.

SANTOSH M., PHILIP R., JACOB M. K. & OMANA P. K. 1992. Highly pure placer gold formation in the Nilambur Valley, Wynad Gold Field, southern India. *Mineralium Deposita* **27,** 336-339.

SCHAETZL R. J. 1998. Lithologic discontinuities in some soils on drumlins: Theory, detection, and application. *Soil Science* **163,** 570-590.

SCHAETZL R. J. & ANDERSON S. 2005. *Soils: genesis and geomorphology*. Cambridge University Press, Cambridge, 817 pp.

SCHLESINGER W. H. 1982. Carbon storage in the caliche of arid soils: a case study from Arizona. *Soil Science* **133,** 247-255.

SCHMITT H. R., CAMERON E. M., HALL G. E. M. & VAIVE J. 1993. Mobilization of gold into lake sediments from acid and alkaline mineralized environments in the southern Canadian Shield: Gold in lake sediments and natural waters. *Journal of Geochemical Exploration* **48,** 329-358.

SCHOONEN M. A. A., FISHER N. S. & WENTE M. 1992. Gold sorption onto pyrite and goethite: A radiotracer study. *Geochimica et Cosmochimica Acta* **56,** 1801-1814.

SCHULZE D. G. 1989. An introduction to soil mineralogy. *In:* DIXON J. B. and WEED S. B., ed. *Minerals in soil environments*, pp. 1-34. Soil Science Society of America, Madison, WI, United States.

SHACKLETTE H. T., LAKIN H. W., HUBERT A. E. & CURTIN G. C. 1970. *Absorption of gold by plants*. U. S. Geological Survey Bulletin 1314-B, Washington, 23 pp.

SHEARD M. J., LINTERN M. J., PRESCOTT J. R. & HUNTLEY D. J. 2006. Great Victoria Desert: New dates for South Australia's ?oldest desert dune system. *MESA Journal* **42,** 15-26.

SIBBICK S. J. & FLETCHER W. K. 1993. Distribution and Behavior of Gold in Soils and Tills at the Nickel Plate Mine, Southern British-Columbia, Canada. *Journal of Geochemical Exploration* **47,** 183-200.

SKIPP G. L. & BROWNFIELD I. K. 1993. Improved density gradient separation techniques using sodium polytungstate and a comparison to the use of other heavy liquids, pp. 16 in *Open-File Report 92-386 U. S. Geological Survey*. U. S. Geological Survey, Reston, VA, United States.

SKIRROW R. G. 2003. Fe-oxide Cu-Au deposits:potential of the Curnamona province in an Australian and global context, pp. 158-161 in *Broken Hill Exploration Initiative: Abstracts from the July 2003 Conference*, edited by PELJO M. Geoscience Australia, Record 2003/13.

SKIRROW R. G. & ASHLEY P. M. 2000. Proterozoic Cu-Au systems of the Curnamona Province. *MESA Journal* **19,** 48-50.

SMECK N. E. & WILDING L. P. 1980. Quantitative evaluation of pedon formation in calcareous glacial deposits in Ohio. *Geoderma* **24,** 1-6.

SMEE B. W. 1998. A new theory to explain the formation of soil geochemical responses over deeply covered gold mineralization in arid environments. *Journal of Geochemical Exploration* **61,** 149-172.

SMEE B. W. 1999. The effect of soil composition on weak leach solution pH: a potential exploration tool in arid environments. *Explore - Newsletter for the Association of Exploration Geochemists* **102,** 4-7.

SMITH B. H. 1987. Dispersion of gold in soils, pp. 55-82 in *Meaningful sampling in gold exploration*. Australian Institute of Geoscientists, Bulletin no. 7, Perth.

SMITH B. H. & KEELE R. A. 1984. Some observations on the geochemistry of gold mineralisation in the weathered zone at Norseman, Western Australia. *Journal of Geochemical Exploration* **22,** 1-20.

SMITH H. & WILDING L. P. 1972. Genesis of argillic horizons in ochraqualfs derived from fine textured till deposits of Northwestern Ohio and Southeastern Michigan. *Soil Science Society of America Proceedings* **36,** 808-815.

SMITH R. E. & SINGH B. 2007. Recognizing, in lateritic cover, detritus shed from the Archean Gossan Hill Cu-Zn-Au volcanic-hosted massive sulphide deposit, Western Australia. *Geochemistry - Exploration, Environment, Analysis* **7,** 71-86.

SOIL SURVEY DIVISION STAFF. 1993. *Soil survey manual*. US Department of Agriculture Handbook no. 18. US Government Printing Office, Washington, DC pp.

SOLOMON S. T. & WALKDEN G. M. 1985. The application of cathodoluminescence to interpreting the diagenesis of an ancient calcrete profile. *Sedimentology* **32,** 877-896.

SOMBROEK W. G., NACHTERGAELE F. O. & HEBEL A. 1993. Amounts, dynamics and sequestering of carbon in tropical and subtropical soils. *Ambio* **22,** 417-426.

STEPHENS C. G. 1971. Laterite and silcrete in Australia: A study of the genetic relationships of laterite and silcrete and their companion materials, and their collective significance in the formation of the weathered mantle, soils, relief and drainage of the Australian continent. *Geoderma* **5,** 5-52.

STEVENS B. P. J., BARNES R. G. & FORBES B. G. 1990. Willyama Block - regional geology and minor mineralisation. *In:* HUGHES F. E., ed. *Geology and mineralisation of Australia and Papua New Guinea*, pp. 1065-1072. The Australasian Institute of Mining and Metallurgy, Melbourne.

STILLE P. & SHIELDS G. 1997. *Radiogenic isotope geochemistry of sedimentary and aquatic systems*. Springer pp.

STOOPS G. 2003. *Guidelines for analysis and description of soil and regolith thin sections*. Soil Science Society of America, Inc., Madison, WI, 184 pp.

STREETER V. L. & WYLIE E. B. 1983. *Fluid Mechanics: First SI Metric Edition*. McGraw-Hill, Singapore, 562 pp.

SUDOM M. D. & ARNAUD R. J. S. 1971. Use of quartz, zirconium and titanium as indices in pedological studies. *Canadian Journal of Soil Science* **51,** 385-396.

TAYLOR G. 2006. Fundamentals of regolith geology. *In:* FITZPATRICK R. W. and SHAND P., ed. *Regolith 2006 - Consolidation and dispersion of ideas*, pp. 343-345. CRC LEME, Perth, Western Australia.

TAYLOR G. & BUTT C. R. M. 1998. The Australian regolith and mineral exploration. *AGSO Journal of Australian Geology and Geophysics* **17,** 55-67.

TAYLOR G. & EGGLETON R. A. 2001. *Regolith geology and geomorphology*. John Wiley & Sons, Chichester, 375 pp.

TAYLOR G. & SHIRTLIFF G. 2003. Weathering: cyclical or continuous? An Australian perspective. *Australian Journal of Earth Sciences* **50,** 9-17.

TAYLOR G. F. 1990. The regolith and associated mineral deposits. *In:* HUGHES F. E., ed. *Geology of the mineral deposits of Australia and Papua New Guinea*, pp. 1569-1572. Australian Institute of Mining and Mettallurgy, Melbourne.

TAYLOR S. R. & MCLENNAN S. M. 1985. *The continental crust: Its composition and evolution*. Blackwell, Oxford, 312 pp.

THALHAMMER O. A. R., STEVENS B. P. J., GIBSON J. H. & GRUM W. 1998. Tibooburra Granodiorite, western New South Wales: emplacement history and geochemistry. *Australian Journal of Earth Sciences* **45,** 775-787.

THOMAS M. 2004. Biogeochemical data ranges from Tunkillia Prospect, central Gawler Craton, South Australia. *In:* ROACH IAN C., ed. *Regolith 2004; proceedings of the CRC LEME regional regolith symposia 2004*, pp. 362-364. Cooperative Research Centre for Landscape Environments and Mineral Exploration. Bentley, West. Aust., Australia. 2004.

TORDIFFE E. A. W., VERMAAK J. J., VAN D. W. W. A. & BEUKES G. J. 1989. The Jacomynspan copper-nickel prospect; a study of secondary dispersion in the calcretes of the northern Cape Province, South Africa. *Journal of Geochemical Exploration* **34,** 31-45.

TORRESAN M. E. 1987. The use of sodium polytungstate in heavy mineral separations, pp. 18 in *Open-File Report 87-590 U. S. Geological Survey*. U. S. Geological Survey, Reston, VA, United States.

TREADWELL-STEITZ C. & MCFADDEN L. D. 2000. Influence of parent material and grain size on carbonate coatings in gravelly soils, Palo Duro Wash, New Mexico. *Geoderma* **94,** 1-22.

TSAI C. C. & CHEN Z. S. 2000. Lithologic discontinuities in ultisols along a toposequence in Taiwan. *Soil Science* **165,** 587-596.

TWIDALE C. R. & CAMPBELL E. M. 1988. Ancient Australia. *Geojournal* **16,** 339-354.

TWIDALE C. R. & CAMPBELL E. M. 1995. Pre-Quaternary landforms in the low latitude context: the example of Australia. *Geomorphology* **12,** 17-35.

TYLKOWSKI L. N. 2004. Origin and genesis of calcrete in the Murray Basin, p. 43. The University of Adelaide, Honours Thesis (*unpublished*).

VAN DER HOVEN S. J. & QUADE J. 2002. Tracing spatial and temporal variations in the sources of calcium in pedogenic carbonates in a semiarid environment. *Geoderma* **108,** 259-276.

VAN DER STELT B. J., BOUNDY M. & FLINT R. B. 2006. PACE initiative: Theme 2, year 2, drilling partnership - New Well and Old Well shear-associated gold mineral prospects project final report, pp. 73. Department of Primary Industries and Resources. Open File Envelope 11,166, South Australia.

VARAJAO C. A. C., COLIN F., VIEILLARD P., MELFI A. J. & NAHON D. 2000. Early weathering of palladium gold under lateritic conditions, Maquine Mine, Minas Gerais, Brazil. *Applied Geochemistry* **15,** 245-263.

VARSHAL G. M., VELYUKHANOVA T. K. & BARANOVA N. N. 1984. The geochemical role of gold(III) fulvate complexes. *Geochemistry International* **21,** 139-146.

VARSHAL G. M., VELYUKHANOVA T. K. & BARANOVA N. N. 1990. Geochemical and analytical aspects of the reactions of gold with humic substances in natural waters, soils and rocks. *Geochemistry International* **27,** 10-19.

VARSHAL G. M., VELYUKHANOVA T. K., CHKHETIYA D. N., KHOLIN Y. V., SHUMSKAYA T. V., TYUTYUNNIK O. A., KOSHCHEYEVA I. Y. & KOROCHANTSEV A. V. 2000. Sorption on humic acids as a basis for the mechanism of primary accumulation of gold and platinum group elements in black shales. *Lithology and Mineral Resources* **35,** 538-545.

VERRECCHIA E. P. & DUMONT J. L. 1996. A biogeochemical model for chalk alteration by fungi in semiarid environments. *Biogeochemistry* **35,** 447-470.

VERRECCHIA E. P., DUMONT J. L. & ROLKO K. E. 1990. Do fungi building limestones exist in semi-arid regions? *Naturwissenschaften* **77,** 584-586.

VERRECCHIA E. P., DUMONT J. L. & VERRECCHIA K. E. 1993. Role of calcium oxalate biomineralization by fungi in the formation of calcretes; a case study from Nazareth, Israel. *Journal of Sedimentary Petrology* **63,** 1000-1006.

VERRECCHIA E. P., FREYTET P., VERRECCHIA K. E. & DUMONT J. L. 1995. Spherulites in calcrete laminar crusts: biogenic $CaCO_3$ precipitation as a major contributor to crust formation. *Journal of Sedimentary Research* **A65,** 690-700.

VLASSOPOULOS D. & WOOD S. A. 1990. Gold speciation in natural waters: I. Solubility and hydrolysis reactions of gold in aqueous solution. *Geochimica et Cosmochimica Acta* **54,** 3-12.

VLASSOPOULOS D., WOOD S. A. & MUCCI A. 1990. Gold speciation in natural waters: II. The importance of organic complexing- Experiments with some simple model ligands. *Geochimica et Cosmochimica Acta* **54,** 1575-1586.

WALTER M. R., VEEVERS J. J., CALVER C. R. & GREY K. 1995. Neoproterozoic stratigraphy of the Centralian Superbasin, Australia. *Precambrian Research* **73,** 173-195.

WATTS N. L. 1980. Quaternary pedogenic calcretes from the Kalahari (southern Africa): mineralogy, genesis and diagenesis. *Sedimentology* **27,** 661-686.

WEBSTER J. G. 1986. The solubility of gold and silver in the system Au-Ag-S-O_2-H_2O at 25°C and 1 atm. *Geochimica et Cosmochimica Acta* **50,** 1837-1845.

WEISS S. 2003. The mineralogy of gold - a review. *In:* COOK R. B., COOGAN E. R., NEUMEIER G. and STAEBLER G. A., ed. *Gold the noble mineral*, pp. 112. Lapis International, LLC, East Hampton, USA.

WHIPKEY C. E., CAPO R. C., CHADWICK O. A. & STEWART B. W. 2000. The importance of sea spray to the cation budget of a coastal Hawaiian soil; a strontium isotope approach. *Chemical Geology* **168,** 37-48.

WHITE P. J. & BROADLEY M. R. 2003. Calcium in plants. *Annals of Botany* **92,** 487-511.

WILLIS I. L., BROWN R. E., STROUD W. J. & STEVENS B. P. J. 1983. The early Proterozoic Willyama Supergroup; stratigraphic subdivision and interpretation of high to low-grade metamorphic rocks in the Broken Hill Block, New South Wales. *Journal of the Geological Society of Australia* **30,** 195-224.

WILSON A. F. 1983. The economic significance of non-hydrothermal transport of gold, and of the accretion of large gold nuggets in laterite and other weathering profiles in Australia. *Special Publication, Geological society of South Africa* **7,** 229-234.

WILSON A. F. 1984. Origin of quartz-free gold nuggets and supergene gold found in laterites and soils - a review and some new observations. *Australian Journal of Earth Sciences* **31,** 303-316.

WITTWER P. D., BAROVICH K. M. & HILL S. M. 2004. Geology and geochemistry of regolith carbonate accumulations of the southwestern Curnamona Province, SA: Implications for mineral exploration. *In:* ROACH I. C., ed. *Regolith 2004*, pp. 402-406. CRC LEME.

WOOD H. K. & MACPHERSON G. L. 2005. Sources of Sr and implications for weathering of limestone under tallgrass prairie, northeastern Kansas. *Applied Geochemistry* **20,** 2325-2342.

WOOD S. A. 1996. The role of humic substances in the transport and fixation of metals of economic interest (Au, Pt, Pd, U, V). *Ore Geology Reviews* **11,** 1-31.

WRIGHT V. P. 1986. The role of fungal biomineralization in the formation of Early Carboniferous soil fabrics. *Sedimentology* **33,** 831-838.

WRIGHT V. P. 1990. A micromorphological classification of fossil and recent calcic and petrocalcic microstructures. *In:* DOUGLAS L. A., ed. *Soil micromorphology; a basic and applied science*, pp. 401-407. Elsevier, Amsterdam.

WRIGHT V. P. 2007. Calcrete. *In:* NASH D. J. and MCLAREN S. J., ed. *Geochemical sediments and landscapes*, pp. 488. Blackwell, Oxford.

WRIGHT V. P., PLATT N. H., MARRIOTT S. B. & BECK V. H. 1995. A classification of rhizogenic (root-formed) calcretes, with examples from the Upper Jurassic-Lower Cretaceous of Spain and Upper Cretaceous of southern France. *Sedimentary Geology* **100,** 143-158.

WRIGHT V. P. & TUCKER M. E. 1991. Calcretes: An introduction. *In:* WRIGHT V. P. and TUCKER M. E., ed. *Calcretes*, pp. 1-22. Blackwell Scientific Publications, Oxford.

YAALON D. H. 1983. Climate, time and soil development. *In:* WILDING L. P., SMECK N. E. and HALL G. F., ed. *Pedogenesis and soil taxonomy. I. Concepts and interactions*, pp. 233-251. Elsevier, Amsterdam.

YANG J., CHEN J., AN Z., SHIELDS G., TAO X., ZHU H., JI J. & CHEN Y. 2000. Variations in (super 87) Sr/ (super 86) Sr ratios of calcites in Chinese loess; a proxy for chemical weathering associated with the East Asian summer monsoon. *Palaeogeography, Palaeoclimatology, Palaeoecology* **157,** 151-159.

YPMA P. J. 1991. The concentration of gold in calcrete and its significance for lower Proterozoic gold-uranium mineralization. *In:* PAGEL M. and LEROY JACQUES L., ed. *Source, transport and deposition of metals.*, pp. 719-722. A. A. Balkema, Rotterdam, Netherlands.